UNIVERSITÉ PIERRE ET MARIE CURIE, PARIS VI

Dossier d'Habilitation à Diriger des Recherches

Spécialité : Biologie

présenté par : **Angelo ARLEO**

NEURAL BASES OF SPATIAL COGNITION AND INFORMATION PROCESSING IN THE BRAIN

Soutenue le 12 Décembre 2005 devant le Jury composé de :

Rapporteurs :	Neil	BURGESS	(University College London)
	Jean-Arcady	MEYER	(CNRS-Université Paris VI)
	Bruno	POUCET	(CNRS-Université de Provence)
Examinateurs :	Daniel	BENNEQUIN	(CNRS-Université Paris VII)
	Jacques	DROULEZ	(CNRS-Collège de France)
	Sidney	WIENER	(CNRS-Collège de France)

Neural Bases of Spatial Cognition and Information Processing in the Brain

Note to the reader: This pdf document is endowed with hyperlinks associated with: the table of contents, references to figures/chapters/sections, and bibliographical citations. After following a hyperlink (e.g., to check a reference in the bibliography), the key combination Alt+Left Arrow returns you to the hyperlink position in the document.

Contents

Chapter 1

General Introduction

The main research topic of this dissertation is the spatial memory function. Similar to other high-level brain functions, spatial memory calls upon parallel processes mediated by multiple neural substrates that interact, either cooperatively or competitively, to promote appropriate spatial learning and goal-oriented behaviour.

As a consequence, studying spatial memory requires/permits to investigate numerous brain functions including: *(i)* **neural information processing** (e.g., information storage and transmission at synapses; rate-based versus spike-time neural coding); *(ii)* **multimodal sensory processing and integration** (e.g., extraction of low-dimensional representations from high-dimensional sensory flows; combination of multimodal signals into unified perceptual representations); *(iii)* **procedural-like memory** (e.g., acquisition of low-level sensory-motor couplings; fine tuning of coordinate movements according to the ongoing sensory context); *(iv)* **declarative-like memory** (e.g., elaboration of abstract representations of the spatio-temporal relationships between spatial events); *(v)* **action selection** (e.g., reward-dependent navigation planning; dynamical weighing of multiple concurrent strategies).

Besides such a broad functional manifold, understanding spatial cognition requires a vertical cross-linking of different description levels including: *(i)* the **molecular level** (e.g., dynamics of gene expression in normal and mutant organisms; dynamics of the molecular influx through receptor channels; neuropharmacological modulation of neural states); *(ii)* the **synaptic level** (e.g., mechanisms regulating the presynaptic neurotransmitter release; biophysics of the transduction of presynaptic spikes into analog postsynaptic potentials; activity-dependent synaptic plasticity providing the basis for spatial learning and memory); *(iii)* the **cellular level** (e.g., electrophysiological properties of single neurons such as selective discharge in relation to spatial correlates; mechanisms regulating the intrinsic electroresponsiveness of nerve cells; temporal dynamics of the emitted spike trains); *(iv)* the **local network level** (e.g., mechanisms underlying the emergence of neural population states; population activity dynamics for encoding, storage, and retrieval of spatial information); *(v)* the **system level** (e.g., anatomo-functional interactions of multiple brain structures mediating spatial learning

functions); *(vi)* the **behavioural level** (e.g., adaptive motor skills; learning mechanisms promoting flexible solutions to solve complex navigation tasks; phylogenetic comparisons and ontogenetic development of spatial learning capabilities).

Integrative neuroscience provides a suitable framework to study wide horizontal sub-function spectra as well as vertical links across different descriptive levels. This cross-disciplinary approach brings together experimental neuroscience (e.g., molecular biology, neurophysiology, neuroanatomy, neurology, psychology), theoretical neuroscience (e.g., physics, mathematics), and neuroengineering (e.g., neuroinformatics, neurorobotics). For instance, biologically plausible models and their validation in real experimental conditions may help to explore potential connections between findings on the neuronal level (e.g., single-cell discharge patterns) and observations on the behavioural level (e.g., animal's action selection policy). Indeed, theoretical models can permit a scale up to large neural populations, organise them in subsystems, and test hypotheses about their anatomo-functional interactions to produce complex behaviour. Therefore, theoretical neuroscience may provide a unique vantage point from which to derive predictions that can then be tested in innovative experiments with animals.

This dissertation presents an integrative neuroscience approach that attempts to unravel the overall spatial memory function by combining electrophysiological studies, behavioural experiments, theoretical modelling, and robotics.

1.1 Roadmap of this dissertation

The main body of this dissertation is organised in five chapters that describe my research line in chronological order. Each chapter begins with a short Preface that outlines the content of the chapter and provides some elements related to the working context (e.g., host institution and laboratory, mentor, collaborations, supervised students). Notice that, thanks to collaborations as well as student supervisions, all the projects depicted in this dissertation are still ongoing (parallel) works.

Chapter 2, titled "Spatial Cognition and Multimodal Sensory Integration", introduces the spatial memory function and discusses some background issues that are useful to understand the overall problem (e.g., the representation of spatial information via allocentric and egocentric reference frames). The chapter also reviews some electrophysiological, pharmacological, and behavioural findings about the neural bases of spatial cognition (e.g., hippocampal place and head direction cells), and it focuses on the importance of multimodal sensory integration for robust spatial learning.

Chapter 3, titled "Spatial Learning and Navigation in Neuromimetic Systems", describes a neuromimetic computational model for the elaboration of spatial representations (i.e., cognitive maps) and their use for goal-oriented navigation. The model attempts to capture some of the mechanisms underlying the location- and

direction-selective activity of hippocampal place and head direction cells, respectively. Population coding and multimodal sensory integration (mediated by Hebbian relational learning) are two major components of the model. The latter was validated through a series of robotic experiments in which a mobile robot had to learn some navigation tasks under experimental conditions similar to those employed for rat spatial learning experiments.

Chapter 4, titled "Head Direction Cells: Electrophysiological Recordings and Theoretical Modelling", outlines the electrophysiological work done to study the interrelation between visual and inertial signals and their relative influence upon the direction-selective discharge of thalamic head direction (HD) cells. The presented findings reveal some new aspects of the visually-driven update of HD cell activity, determined by both static and dynamic visual cues (e.g., optic field flow). The second part of the chapter depicts a theoretical study (done in parallel to the experiments) that focuses on the generation and maintenance of the HD representation. The theoretical results (both analytical and numerical) permitted to reproduce some of our experimental data and provided some experimentally testable predictions.

Chapter 5, titled "Motor Behaviour Adaptation for Optimal Goal-oriented Navigation", presents a behavioural study focusing on the role of the cerebellum in spatial navigation. The work investigated the contribution of cerebellar long-term plasticity (in particular long-term depression, LTD, at the parallel fibre-Purkinje cell, PF-PC, synapses) to the procedural component of navigation. A mutant mouse model (namely L7-PKCI, having a specific LTD deficit at the PF-PC synapses) was employed for this study. The second part of the chapter describes an automated analysis tool that was developed to assess the navigation skills of mice solving a spatial learning task. This tool pays a particular attention to the characterisation of the trajectory patterns, which are likely to inform us about procedural-like abilities of the subjects.

Chapter 6, titled "Exploring the Neural Code via Information Theory", presents a project aiming at quantifying the information transfer properties of single neurons. The study focused on the cerebellar granule cells (GCs), whose characteristics (e.g., the fact they receive, on average, only four afferents) are suitable for performing an information theoretic analysis exploring the input-output neural space extensively. Both experimental (i.e., single-cell patch clamp recordings) and computational (i.e., an Hodgkin-Huxley-like GC model) investigations were done to measure how long-term synaptic plasticity affects information transmission, and to characterise the spike train features (e.g., spike time correlations across the neuron's afferents) that most contribute to the overall information transfer.

Chapter 2

Spatial Cognition and Multimodal Sensory Integration

Preface. *This chapter reviews some basic concepts relevant to the understanding of the spatial learning problem (e.g., allothetic vs idiothetic signals, allocentric vs egocentric representations), and it outlines some behavioural, electrophysiological, and pharmacological findings that shed light on the nature of the neural mechanisms underlying the spatial memory function in animals. Special emphasis is given to the importance of multisensory integration for robust spatial learning. This chapter provides a suitable introduction to Chapters 3, 4, and 5 titled, respectively, "Spatial Learning and Navigation in Neuromimetic Systems", "Head Direction Cells: Electrophysiological Recordings and Theoretical Modelling", and "Motor Behaviour Adaptation for Optimal Goal-oriented Navigation". The content of the present chapter has been adapted from Arleo and Rondi-Reig (2005).*

2.1 Spatial memories rely upon idiothetic and allothetic signals

Spatial cognition involves the ability of a navigating agent (be it an animal or an autonomous artifact) to acquire spatial knowledge (e.g., spatio-temporal relations among environmental cues or events), organise it properly, and employ it to adapt its motor behaviour to the specific context (e.g., performing flexible goal-oriented navigation).

At the sensory level, **different perceptual modalities provide the navigator with a manifold description of the currently experienced spatial context**. The integration of these multimodal signals (that are processed by interrelated brain regions) into a coherent representation is at the core of spatial cognition. The variety of sensory modalities conveying spatial information can be separated into two main categories, namely **idiothetic and allothetic cues**. Idiothetic stimuli are self-motion related signals and include vestibular (inertial), kinesthetic (e.g., information from muscle and joint receptors), motor command efferent copies, and sensory flow information (e.g., optic

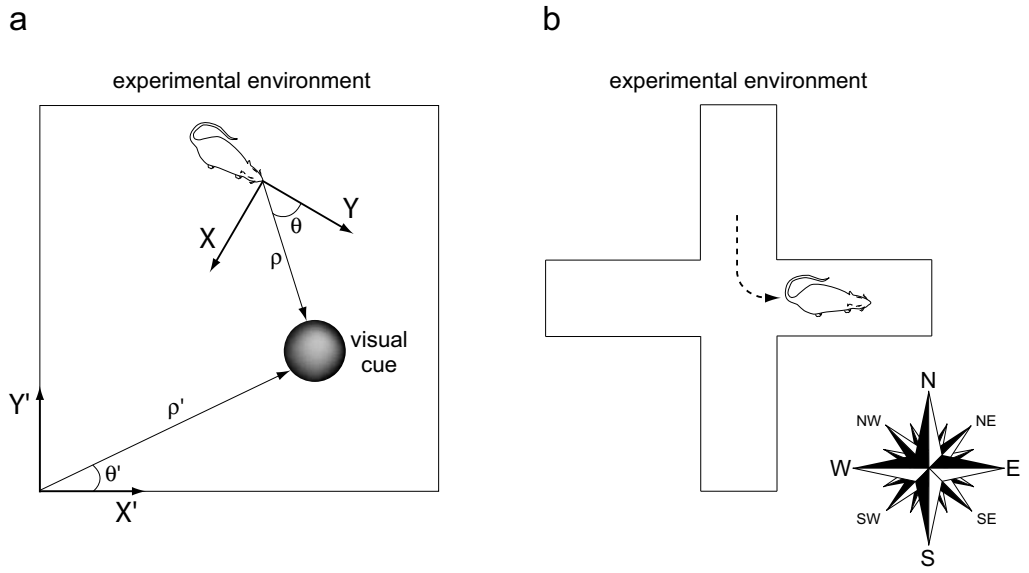

Figure 2.1: Encoding spatial information within a reference frame. **(a)** The circular object provides an allothetic (visual) spatial cue to the navigator (rat). The latter can represent the spatial position of the external cue within the egocentric reference frame X-Y (centered on its head), that is estimate the distance ρ between its head and the object, as well as the angle θ between its heading and the direction to the object. Alternatively, the rat can encode the same spatial information within the allocentric coordinate system X'-Y' (centered on the bottom-left corner of the experimental environment), that is estimate the distance ρ' and the angle θ'. **(b)** In this example, the navigator can employ idiothetic information (e.g., vestibular signals) to represent the change of its motion direction within an egocentric reference frame, that is "I turned to my left". Alternatively, it can refer to the allocentric directional system based on the geomagnetic north, that is "I turned eastward". (Taken from Arleo and Rondi-Reig 2005)

field flow signals informing the navigator about its own movements). Allothetic signals provide information about the external environment and include visual (e.g., environmental landmarks), olfactory, auditory, and somatosensory (e.g., tactile or texture) cues. **Learning spatial memories requires the extraction of coherent information from such a redundant and multidimensional sensory input space**. This learning process implies, for instance, maintaining idiothetic and allothetic cues congruent (e.g., minimisation of interferences or conflicts) both during the exploration of a novel environment and across subsequent visits to a familiar environment.

A given sensory modality is labelled as allothetic or idiothetic to characterise the type of information it conveys. On the other hand, if we want to characterise the way this information is represented by the navigator, we need to introduce the concept of **reference coordinate system** (or simply reference frame). This system defines the **framework in which spatial information (e.g., the position of an object) can be represented relative to an origin point**. Depending on the anchorage of the origin of the reference coordinate system, the same information can be encoded egocentrically or allocentrically. If the reference frame is centred on the subject (e.g., on a body part such as the head) the representation is said **egocentric**. If the origin of the frame-

work is a fixed point of the environment (e.g., a corner of the room) the representation is called **allocentric**. As shown in Fig. 2.1a, the same allothetic spatial information (e.g., the position of a visual cue in the environment) can be represented either egocentrically (e.g., relative to the body of the navigator) or allocentrically (e.g., relative the room corner). Similarly, as shown in Fig. 2.1b, idiothetic signals (e.g., vestibular information) can be employed to describe self-motion either egocentrically or relative to an allocentric reference frame. Egocentric coding is simple to build but it varies as the navigator moves in the environment (because the reference frame translates and rotates as the subject moves). Allocentric coding requires more complex processing (e.g., to relate the visual cue position to the world-centred origin), but it is invariant with respect to the subject's position and orientation in the environment. One factor of the complex multisensory integration process is that different sensory modalities are encoded within different reference frames. Thus, in order **to combine different sensory modalities, a navigating system has to integrate different representations into a unified spatial framework**.

Animals employ both idiothetic and allothetic cues to maintain memory traces of the spatial components (e.g., their body position and orientation) of experienced events. For instance, they are capable of estimating their current location relative to a starting point (i.e., homing vector) by integrating linear and angular self-motion signals over time (Figs. 2.2a,b). This process, termed path integration or dead reckoning (Mittelstaedt and Mittelstaedt 1980; Etienne and Jeffery 2004), relies upon idiothetic cues like vestibular and kinesthetic signals, motor command efferent copies, and sensory (e.g., optic) flow information. On the other hand, self-localisation can occur solely on the basis of allothetic cues like vision, auditory, olfactory, and tactile signals. Indeed, locations can be characterised by specific allothetic sensory patterns (e.g., configurations of visual cues), such that memorising these sensory patterns can enable a subject to recognise familiar places.

Idiothetic and allothetic spatial information have complementary strengths and weaknesses. Since path integration does not depend on external references, it allows a subject to self-localise in an unfamiliar environment from its very first exploring excursion (Etienne and Jeffery 2004). Also, path integration is a basic mechanism suitable for all types of environments (i.e., with or without external cues) and navigators (e.g., agents that can not exploit their interaction with the external world effectively). A limitation of path integration is its vulnerability to cumulative drift over time. Indeed, the idiothetic-based dynamics, consisting of integrating translational and rotational signals over time, is prone to systematic as well as non-systematic errors that quickly disrupt the position estimate (Mittelstaedt and Mittelstaedt 1982; Etienne et al. 1998).

Allothetic spatial information permits the formation of local sensory views directly suitable for self-localisation (McNaughton et al. 1991). Also, if the spatial configuration of the environmental cues (e.g., distal landmark arrays) remains fairly stable over time, the position assessment process is not affected by cumulative errors. However, allothetic (e.g., visual) cues are not always available to the navigator (e.g., in darkness conditions). Additionally, since self-localisation based on allothetic cues involves sensory pattern recognition, *perceptual aliasing* phenomena may occur, that is distinct areas

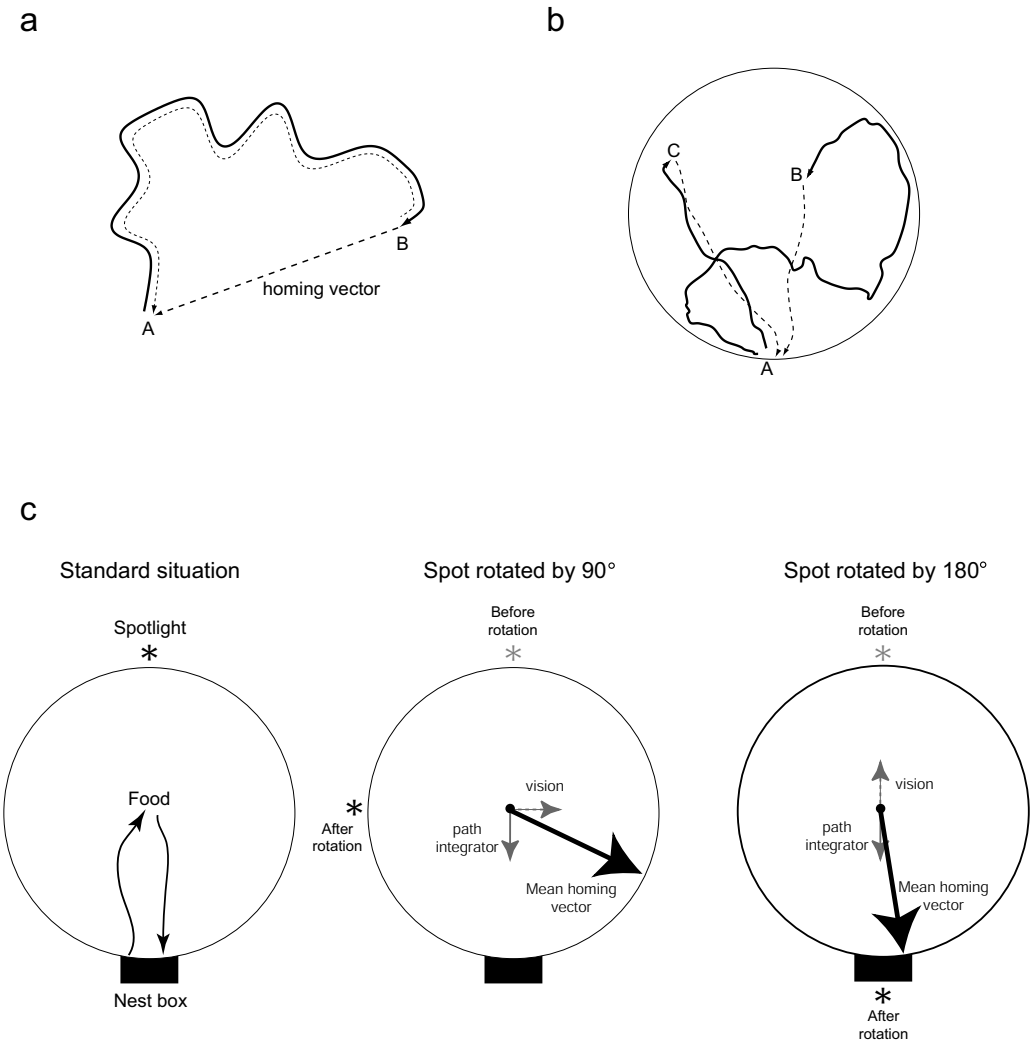

Figure 2.2: Homing behaviour based on path integration (PI). **(a)** Difference between path reversal (i.e., inverting the sequence of movements performed from a starting point A to a current location B), and path integration (i.e., integrating translations and rotations over time to generate a homing vector leading the animal directly to the departure point A). The solid line represents the outward journey; the dotted line indicates the return journey based on path reversal; the dashed line is the homing vector obtained by path integration. Adapted from Etienne et al. (1998). **(b)** Two examples of homing behaviour performed by two hamsters. After having been guided by a bait from the nest location A to points B and C (solid lines), the two animals returned home following direct trajectories (dashed lines). The experiment was performed in the dark in a circular arena of $2\,m$ of diameter. Adapted from Etienne et al. (1998). **(c)** Hamsters' homing behaviour in conflict situations. During training (left), a distal spotlight (asterisk) provided a stable landmark to the animal performing hoarding excursions to a feeder. In probe trials, the spotlight was rotated by either 90° (centre) or 180° (right). Animals were guided from the nest to the feeder in darkness conditions, then the spotlight was turned on, which created a conflict between self-motion (continuous gray arrows) and visual (dashed gray arrows) information. Large arrows indicate the homing vectors followed by the animals and show that in the case of 90° conflicts the visual landmark signal tended to dominate over self-motion, whereas for a 180° mismatch the path integration component became predominant. Adapted from Etienne and Jeffery (2004). (Taken from Arleo and Rondi-Reig 2005)

of the environment may be characterised by equivalent local patterns. For instance, visual sensory aliasing can lead to singularities (i.e., ambiguous state representations) in a purely vision-based space coding (Sharp et al. 1990).

Therefore, neither idiothetic nor allothetic cues are sufficient by themselves to establish reliable spatial memories. One **solution is to combine allothetic and self-motion signals into a unified representation** (e.g., O'Keefe and Nadel 1978; Jeffery and O'Keefe 1999; Redish 1999; Arleo and Gerstner 2000b). The combination of allothetic and idiothetic information may yield a mutual benefit in the sense that idiothetic cues may compensate for perceptual aliasing (e.g., discriminate between two locations in a visually symmetrical environment) and, conversely, environmental landmarks may be used to occasionally reset the integrator of self-motion signals. Idiothetic information might provide the spatial framework suitable for 'grounding' the knowledge gathered by a navigating animal (McNaughton et al. 1991; Knierim et al. 1995a). According to this hypothesis, allothetic local views might be tied onto this framework as the exploration of a novel environment proceeds.

But how is this idiothetic-allothetic coupling established and maintained consistent over time? How are the conflicts between self-motion and landmark cues solved? Ethologists have largely investigated the interaction between path integration and landmark cues for spatial navigation (Etienne and Jeffery 2004). Numerous behavioural studies involved homing tasks in which animals had to perform hoarding excursions and then return home with the collected food. One method to distinguish the idiothetic and allothetic determinants of the animals' homing behaviour consists of setting a conflict between environmental (proximal or distal) landmarks and self-motion cues. Then, observing the homing vector makes it possible to assess the relative influence of allothetic and idiothetic information. Etienne et al. (1990) examined the homing behaviour of golden hamsters during hoarding trips within a circular open arena (Fig. 2.2c). During training, a stable distal spotlight provided a unique visual landmark on an otherwise dark background. Other allothetic cues (e.g., tactile and olfactory stimuli) were masked. In probe trials, hamsters were guided in the dark from the nest (a box located at a fixed peripheral position) toward a feeding location at the centre of the arena. During the uptake of food, visual and self-motion information were set in conflict by rotating the spotlight (either by 90° or 180° relative to its standard position) and turning it on. The authors reported that animals tended to return home following compromise homing vectors whose visual component dominated over the self-motion component in the case of 90° conflicts (Fig. 2.2c, centre). By contrast, when the divergence between the two types of information was further increased (i.e., 180°) the path integration component became predominant (Fig. 2.2c, right). In another series of experiments, Etienne et al. (2000) tested the realignment of the path integrator relative to distal landmarks. The arena and the peripheral home base were both rotated before each hoarding excursion. Then, in the darkness, the hamsters were guided from the rotated nest toward a feeding location along a two-leg (L-shaped) journey. Under this condition, the subjects mainly relied on their internally generated homing vector and returned to the new rotated home base. By contrast, if the environmental lights were briefly turned on at the end of the first outward leg and then switched off again, the

animals tended to return to the original un-rotated home location, suggesting that a reset of the path integrator had occurred on the basis of the (unchanged) visual cues.

2.2 The neural bases of spatial learning

In addition to behavioural studies, an extensive body of electrophysiological work has been done to investigate the neural bases of animals' spatial learning capabilities. Extracellular single-neuron recordings have largely focused on the properties of pyramidal neurons in the hippocampal formation. This limbic region has been thought to mediate spatial memory functions ever since location-sensitive cells (Fig. 2.3a) in the hippocampus of freely moving rats were found (O'Keefe and Dostrovsky 1971). These neurons, termed **hippocampal place (HP) cells**, **are likely to provide a spatial representation in allocentric (i.e., world centred) coordinates**, thus providing a 'cognitive map' to support flexible navigation (e.g., O'Keefe and Nadel 1978; Leonard and McNaughton 1990; Poucet 1993; Jaffard and Meunier 1993; McNaughton et al. 1996; Burgess and O'Keefe 1996; Redish 1999; Lenck-Santini et al. 2001; Fyhn et al. 2004; Hafting et al. 2005). Furthermore, since the spatially selective responses of HP neurons might result from the projection of contextual (relational) memories onto the two-dimensional locomotion space of the animal, a role for the hippocampal formation in a larger class of memories, namely episodic memory, has been suggested (e.g., Burgess et al. 2002; Fortin et al. 2002).

The hippocampal formation is well suited for subserving the integration of multimodal spatial information into a unified representation. It receives afferents from numerous subcortical regions (e.g., brainstem, amygdala, septum) via the fornix fibre bundle, and it is the recipient of highly processed sensory-motor signals conveyed by neocortical areas mainly via the entorhinal cortex (Witter 1993). Among the neocortices projecting onto the hippocampus, the parietal lobe seems, for example, to be involved in spatial cognition (Burgess et al. 1999; Save and Poucet 2000). Inputs from sensory receptors and motor effectors, likely to be encoded within different egocentric frameworks, reach the parietal lobe from sensory cortices like visual, sensory-motor, and somatosensory areas. Then, these multiple egocentric representations converge from the parietal cortex onto the hippocampal formation in which they might be translated into an allocentric spatial reference frame. According to this theory, the parietal cortex and the hippocampus might cooperate by promoting the egocentric and allocentric components of a navigation task, respectively (Burgess et al. 1999).

Binding of multiple egocentric representations into a unified allocentric framework may occur via correlational learning. According to Hebb's postulate (1949), it is now admitted that correlated spiking of pre- and post-synaptic neurons can result in strengthening or weakening of synapses, depending on the temporal order of spiking. The activity-dependent long-term synaptic plasticity in the hippocampus constitutes a mechanism suitable for this type of learning (Morris and Frey 1999). Both pharmacological and genetic approaches have shown that **hippocampal NMDA** (N-methy-D-Aspartate) **receptors are required for the induction of hippocampal long-term**

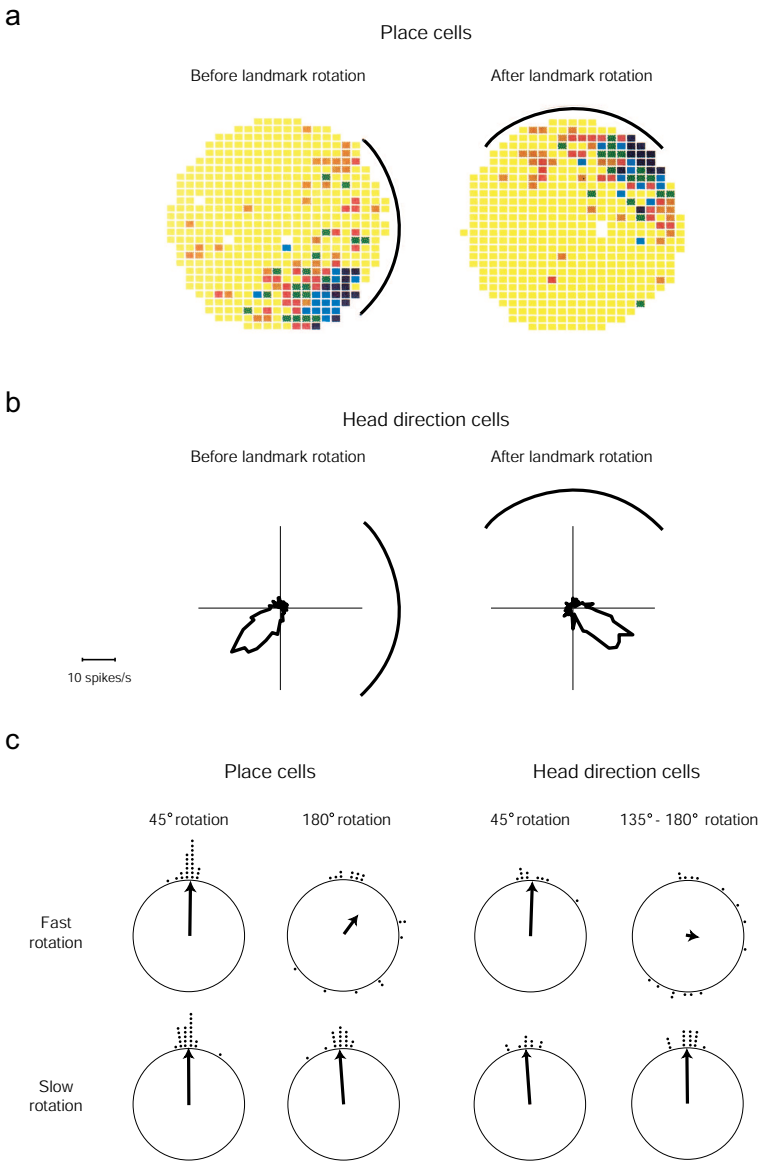

Figure 2.3: **(a)** Sample of receptive field of a place cell recorded from the rat hippocampus. The plots show the mean discharge of the neuron (blue and yellow denote peak and baseline firing rates, respectively) as a function of the animal position within the environment (a cylindrical arena with a cue card attached to inner wall). The location-selective response of the cell is controlled by the cue card in that rotating the card by 90° induces an equivalent rotation of the receptive field. Adapted from Muller and Kubie (1987). **(b)** Sample of tuning curve of a head direction cell recorded in the rat anterodorsal thalamic nucleus. The polar plots indicate that the cell has a unique 'preferred' direction and that the response of the cell is controlled by the visual landmark. Data by Arleo and Wiener. **(c)** Interrelation between visual and self-motion cues in controlling place (left) and head direction (right) cells. Plots indicate the angular deviations of the responses of place and head direction cells relative to the visual landmark in the case of small (45°) and large (135° − 180°) conflicts, and for fast and slow induction of the conflict. The angular deviation of 0°, indicating the absolute control of the visual landmark over the cells' response, is plotted at the 12 : 00 position. Dots indicate individual trials, whereas arrows are averages over all trials. Adapted from Knierim et al. (1998). (Taken from Arleo and Rondi-Reig 2005)

potentiation (LTP), a temporally correlational learning process that can be understood in terms of Hebbian synaptic modification (Collingridge et al. 1983; Morris et al. 1986; Tsien et al. 1996). NMDA-mediated plasticity in the recurrent connections of the CA3 hippocampal region is crucial for the rapid encoding of novel experiences (Lee and Kesner 2002). CA3-NR1-knockout mice are deficient in acquiring novel place/reward information, and CA1 HP cells in these animals are significantly impaired when recorded in a novel environment (e.g., Nakazawa et al. 2002).

Complementing the allocentric place responses of hippocampal neurons, **head direction (HD) cells provide an allocentric representation of the orientation of the animal** (Ranck 1984; Wiener and Taube 2005). The discharge of these neurons is highly correlated with the direction of the head of the animal in the azimuthal plane, regardless of the orientation of the head relative to the body, of the animal's ongoing behaviour and of its spatial location (see Taube 1998, for a review). Each HD cell is selective for one specific 'preferred' direction (Fig. 2.3b), and the preferred directions of a population of HD cells tend to be evenly distributed over $360°$. Direction-sensitive neurons have been found in numerous brain regions centred on the limbic system, including postsubiculum (Ranck 1984; Taube et al. 1990a), anterodorsal thalamic nucleus (Blair and Sharp 1995; Taube 1995), lateral mammillary nucleus (Stackman and Taube 1998), retrosplenial cortex (Chen et al. 1994), and dorsal tegmental nucleus (Sharp et al. 2001). Similar to the HP cell system, the HD circuit receives multimodal afferent information, including angular self-motion signals from the medial vestibular nucleus and visual inputs from neocortical areas (e.g., parietal cortex).

2.3 Allothetic *vs* idiothetic control of head direction and hippocampal place cell activity

The discharge of HP and HD cells is determined by the interaction between allothetic and idiothetic cues. Several studies have attempted to identify the nature of the signals relevant for the establishment and maintenance of their firing properties (see Best et al. 2001 for a review).

The responses of HP and HD cells are anchored to visual landmarks of the environment (e.g., O'Keefe and Conway 1978; Muller and Kubie 1987; O'Keefe and Speakman 1987; Taube et al. 1990b; Bostock et al. 1991; Knierim et al. 1998; Zugaro et al. 2003). A classical experimental apparatus employed to record HP and HD cells consists of a black cylindrical arena in which the rat freely moves while searching for chocolate pellets. The high walls of the cylinder prevent the animal from seeing outside the arena. A large white card, attached to the inner wall of the otherwise black cylinder, is used as a unique salient visual cue. Data show that rotating the white card causes an equal rotation of the receptive fields of HP and HD cells (Fig. 2.3a,b). More generally, experimental findings indicate that **distal (background) visual cues tend to dominate over proximal (foreground) visual cues in controlling HP** (Cressant et al. 1997) **and HD cells** (Zugaro et al. 2001; Zugaro & Arleo et al. 2004). The

dominance of background cues may be due to the fact that they provide more stable references than proximal landmarks as the animal moves around. Consistent with this hypothesis, the more stable an animal perceives an allothetic cue to be, the higher its influence upon HP and HD cell dynamics (Biegler and Morris 1993; Knierim et al. 1995b; Jeffery 1998).

Despite their dependence on exteroceptive signals, both HP and HD cells can maintain stable location and direction tunings for several minutes in the absence of environmental landmarks (Muller and Kubie 1987; Quirk et al. 1990; Chen et al. 1994; Markus et al. 1994), which suggests an **important role for idiothetic cues**. HP and HD cells continue to discharge when the animal moves about in complete darkness (see Wiener and Arleo 2003 for a review on persistent activity in limbic neurons). Also, the location-selective responses of HP cells can develop in blind animals exploring a novel environment (Hill and Best 1981). Save et al. (1998) studied the HP cell activity in blind rats and found receptive fields and response specifics (e.g., spike parameters) very similar to those recorded from sighted rats. The only major difference concerned the mean peak firing rates that were prominently lower in HP cells from blind animals. Vestibular information seems to be important for maintaining the selectivity properties of HP and HD cells (Stackman and Taube 1997). Also, motor signals influence the dynamics of both types of cells, since HP and HD neurons exhibit a dramatic attenuation of their responses if the animal is tightly restrained (Foster et al. 1989; Taube 1995).

Recently, electrophysiological studies of HP and HD neurons have focused on the interaction between idiothetic and allothetic cues and their relative importance under different experimental conditions. Knierim et al. (1998) made self-motion and visual cues incongruent (by rotating the animal and a salient familiar landmark relative to each other) and recorded both HP and HD cells before and after the onset of the conflict (Fig. 2.3c). For small angular mismatches ($45°$) between idiothetic and landmark information, the responses of HP and HD cells remained anchored to the visual stimulus. When larger discrepancies ($180°$) were induced by slow continuous rotations, the landmark still controlled the cell responses. By contrast, for sudden large ($180°$) rotations, either HP and HD cells followed the landmark, or self-motion cues predominated, or a reorganisation (remapping) of HP fields occurred. Jeffery and O'Keefe (1999) further examined HP cell responses in the presence of $180°$ conflicts and found that the ability of visual cues to dominate self-motion signals might depend on the 'confidence' of the idiothetic information. When animals were prevented from visual update for about three minutes while the conflict was introduced, the visual landmark tended to predominate. Conversely, when animals underwent visual isolation during only $30\,s$, a marked attenuation of the visual control was observed.

Finally, HD cells maintain their directional coding even after the removal of landmarks, but their preferred directions may drift over time (Taube 1998). When landmarks are put back to its standard position, HD cells tend to realign their preferred directions with the external reference (Goodridge et al. 1998). However, this resetting does not always occur during subsequent light-dark-light recording phases (Knierim et al. 1998).

Chapter 3

Spatial Learning and Navigation in Neuromimetic Systems

Preface. *I began to study the mechanisms underlying the spatial learning capabilities of animals during my stay at the Laboratory of Computational Neuroscience at the Ecole Polytechnique Fédérale de Lausanne, EPFL, (Ph.D. studentship 1997-2000). Under the supervision of W. Gerstner, I developed a model belonging to the class of computational approaches termed neuromimetic, in the sense their main principles take inspiration from behavioural, anatomo-functional, and neurophysiological findings. The model focused on the properties of hippocampal place (HP) cells and head direction (HD) cells, and addressed two overall issues: (i) How can animals establish stable allocentric spatial representations based on locally available multisensory inputs? (ii) How can HP and HD cells serve as a basis for goal-oriented navigation? The spatial learning model was validated on a mobile robot by adopting experimental protocols similar to those employed for rat experiments. These robotic experiments showed that as long as the system was capable of combining allothetic and idiothetic cues to drive HP and HD cells, the generated space code was stable over time, and goal-oriented navigation could be performed in a straightforward manner based on a reward-dependent learning scheme.*

From 2001 onwards, the model has been extended and improved thanks to the collaboration with: (i) J.-A. Meyer and A. Guillot of the Animatlab (University Paris VI) who allowed me to co-supervise several student projects (including an ongoing Ph.D. work, see d'Erfurth et al. 2005), and who employed the above spatial learning system as a module for their ICEAbot navigation system (EU Integrated Project funded for the period 2006-2010); (ii) W. Gerstner (Laboratory of Computational Neuroscience, EPFL) who used the original model as a basis for three Ph.D. projects (Strösslin et al. 2002; Chavarriaga and Gerstner 2004; Chavarriaga et al. 2005; Strösslin et al. 2005; Sheynikhovich et al. 2005).

This chapter reviews the main model features and presents some relevant results. The reader is referred to the reprints of Arleo and Gerstner (2000b), Arleo and Gerstner (2001), and Arleo et al. (2004) in Appendix C for further details.

3.1 Binding of allothetic and idiothetic information for robust spatial learning

The perspective of emulating the spatial navigation capabilities of animals has given rise to a large number of bio-inspired (or neuromimetic) spatial learning models (see reviews in Arleo 2000; Arleo and Gerstner 2005). A few of these computational models were validated by means of robotic platforms (e.g., Burgess et al. 1994; Schölkopf and Mallot 1995; Trullier and Meyer 2000; Gaussier et al. 2002). These control architectures relied solely on vision to elaborate space representations allowing the robot (often referred to as 'animat') to self-localize. The model outlined here provides an example of spatial learning system stressing the importance of integrating allothetic cues (visual landmarks) and idiothetic (self-motion related) signals (Arleo and Gerstner 2000b; Arleo and Gerstner 2001; Arleo et al. 2004). In the model, these two sensory streams were combined by means of unsupervised Hebbian learning to generate stable head direction (HD) and hippocampal place (HP) cell representations (Fig. 3.1). Then, goal-oriented navigation was obtained via a reinforcement learning scheme that mapped places onto allocentric local actions based on reward-dependent signals.

3.1.1 Modelling head direction cells

The circuitry of the HD cell model (Fig. 3.1) involved the postsubiculum (PoSC), the anterodorsal nucleus (ADN) of the thalamus, the lateral mammillary nucleus (LMN), and the dorsal tegmental nucleus (DTN). Each anatomical region was modelled by a population of formal spiking neurons with evenly distributed preferred directions relative to an absolute directional reference (Degris et al. 2004).

In the model, **the dynamics of the HD system was primarily determined by the integration of angular velocity signals** that permitted to maintain an estimate of the animat heading over time. The formal DTN and LMN populations constituted a **distributed attractor-integrator network** (Amari 1977; Ermentrout 1998) to bear, at any time, a stable directional state corresponding to a gaussian-shaped activity profile in which a subpopulation of LMN units with preferred directions discharged tonically, whereas the others exhibited a very low baseline frequency (Fig. 3.2). This attractor state persisted in the absence of any sensory input (e.g., when the animat was immobile in darkness). The angular velocity signal entering the circuit via DTN was integrated over time through the DTN-LMN interaction. This yielded a shift of the activity profile over the continuous attractor state space and provided an ongoing neural trace of the animat's orientation. The direction representation encoded by the LMN ensemble activity was transmitted to the PoSC via the ADN network. In the model, the PoSC constituted the output interface of the HD system. In order to reconstruct the robot's current heading, a population vector decoding scheme was applied (Georgopoulos et al. 1986). That is, the direction was estimated by taking the centre of mass of the PoSC activity profile.

The integration of the angular velocity signal was affected by a cumulative error

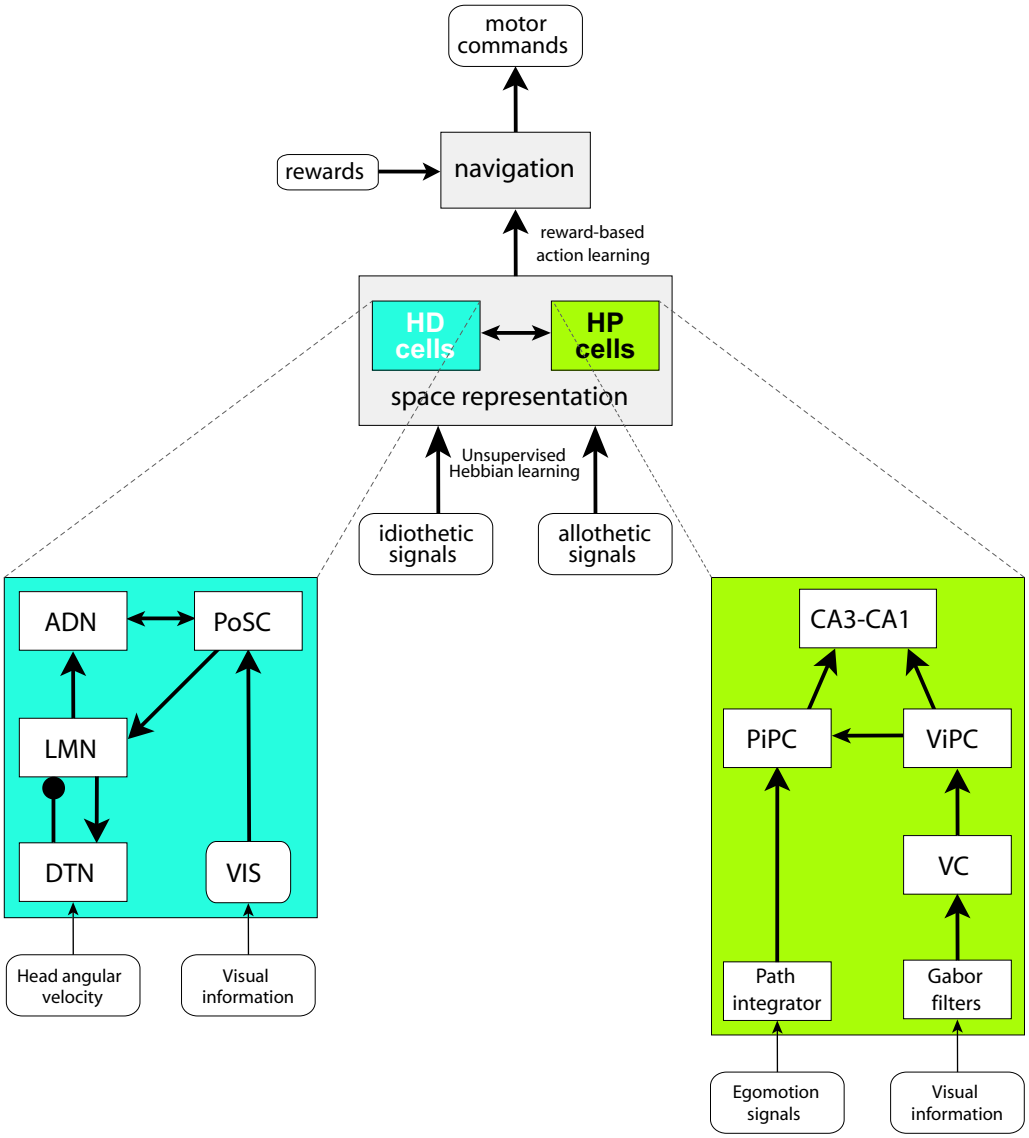

Figure 3.1: Overview of the spatial learning model. The system processed idiothetic and allothetic sensory inputs in parallel. The spatial information extracted from these two processing streams was combined by means of LTP-LTD Hebbian learning to generate place and directional coding. Goal-oriented navigation was achieved by mapping places onto allocentric locomotor actions by means of reward-based learning. The HD model (blue module) included the postsubiculum (PoSC), the anterodorsal thalamic nucleus (ADN), the lateral mammillary nucleus (LMN), and the dorsal tegmental nucleus (DTN). Arrows and circles indicate excitatory and inhibitory projections, respectively. Head angular velocity signals entering the system via the DTN and were integrated over time by the DTN-LMN attractor-integrator network. Visual signals entered the system via a population of formal units (VIS) encoding the agent's egocentric bearing relative to a visual landmark. In the hippocampal place cell model (green module), the visual pathway included a set of Gabor filters for image processing, a network of formal cells (VC) to encode views, and a population of vision-based place cells (ViPC). The idiothetic pathway included the path integrator and a network of units (PiPC) encoding locations based on self-motion signals only. ViPC and PiPC were combined to form a stable space representation in the CA3-CA1 layer of the model. (Adapted from Arleo and Gerstner 2005)

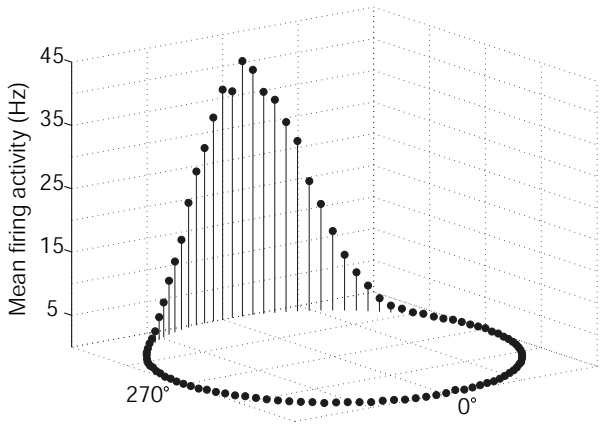

Figure 3.2: A sample of population activity pattern in the LMN layer of the model. Each cell has a specific preferred direction and the set of all preferred directions covers the 360° uniformly. In the figure, each formal cell is represented by a black circle and the whole population forms a ring in the x-y plane. The mean firing rate of each formal HD cell is proportional to the height of the vertical bar below the black circle. (Taken from Arleo and Gerstner 2001)

which could rapidly disrupt the HD coding. The gray area in Fig. 3.3a shows the mean deviation between the animat's actual heading and the direction estimated by the HD system over time. **Static visual information was employed to** modify the intrinsic dynamics of the system in order to *(i)* **prevent the angular velocity integrator from cumulative error, and** *(ii)* **polarise the directional representation whenever the animat entered a familiar environment**. Let L denote a distal visual landmark and let VIS be the population of formal units encoding the animat's egocentric bearing α relative to L. At any time t, the ensemble VIS activity was characterised by a gaussian profile whose centre of mass estimated the egocentric angle $\alpha(t)$. The synaptic projections from VIS to PoSC cells were established by means of a Hebbian learning rule that correlated the egocentric signal encoded by VIS cells with the allocentric HD representation encoded by PoSC cells. A corollary effect of applying this Hebb rule was that only those visual cues that were perceived as stable by the animat could be strongly coupled with its internal directional representation (see Sec. 3.2.2). The black area in Fig. 3.3a represents the mean HD reconstruction error when the system was calibrated by a stable visual input. In contrast to the purely idiothetic coding (gray area), the representation obtained by combining visual and self-motion signals displayed an error that remained bounded over time. Finally, Fig. 3.3b shows an example of tracking of the robot's ongoing heading by means of the HD model signal.

3.1.2 Modelling hippocampal place cells

In the model, **spatial learning occurred via two processing streams** that drived two hippocampal place (HP) cell populations and produced two parallel spatial representations: **a place code based on visual landmark information (ViPC), and a representation obtained by path integration (PiPC)** (see Fig. 3.1).

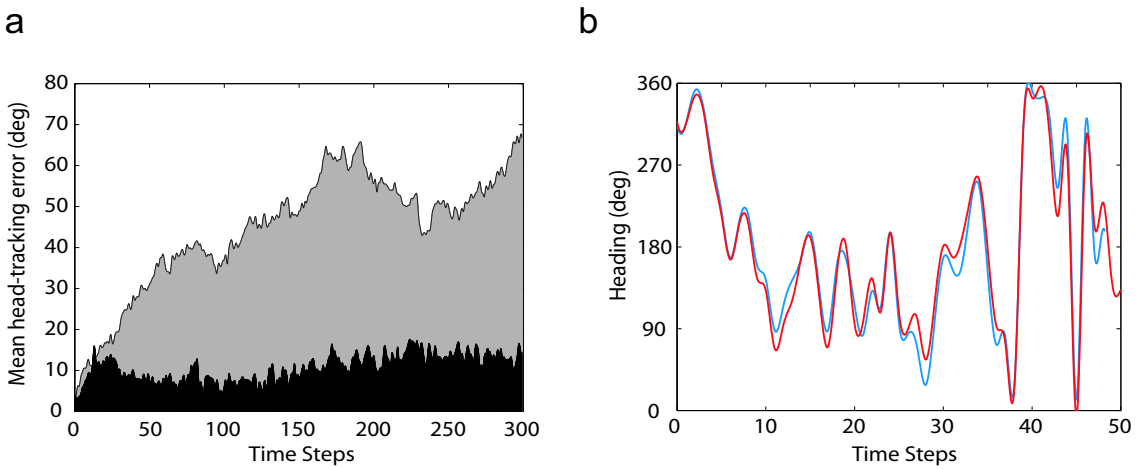

Figure 3.3: **(a)** Mean error over time when estimating the animat's heading based on the HD coding. The gray region represents the angular deviation resulting from idiothetic-based dynamics alone. The black area shows that the error remains bounded when visual signals are used to calibrate the HD system occasionally. (Taken from Arleo and Gerstner 2001) **(b)**Example illustrating the ability of the HD system to track the robot's heading over time. The solid line represents the robot's current orientation, whereas the dashed line is the direction encoded by the HD cells. (Original source Arleo 2000)

Vision-based place coding was a three-step process. First low-level features were extracted by sampling each image by means of a family of local visual filters (Fig. 3.4a,b). Second, the responses of the filters were combined to drive a population of units whose activity became correlated to more complex spatial relationships between visual features. We called these units 'view cells' (VCs) because they provided a neural encoding of the views perceived by the animat. However, the activity of the VCs was not invariant with respect to the animat's gaze direction and position. Therefore, the third step to achieve vision-based space coding consisted of combining multiple gaze-dependent views at each animat's position. This combination produced a local view encoding the spatial relationships between the perceived visual cues and generated allocentric place cell activity (Fig. 3.4c).

As discussed in Chapter 2, unimodal allothetic information is prone to perceptual aliasing and can lead to ambiguous space representations. Indeed, **due to visual aliasing, the vision-based place cells could have multiple subfields and could not differentiate spatial locations effectively** (Fig. 3.4c, third plot from the left). As a consequence, the accuracy of the vision-based representation was not uniformly distributed over the surface explored by the simulated animal (Fig. 3.4d,e).

In the model, **path integration** (Mittelstaedt and Mittelstaedt 1980; Etienne and Jeffery 2004) **was employed to compensate for ambiguities in the visually driven place coding**. The navigator integrated its linear and angular displacements over time to generate an environment-independent representation of its position relative to a starting point. Such a dead-reckoning mechanism was used to drive a population of cells (PiPCs) whose activity depended on self-motion signals only (i.e., it provided a space coding based solely on idiothetic information). **PiPCs had preconfigured**

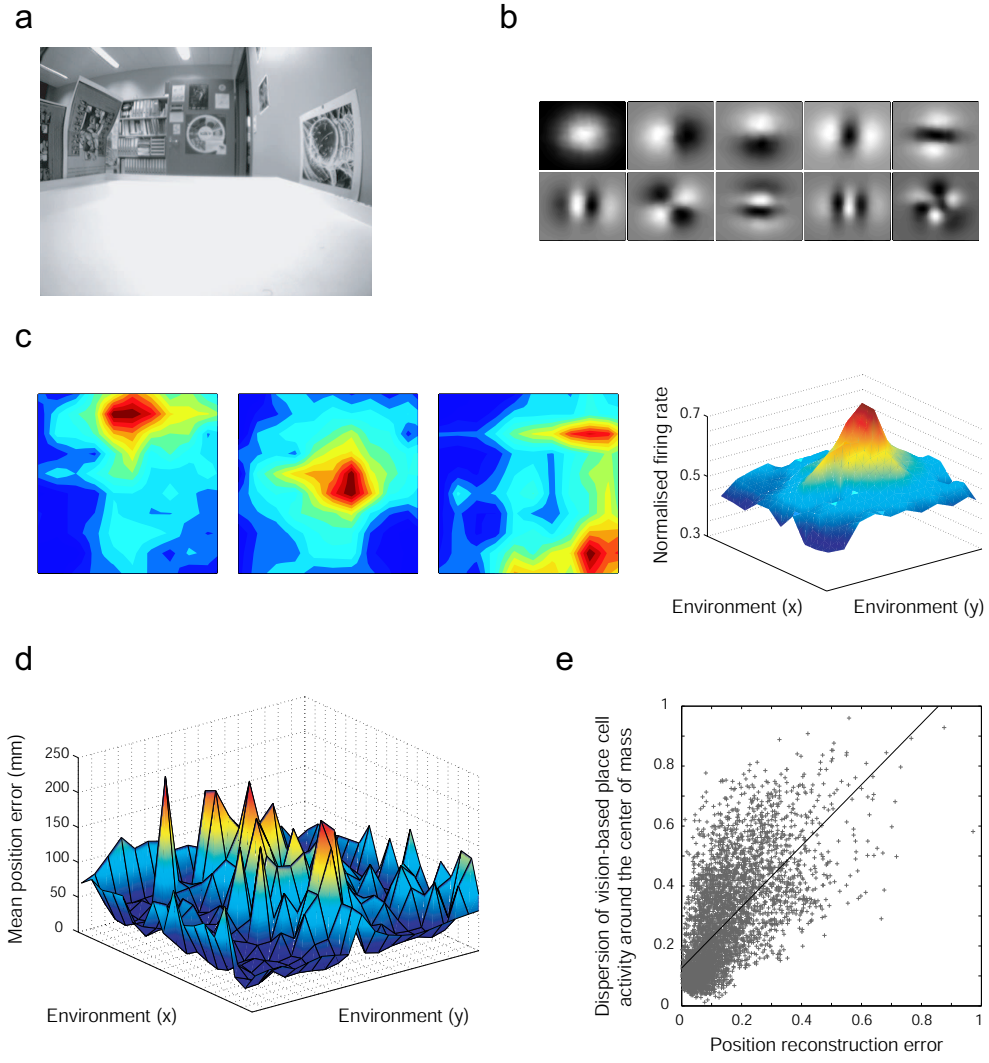

Figure 3.4: Vision-based place coding. **(a)** A sample image taken by the robot while exploring an open-field square environment. **(b)** The receptive fields of a set of filters used to sample the images and detect low-level visual features (the ten filters correspond to the first ten principal components, numbered from left to right, top to bottom, obtained by applying the learning algorithm proposed by Sanger 1989). The model was also tested by employing a set of Gabor filters and a retinotopic sampling method. **(c)** Some samples of vision-based place fields. The squares represent overhead views of the environment. The mean firing rate of each recorded cell was plotted as a function of the locations visited by the robot (red regions denote high activity). Due to visual aliasing, some cells exhibited multipeak receptive fields (third plot from the left). The three-dimensional diagram suggests that visually driven place cells tended to have rather high baseline firing rates. **(d)** Accuracy of the vision-based place representation. By averaging the error function over the whole environment, we obtain a mean position error of about $60\,mm$. **(e)** In the model, the reliability of the visual space coding is assessed by measuring the dispersion of the ensemble activity around the center of mass (computed by population coding). The diagram shows the correlation between this dispersion measure and the vision-based position reconstruction error (number of data points: 4600, correlation coefficient: 0.67). The robot utilises such an on-line reliability criterion to select those local views that are suitable for calibrating its path integrator. (Taken from Arleo and Rondi-Reig 2005)

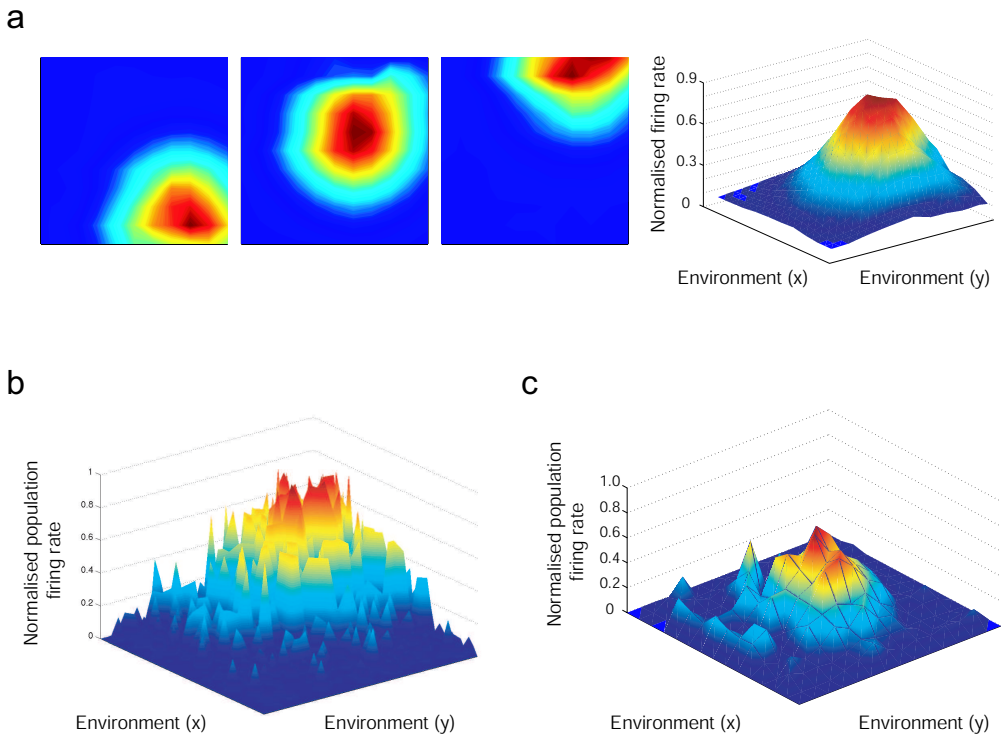

Figure 3.5: Place cell coding based on multisensory integration. **(a)** Samples of model place fields obtained by combining vision and path integration. They did not exhibit multiple subfields and had very low baseline firing (right diagram). **(b)** The animat used the ensemble HP cell activity to self-localize. The diagram shows an example of population activity when the robot was located at the upper-right corner of the arena. **(c)** In the absence of visual information (e.g. in the dark) place cell firing could be sustained by the input provided by the path integration signal. The figure illustrates the population activity recorded in the dark when the robot was approximately at the centre of the arena. (Taken from Arleo and Rondi-Reig 2005)

metric interrelations within an abstract allocentric reference frame S' that was mapped onto the physical space S according to the animat's entry position and the absolute directional reference provided by HD cells. As discussed below, during spatial learning the animat coupled the activity patterns of PiPCs with the local views encoded by ViPCs. This allowed the system to learn a mapping function $S' \rightarrow S$ such that PiPCs could maintain coherent firing patterns across different entries in a familiar environment.

The efferents of the two place cell populations (driven by vision and path integration, respectively) converged onto a third downstream network of HP cells (CA3-CA1 cells, Fig. 3.1). **Hebbian learning**, inducing both long-term synaptic potentiation (LTP) and depression (LTD), was employed **to combine allothetic and idiothetic information based on the agent-environment interaction**. This generated a stable space representation consisting of localised place fields similar to those found in hippocampal CA3-CA1 regions (Fig. 3.5a). These place fields were less noisy than those solely driven by vision and did not exhibit multi-peak fields, meaning that the system over-

came the sensory aliasing problem of purely vision-based representations.

The goal of the spatial learning process was to generate a large population of overlapping place fields covering the two-dimensional space uniformly and densely. The navigator utilised this ensemble HP cell activity to self-localise (Fig. 3.5b). **Population vector decoding scheme** (Georgopoulos et al. 1986; Wilson and McNaughton 1993) computed the centre of mass of the ensemble activity pattern **to estimate the animat's current position**. The use of the population activity, rather than single cell activity, helped in terms of stability and robustness of the self-localisation process.

In the model, **a place map could emerge and persist even in the absence of visual information (e.g., in darkness conditions)**. This property is consistent with the experimental observation that hippocampal place fields can arise in darkness (Quirk et al. 1990). Since the activity of the modelled HP cells relied on convergent excitation from both vision and path integration, their mean peak firing rates were lower in vision-less conditions than when the animat could use visual spatial cues (Fig. 3.5c). The **reduced firing activity of the HP units of the model in darkness conditions** is in agreement with the experimental findings indicating that HP cells recorded from blind rats exhibit lower discharge frequencies than those observed in sighted animals (Save et al. 1998).

The model postulated a role for the medial entorhinal cortex (MEC) as a possible anatomical locus for the path integration based (PiPC) representation. Experimental data suggest that the place field topology of location-sensitive cells in MEC does not change across different environments (Quirk et al. 1992). The model proposed also that the lateral entorhinal cortex might be involved in allothetic space coding, suggesting it as a possible locus for the ViPC space representation. The entorhinal cortex constitutes the main 'cortical gate' to the hippocampal formation, in the sense it receives highly processed inputs, via the perirhinal and parahippocampal cortices, from several neocortical associative areas (e.g., the parietal lobe) and conveys such information to the hippocampus via the perforant path (Witter 1993).

3.2 Maintaining allothetic and idiothetic information coherent over time

3.2.1 Exploring a novel environment

The animat initially explored an unfamiliar environment by relying upon path integration only. As exploration proceeded, local views (encoded by the visually driven ViPCs) were coupled (by means of LTP/LTD correlational learning) to the spatial framework provided by the path integrator such that vision and self-motion signals could cooperate to form the hippocampal space code (i.e., the CA3-CA1 place representation). However, to maintain this allothetic-idiothetic coupling coherent over time, the path integrator must be prevented from accumulating errors. In order to do that, the animat adopted an **exploration strategy consisting of looped excursions** (i.e., outward and

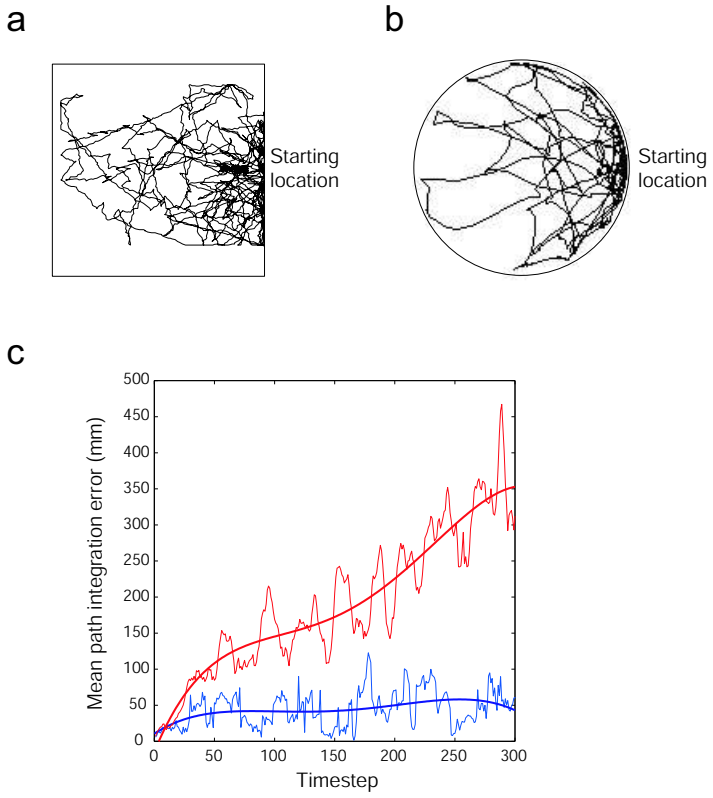

Figure 3.6: Exploratory behaviour and path integration (PI) calibration. **(a)** To establish a coherent allothetic-idiothetic coupling, the robot started exploring a novel environment (in this example a square arena) by means of looped excursions centred at the starting location. **(b)** Example of rat's behaviour at the beginning of exploration in a novel circular environment (data issued from a collaboration with C. Brandner, Inst. of Psychology, Univ. of Lausanne, Switzerland). **(c)** Uncalibrated (red curves) and calibrated (blue curves) mean PI error (thin lines are raw data, whereas thick lines are polynomial fittings). The red curves show that this mean PI error tended to grow over time. By contrast, if the system used the vision-based place representation to calibrate the PI occasionally, this error remained bounded over time (blue curves). (Taken from Arleo and Rondi-Reig 2005)

homing journeys) **centred at the starting location** (Fig. 3.6a). During an outward excursion the system acquired new spatial knowledge and updated its space code. After a while, it started following its homing vector and as soon as it arrived and recognised a previously visited location (not necessarily the starting location), it utilised the vision-based representation to realign the path integrator. Once vision had calibrated the path integrator, a new outward excursion was initiated. By iterating this procedure the robot could keep the dead-reckoning error bounded (Fig. 3.6c), and propagate exploration over the entire environment (the probability of calibrating the path integrator at locations other than the starting region increased over time). Behavioural findings concerning the locomotion of rodents exploring novel environments (Drai et al. 2001) (also Brandner and Arleo, unpublished results) show a typical exploratory pattern consisting of looped excursions centred at their home base (Fig. 3.6b). **The model postulated that maintaining the idiothetic and allothetic signals mutually consistent might**

be one of the factors determining such a loop-based exploratory behaviour of animals.

3.2.2 Importance of landmark stability

The LTP-LTD Hebbian learning used to couple external and internal representations made stable visual configurations more likely to be correlated to self-motion signals than unstable ones (Fig. 3.7a). As a consequence, only those visual configurations that were taken as stable by the animat could influence the dynamics of the space coding process. Stable landmarks could polarise the allocentric representation across different entries in an environment. This polarisation helped the system to realign the allothetic and idiothetic components of its directional and spatial code and, then, to reactivate a previously learned description of a familiar environment. Failure of such a reactivation process might result in creating a new superfluous representation (Knierim et al. 1998).

In a series of robot experiments (Arleo and Gerstner 2001) the constellation of visual cues was kept stable during spatial learning. Then, the path integrator was reinitialised randomly (simulating a disorientation procedure) and the robot was placed back in the familiar environment. Since the system learned a stable coupling between the idiothetic and allothetic signals, the robot could use the visual information to anchor its allocentric spatial representation, reset its path integrator, and reactivate the previously learned place map (Fig. 3.7b, top row). In a second series of experiments, the constellation of visual cues underwent arbitrary rotations during spatial learning. Thus, the Hebbian learning scheme failed to establish stable correlations between idiothetic and allothetic inputs. As a consequence, when the robot was disoriented and placed back in the explored environment, it was unable to reactivate the learned spatial representation properly and intersession remapping occurred (i.e., HP cell response patterns varied across subsequent visits of the same environment, (Fig. 3.7b, bottom row). These results are in agreement with those reported by Knierim et al. (1995a) who recorded HP cells and HD cells from freely moving rats.

Finally, notice that because the realigning procedure relied on the allothetic-idiothetic coupling established by the robot via Hebbian learning, impairing this latter mechanism would also lead to unstable intersession representations (i.e., remapping). This result is consistent with experimental findings showing that animals with impaired hippocampal LTP exhibit stable place cell firing patterns within sessions, but unstable mapping between separate runs (Barnes et al. 1997).

3.2.3 Conflict situations

In the above experiments the animat used external visual fixes to recalibrate an otherwise untrustworthy path integrator (e.g., after disorientation or because of cumulative integration error). Here we consider the situation in which stable allothetic inputs and reliable idiothetic signals provide conflicting spatial information. **In the model, the rel-**

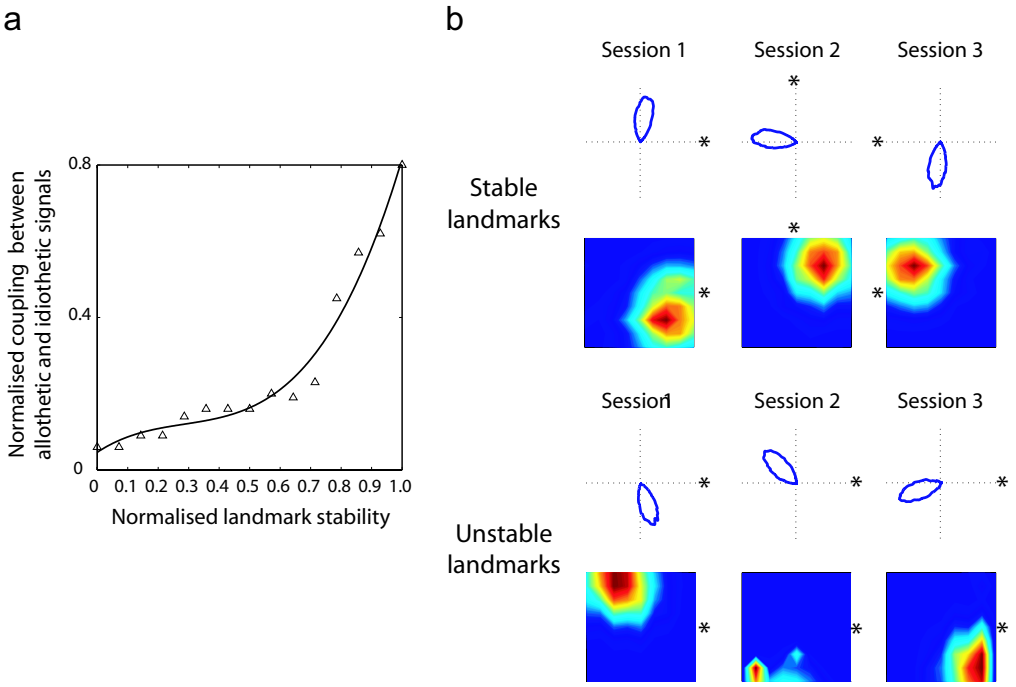

Figure 3.7: Interaction between visual and self-motion signals. **(a)** Due to Hebbian learning, the larger the stability of a visual cue configuration, the strongest its coupling with the path integration-based representation (triangles are sampled data, the curve is a polynomial fitting). **(b)** Intersession responses of one formal HD cell and one HP cell after spatial learning. At the beginning of each probe session the robot was disoriented. Top: Visual cue configurations that remained stable during spatial learning were able to polarize HD and HP firing at the beginning of each probe session. The cells reoriented their receptive fields according to the 90° visual cue rotations (the asterisk indicates the centroid of the visual cue configuration). Bottom: Unstable visual cues did not allow the disoriented robot to reactivate coherent representations across sessions and remapping might occur. (Adapted from Arleo and Gerstner 2005 and Arleo and Rondi-Reig 2005)

ative importance of coupled external and internal spatial cues was a function of: *(i)* **the degree of confidence of the robot about its self-motion signals; and** *(ii)* **the degree of discrepancy between allothetic and idiothetic spatial information**. A series of tests was run inspired by the behavioural experiments by Etienne et al. (1990), who studied the homing behaviour of hamsters in perceptual conflict situations (see Chapter 2, Sec. 2.1 for a discussion of these experiments). First, we let the animat learn the coupling between a stable visual configuration and its path integrator. Then, during testing, we created both a $90°$ and a $180°$ conflict between external and internal cues and examined the homing behaviour of the robot. Results in Fig. 3.8a (top row) show that when a $90°$ conflict occurred the visual component tended to influence the robot's homing trajectory more than self-motion signals. By contrast, for $180°$ conflicts (Fig. 3.8a, bottom row) the system's response was twofold: if the robot had not been disoriented, then its homing behaviour was mainly determined by self-motion signals (bottom row, central plot); on the other hand, if the robot had been disoriented, then it relied on allothetic spatial information even for large discrepancies (i.e., $180°$) between

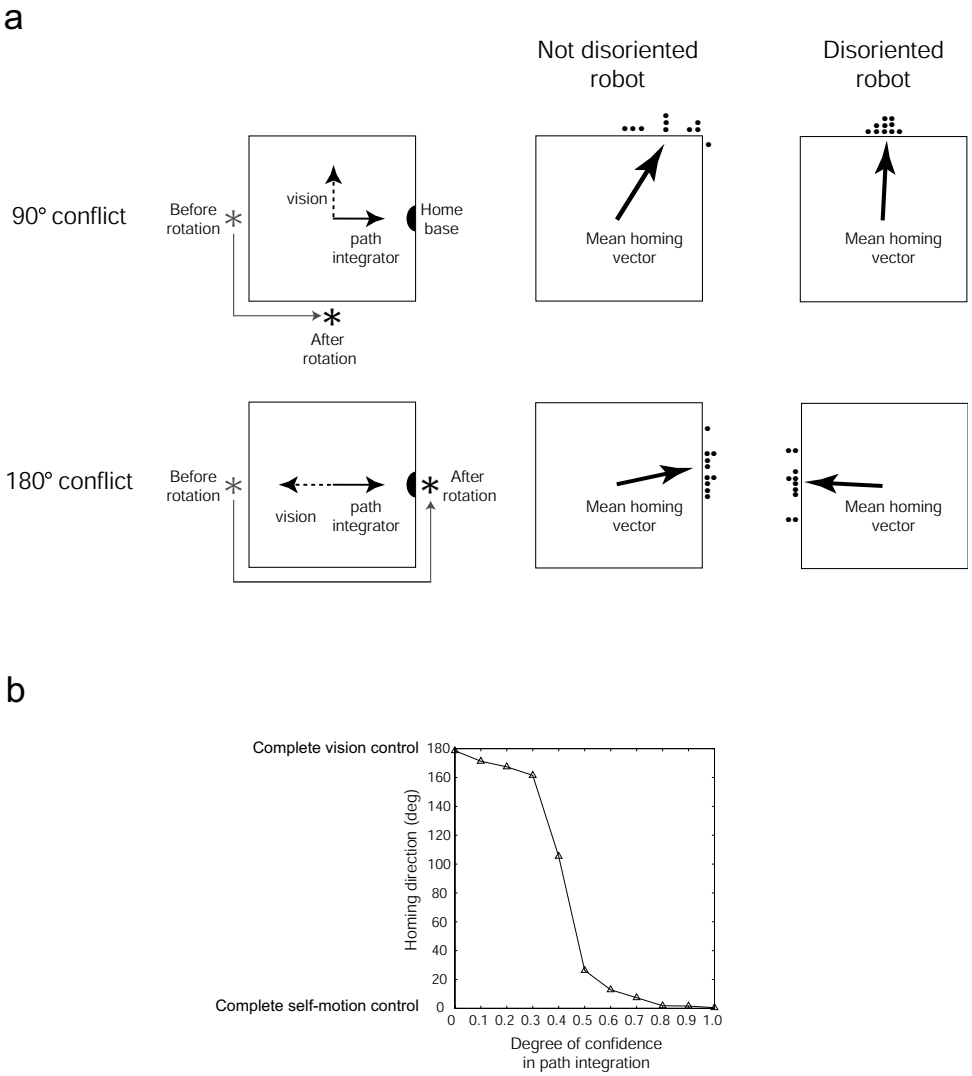

Figure 3.8: Conflict situations between vision and path integration. **(a)** During spatial learning the visual cue configuration was maintained stable. The protocol for the probe trials includes: *(i)* An outward journey during which the robot moved directly from its home base to the centre of environment in the dark. *(ii)* A 'hoarding' phase during which the robot actively rotated on the spot for a random amount of time (both the amplitude and the sign of the rotation were selected randomly). During hoarding, the visual cue configuration was rotated by either 90° or 180° and the light was switched on. *(iii)* A backward journey during which the robot must compute the homing vector to return home. A conflict occurred between vision and path integration (dashed and continuous arrows, respectively, in the first column). The thick arrows in the second and third columns indicate the resulting mean homing behavior of the robot averaged over ten trials (black dots). In the case of nondisoriented robot (second column), the familiar visual cues tended to influence the robot's behaviour when a 90° conflict occurred. By contrast, the visual control vanished when the conflict was further increased (i.e., 180°). If the robot was disoriented during the hoarding phase (third column), visual cues predominated for both 90° and 180° conflicts. **(b)** The response of the robot to a 180° conflict depended on its confidence about the path integrator. (Taken from Arleo and Rondi-Reig 2005)

allothetic and idiothetic cues (bottom row, right plot). Finally, Fig. 3.8b shows the average response of the robot to a 180° conflict situation as a function of the degree of confidence about its path integrator. The diagram indicates that as long as self-motion information was given confidence above chance, the animat tended to use it to perform homing behaviour. If the confidence went below chance, then a priority switch occurred and visual information became predominant.

3.3 Action learning: goal-oriented navigation

The above spatial learning model enabled the animat to self-localise based upon the ensemble firing of a population of HP cells. But, how can the place field representation support goal-oriented navigation? In the model, HP cells drove a downstream population of extra-hippocampal action cells whose ensemble activity mediated allocentric motor commands and guided navigation (Fig. 3.1) (Arleo and Gerstner 2000a; Arleo et al. 2001; Arleo et al. 2004).

The navigation problem, then, was: **how can the system establish a mapping function $\mathrm{M} : \mathbf{P} \rightarrow \mathbf{A}$ from the place cell activity space P to the action space A?** A reinforcement learning scheme (Sutton 1988; Sutton and Barto 1998) was employed to acquire this mapping function based on the animat's experience. The system interacted with the environment and **reward-dependent stimuli elicited the synaptic changes of the connections from place units to action units in order to learn the appropriate action-selection policy**. After training, the system could relate any physical location to the most suitable local action to navigate toward the goal while avoiding obstacles. This resulted in an ensemble pattern of activity of the action units that provided a navigational map to support goal-directed behaviour. Notice that because the CA3-CA1 space coding solved the problem of ambiguous inputs or partially hidden states, the current state was fully known to the system and reinforcement learning could be applied in a straightforward manner.

Action learning consisted of a sequence of training paths starting at random positions and ending either when the animat reached the rewarding location or after a timeout. At the beginning of each trial, the navigator determined its starting location and orientation based upon its HP and HD representations, respectively. Then, it started searching for the goal while improving its action-selection policy. Temporal difference (TD) reinforcement learning (Sutton 1988; Dayan and Sejnowski 1994; Sutton and Barto 1998) was applied to allow the system to learn to predict the outcome of its actions with respect to a given target. A prediction error was used to estimate the difference between the expected and the actual future reward when, at a given location, the animat took a chosen action. Training enabled the system to minimise this error locally. The convergence condition was that, given any state-action pair, the deviation between the predicted and the actual reward tended to zero.

Goal-learning performance was measured in terms of: (i) the mean search latency, i.e. the mean time needed by the robot to find the target, over training trials; (ii) the generalisation capabilities of the system, i.e. the ability to initiate

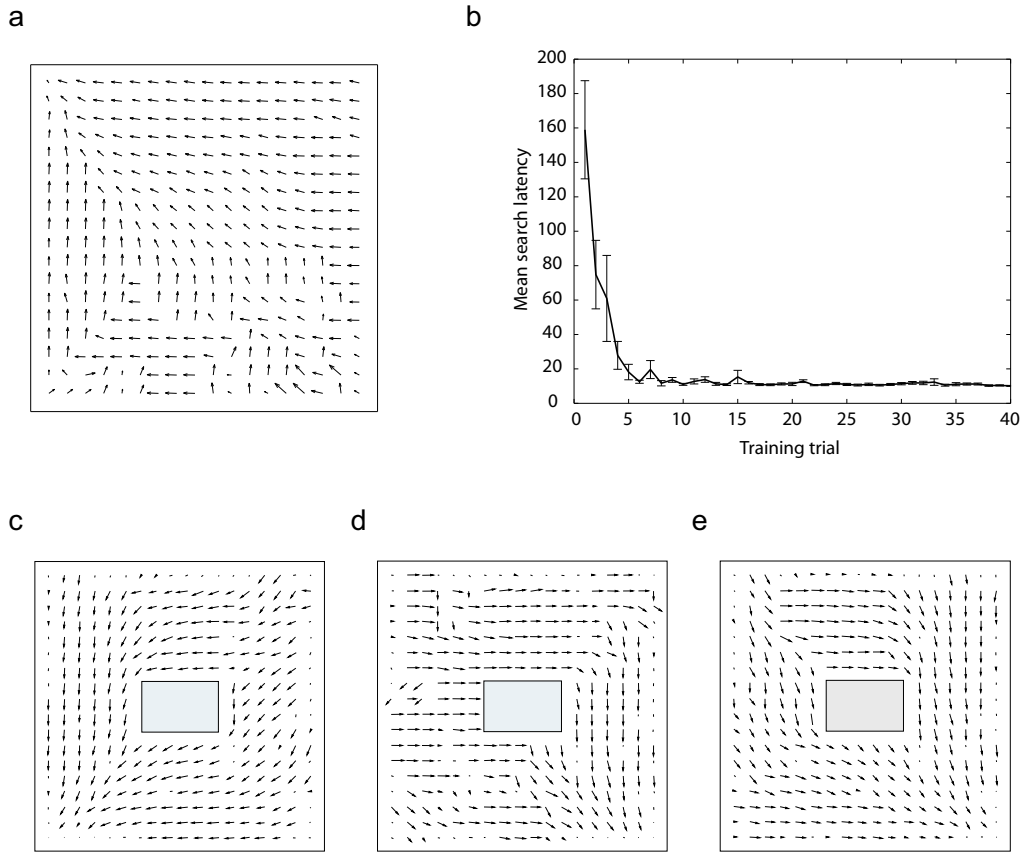

Figure 3.9: Learning navigation maps. **(a)** Vector field representation of a navigation map learned by the robot after only training trials. The target location is near the upper left corner of the environment. Arrows represents the local motion directions encoded by the ensemble action cell activity after learning. **(b)** Mean search latency as a function of training trials. The reward-based learning algorithm converges after approximately ten trials. **(c)** Navigation task in the presence of one obstacle (gray object) and two distinct targets, G_1 nearby the bottom left corner and G_2 nearby the bottom right corner. The vector field was learned by the robot after thirty trials when searching for G_1. **(d)** Partial navigation map for G_2 learned by the robot when focusing on G_1. **(e)** Final navigation map learned by the robot after ten trials when searching for G_2. (Taken from Arleo and Gerstner 2005)

goal-directed actions at locations never experienced during training. Fig. 3.9a shows a navigation map learned by the robot when the rewarding location was in proximity of the upper left corner of a square environment. The map was acquired after only five training trials and enabled the robot to navigate toward the goal from any position in the environment. The vector field representation was obtained by rastering uniformly over the environment and computing, for each sampled position, the local action (arrow) encoded by the ensemble action cell activity. Many sampled locations were not visited by the animat during training, that is, the navigator was able to associate appropriate goal-oriented actions to never experienced spatial positions. The mean amount of generalisation, defined as the percentage of sampled positions that were not visited by the animat during training, is of about 45% for the map of Fig. 3.9a. This large

generalisation property was mainly a consequence of the coarse coding state representation provided by the CA3-CA1 place cells of the model. Fig. 3.9b shows the mean search latencies as a function of training trials. The search latencies decreased rather rapidly and reached the asymptotic value (corresponding to appropriate goal-directed behaviour) after approximately ten trials. This convergence time is comparable to that of rats solving the reference memory task in the Morris water maze (Steele and Morris 1999; Foster et al. 2000).

Fig. 3.9c shows the navigation vector fields learned by the robot in the presence of one obstacle and two distinct types of rewarding locations, G_1 (simulating for instance a feeder position located at the bottom left corner of the arena) and G_2 (simulating for instance the location of a water reservoir at the bottom right corner). First, the robot was trained to navigate toward G_1. Fig. 3.9c represents the navigation map for G_1 learned by the robot after thirty training trials. While optimising the navigation policy for G_1, the robot might encounter the rewarding location G_2 and start learning a partial navigation map for it, even if G_2 was not its current primary target. Fig. 3.9d shows the knowledge about G_2 acquired by the robot while searching for G_1. Thus, when G_2 became the primary target, the robot did not start from zero knowledge and needed a short training period to learn an optimal policy to navigate toward it. Fig. 3.9e displays the navigation map acquired by the robot after ten training trials when searching for G_2.

Similar to the previous hypothesis by Brown and Sharp (1995), the model postulated that **the anatomical interaction between the hippocampus and the ventral striatum**, and in particular the fornix projection from the CA1 region to the nucleus accumbens, **might be a part of the system where the reward-dependent action learning would take place**. The nucleus accumbens seems involved in processing information concerning goal-oriented behaviour (Tabuchi et al. 2000). Ventral striatal neurons receive space coding information from the hippocampal formation and are activated in relation to the expectation of rewards (Schultz et al. 1997). The presence of **dopamine-dependent plasticity in the striatum suggests that dopamine responses might be involved in synaptic adaptation yielding reward-based learning**. In particular, dopamine neurons in the mammalian midbrain seem to encode the difference between expected and actual occurrence of reward stimuli (Schultz et al. 1997). Thus, the temporal difference error used in the model to update the synaptic weights from CA3-CA1 cells to action cells may be thought of as a dopamine-like teaching signal.

Chapter 4

Head Direction Cells: Electrophysiological Recordings and Theoretical Modelling

Preface. *During my stay at the Laboratoire de Physiologie de la Perception et de l'Action (CNRS-Collège de France, Paris, post-doctoral fellowship 2001-2003, associate researcher 2003-2004), I had the opportunity to undertake a training on neurophysiology and extra-cellular recordings from freely-moving rats. With the team directed by S. I. Wiener, we focused on the discharge properties of anterodorsal thalamic head direction (HD) cells. The experiments mainly investigated the interrelation between visual and inertial (e.g., vestibular) cues controlling HD cell responses. New insights were provided about* (i) *the update of the HD representation following reorientation of static landmarks (Zugaro et al. 2003);* (ii) *the role of dynamic visual information (e.g., optic field flow) in controlling HD cell activity (Zugaro & Arleo et al. 2004; Arleo et al. 2004; Arleo et al. 2006);* (iii) *the relationship between the discharge of HD neurons and the theta EEG signal (Arleo et al. 2005; Arleo & Battaglia et al. 2005).*

In parallel to cell recordings, I could also accomplish theoretical studies by supervising undergraduate students and thanks to a collaboration (ACI Neurosciences Intégrative et Computationnelles, 2001-2004) with N. Brunel (Lab. of Neurophysics and Physiology of the Motor System, Univ. Paris 5). The objective of this theoretical work was to reproduce our experimental data about the interaction between vestibular and visual signals, and to put forth new hypotheses about the mechanisms underlying the HD cell properties. We studied the dynamics of a population of HD cells by means of both analytical and numerical approaches, and we focused on the generation and maintenance of their ensemble activity based upon a distributed continuous attractor network without recurrent excitation (Boucheny et al. 2005).

This chapter reviews our main experimental findings about HD cell activity, and it also outlines the theoretical HD cell model and its principal results/predictions. The reader is referred to the Appendix C for reprints of Zugaro et al. (2003), Zugaro & Arleo et al. (2004), and Boucheny et al. (2005). (Notice that the articles Arleo & Battaglia et al. 2005, and Arleo et al. 2006 could not be included because still under submission procedure.)

4.1 Experimental work on head direction cells

As discussed in Chapter 2, head direction (HD) neurons fire selectively as a function of the allocentric orientation of the head of the animal in the azimuthal plane (Ranck 1984; Taube 1998; Wiener and Taube 2005). Therefore, the HD cell system is likely to constitute a physiological basis for the animals' sense of direction. HD neurons can be found in a network of interconnected brain structures which are anatomo-functionally coupled to the hippocampal place cell network (Knierim et al. 1998). HD cells were first electrophysiologically recorded in the rat postsubiculum (PoSC) (Ranck 1984; Taube et al. 1990a), and then found in numerous other structures including the laterodorsal thalamic nucleus (Mizumori and Williams 1993), the dorsal striatum (Wiener 1993), the retrosplenial cortex (Chen et al. 1994), the anterodorsal thalamic nucleus (ADN) (Taube 1995; Blair and Sharp 1995), the lateral mammillary nucleus (LMN) (Stackman and Taube 1998), and the dorsal tegmental nucleus (DTN) (Sharp et al. 2001).

Each HD cell is selective for one specific 'preferred' direction, regardless of the animal's ongoing behaviour and position. The response curve of a HD cell can be approximated by means of a Gaussian tuning profile. The preferred directions of a population of HD cells tend to be evenly distributed over 360° such that the HD cell system may work as an allocentric neural compass. Fig. 4.1a shows the tuning curves of four HD cells we recorded simultaneously from the ADN of a freely-moving rat.

The intrinsic dynamics of the HD cell system seems to rely upon the integration of self-motion inertial signals (e.g., vestibular information) (Taube 1998; Wiener and Taube 2005). During head turns (both in light and in darkness conditions) the ensemble activity profile, determined by the sub-population of HD cells active at a particular time, varies according to the instantaneous head angular velocity. Thus, the HD cell system seems to have the additional property of integration of head velocity signals and provides an ongoing memory trace of the direction of the head.

Anatomical, electrophysiological, and lesion data suggest that **LMN and DTN might constitute an essential sub-circuit of the HD cell system for generating and maintaining the HD signal** (Blair et al. 1998; Bassett and Taube 2001b; Taube and Bassett 2003). This would yield the following ascending processing scheme: DTN $\rightarrow$ LMN $\rightarrow$ ADN $\rightarrow$ PoSC. Lesions to DTN disrupt the directional selectivity in ADN (Bassett and Taube 2001a). Bilateral lesions of LMN abolish the HD signal in ADN (Blair et al. 1998). The directional selectivity of PoSC cells is seriously impaired when lesioning ADN (Goodridge and Taube 1997), but lesions of the PoSC leave the signal in ADN largely intact (Goodridge and Taube 1997). A further evidence for the above processing pathway is provided by a series of studies that have investigated the temporal properties of HD cells in LMN, ADN, and PoSC. During head turns, LMN neurons tend to anticipate the future head direction by approximately $40 - 75\,ms$ (Stackman and Taube 1998; Blair et al. 1998), ADN cells show a smaller anticipatory time delay of about $25\,ms$ (Taube and Muller 1998; Cho and Sharp 2001), and PoSC cells tend to encode the current directional heading (Blair and Sharp 1995). The DTN-LMN circuit seems also well suited to account for the additional property of the HD cell system of integrating the head angular velocity. The DTN receives ascending inputs from the

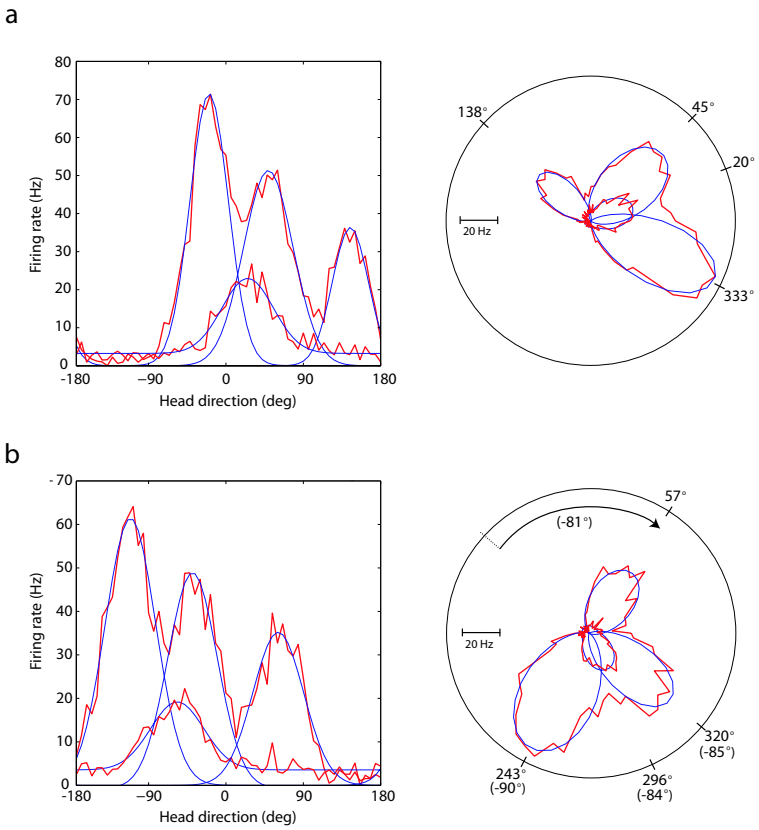

Figure 4.1: **(a)** Tuning curves of four simultaneously recorded ADN HD cells (left column: cartesian representation of the discharge frequency as a function of head direction; right column: polar representation). Three cells were recorded on the same electrode while the fourth (with the lowest peak firing rate) was recorded from another electrode. The red jagged traces are the actual firing rate histograms. The blue lines are Gaussian best-fit approximations of the individual response curves. **(b)** The response curves of the same four cells after a 90° clockwise rotation of a visual landmark. The four preferred directions shifted coherently ($-81°$, $-85°$, $-84°$, and $-90°$) such that, after rotation, their mutual angular deviations remained almost unchanged). This was consistent with all previous literature indicating that the preferred directions of the HD cells always shift coherently, and thus that the shift in preferred direction for one cell is indicative of the shifts for all other cells in the network. (Data Arleo and Wiener).

medial vestibular nucleus, directly and indirectly via the nucleus prepositus hypoglossi (Liu et al. 1984; Bassett and Taube 2001b), and both DTN and LMN contain neurons whose activity is correlated with the angular velocity of the head in the horizontal plane (Bassett and Taube 2001b).

Although the generation of the direction selective activity of **HD neurons** seems to depend upon idiothetic signals, their responses can be influenced by various multisensory signals and they are primarily **anchored on stable visual cues of the environment** (e.g., Blair and Sharp 1996; Stackman and Taube 1997; Goodridge et al. 1998; Zugaro et al. 2001; Zugaro et al. 2001; Zugaro & Arleo et al. 2004; or see Wiener and Taube 2005 for a review). Fig. 4.1b shows the control exerted by a salient visual cue upon the preferred directions of the four HD cells recorded simultaneously. Notice

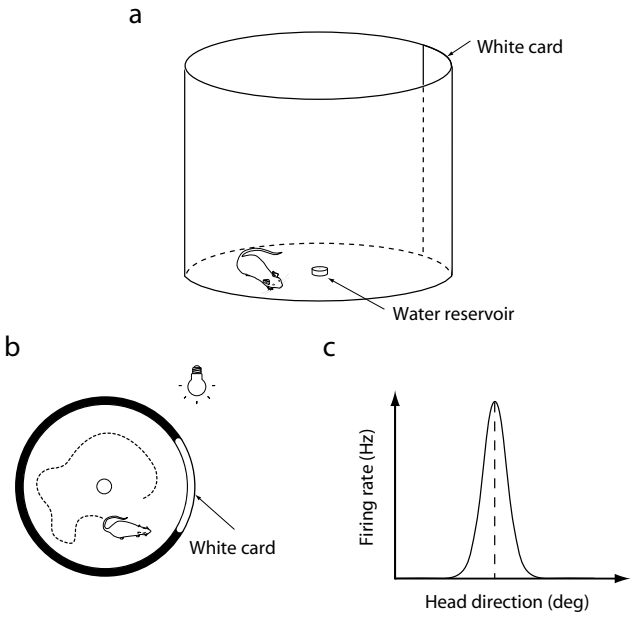

Figure 4.2: **(a)**The experimental apparatus was a circular platform, enclosed by a black cylinder. A large white card attached to the inner wall served as the principal visual cue. A reservoir at the center of the arena permitted to deliver drops of water at specific time intervals. **(b)**In the first stage of the experiment, the rat freely explored the platform. **(c)**A directional response curve was constructed by associating neuronal discharges with smoothed corrected head position samples and then fitting the data with a Gaussian function.

how the four responses are updated coherently to changes of the orientation of the environmental cues. That is, the **preferred directions of a population of HD cells tend to rotate rigidly as a whole** (such that the mutual deviations between preferred directions remain unchanged, Taube 1998; Wiener and Taube 2005).

4.1.1 How rapidly are the HD cell responses updated after rotation of visual landmarks?

Although this issue was already addressed by previous studies (Knierim et al. 1998; Zugaro et al. 2000), the employed experimental protocols could not measure updates occurring faster than $15\,s$, in contrast with theoretical results predicting update latencies of few hundred ms (Zhang 1996; Redish 1999). The experiment outlined in this section was performed to test this prediction (see the reprint of Zugaro et al. 2003 in Appendix C for further details).

We employed the classical experimental setup depicted in Fig. 4.2 and we adopted the experimental protocol described in Fig. 4.3. The main result of this study was the following:

- a **mean latency of** $80 \pm 10\,\mathrm{ms}$ (Fig. 4.4, left column) was observed **for a HD cell to go from baseline to peak firing activity** (i.e., for the establishment of a new

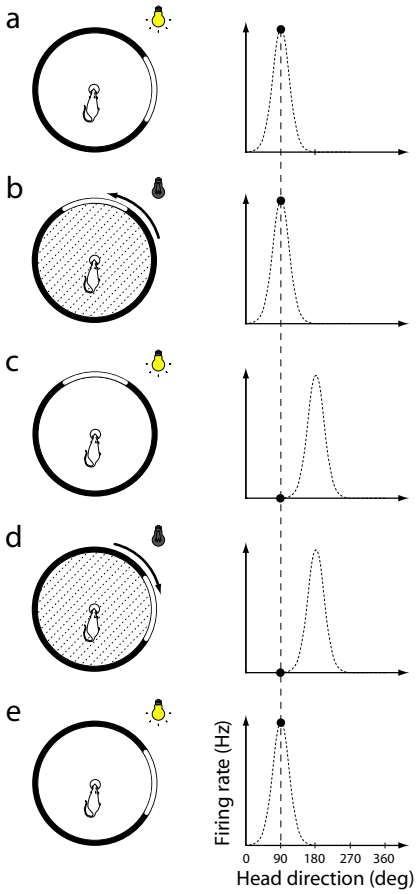

(a) Once the preferred direction of the recorded HD cell had been determined, water drops were delivered to the small reservoir at the centre of the cylinder to keep the lightly water-deprived rats immobile with its head oriented in the preferred direction while drinking. The rat had previously been trained to remain immobile at the water spout with a behavioural shaping procedure: water delivery was triggered only when the rat was positioned at the reservoir at the appropriate orientation, and water was ceased as soon as it moved away from the preferred direction. The solenoid valve that released the water made a distinct clicking sound that likely served as a cue. Notice that it was important to not apply any physical restraint, which is known to depress directional responses (Taube 1995). **(b)** The light was turned off, and the card is rotated by 90° along the cylinder wall. **(c)** The light was turned back on. This triggered a shift in the directional response curve of the neuron since this activity was anchored to visual cues (right panel). Accordingly there should be a marked decrease in firing rate. **(d)** The light was turned off again, and the card was returned to the standard position. **(e)** The light was turned back on. The preferred direction shifted back to its initial orientation. This corresponded to a marked increase in discharge frequency. Steps (b) through (e) were repeated until the rat was satiated and no longer remained immobile at the center. Notice that because the rat remained immobile oriented in the (previously determined) preferred direction while drinking water from the reservoir, full response curves could not be sampled. Rather, only the cell responses corresponding to this particular head direction could be recorded (black circles in the diagrams).

Figure 4.3: Experimental procedure (see right column). (Taken from Zugaro et al. 2003)

bump following the reorientation event);

- on the other hand, we found that the cessation of activity after the cue card was shifted away from its original orientation (i.e., extinction of the bump existing prior the reorientation event) occurred at a slower rate: the **return to baseline occurred only after** $\mathbf{140 \pm 10\,ms}$ (Fig. 4.4, right column).

A possible (theoretical) explanation for the longer latency observed when the firing rates returned to baseline might be that recurrent inhibition triggering this decrease in firing rates would occur after the increase in overall activity within the HD cell network (see Sec. 4.2 about attractor network models of HD cells).

These results showed that, in ADN HD cells, preferred direction updates benefit from very rapid processing of visual signals. The very short latencies observed are consistent with the fact that ADN receives direct projections from the retina (Itaya et al. 1981; Ahmed et al. 1996) as well as indirect projections from the visual cortex via the postsubiculum (Vogt and Miller 1983) and the retrosplenial cortex (Reep et al. 1994), and that visual stimulation of the retina evokes field potentials in the primary visual cortex with delays as brief as $30 - 40\,ms$ (Galambos et al. 2000).

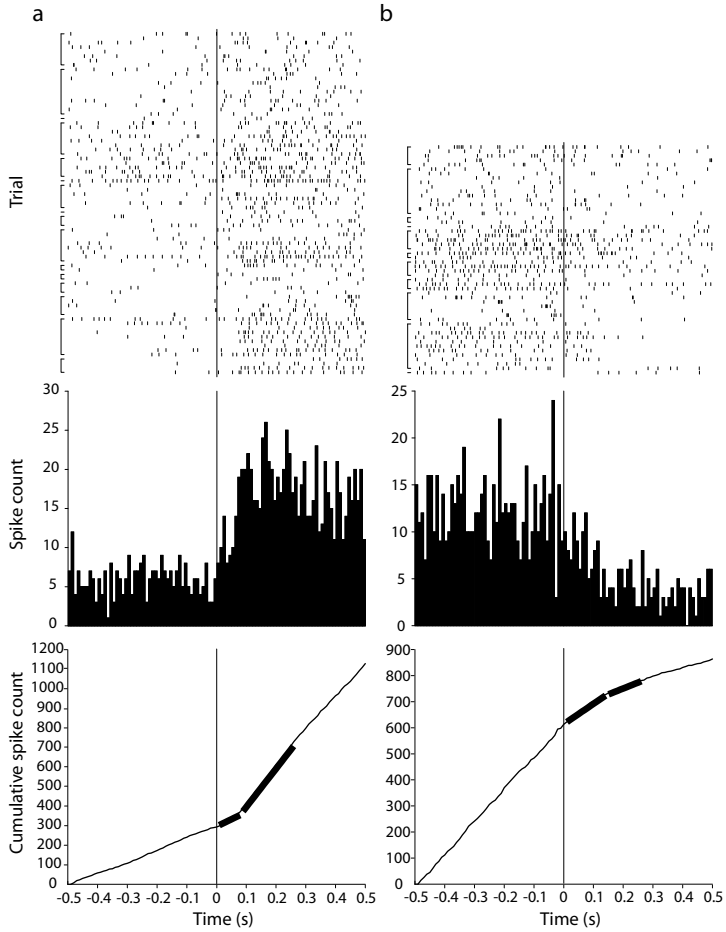

Figure 4.4: Latency of preferred direction updates in HDcells. Raster plots (above), peri-event histograms (middle) and cumulative histograms (below) (binwidth = $10\,ms$) of action potentials. Time zero indicates when the lights were turned on again. After light onset, the preferred directions returned to their initial orientations **(a)**, or shifted to the rotated (non-preferred) orientations **(b)**. To determine the average latency of the preferred direction update, least squares estimates were computed from the cumulative histograms using the first $250\,ms$ of data after light onset (thick curves). Transition points were at $80\pm10\,ms$for returns to the preferred orientation **(a)** and $140\pm10\,ms$for shifts to the non-preferred orientation **(b)**. Brackets indicate trials from the same cell within a given session; the variations in spike density among the rows of rasters reflects differences in peak and background firing rates among the neurons. (Taken from Zugaro et al. 2003)

4.1.2 Head direction cells depend upon dynamic visual signals to select anchoring landmark cues

Cressant et al. (1997) showed that background cues tend to prevail over foreground cues in controlling hippocampal place cell responses. Likewise, Zugaro et al. (2001) showed that **HD cells tend to be anchored to visual landmarks only when these are in the background**. There is a clear adaptive advantage to selecting background cues because they provide more stable (and then reliable) spatial information as the

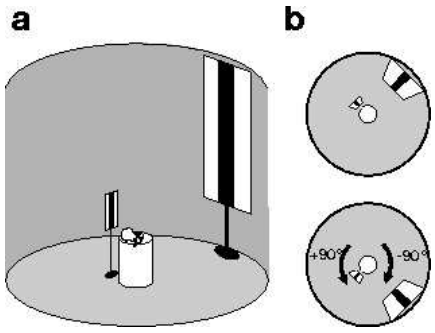

Figure 4.5: Experimental protocol. **(a)** The rats freely foraged for food pellets on an elevated small platform (diameter $22\,cm$) located at the center of a cylindrical black curtain (diameter $3\,m$). A foreground card (height $60\,cm$, distance $36\,cm$) and a background card (height $240\,cm$, distance $144\,cm$), bearing two vertical white stripes, served as principal orienting cues. The cards' respective sizes and distances to the platform center were proportioned so that they occupied the same visual angles. They were separated by $90°$. **(b)** After an initial recording (top panel), the animal was removed from the platform, and the two cards were rotated in opposite directions (bottom panel). The rat was then disoriented in complete darkness and returned to the platform as the light was turned back on, and a second recording began. Recording sessions including baseline and double cue rotations were conducted in continuous or stroboscopic light (flashes at $1.5\,Hz$). (Taken from Zugaro & Arleo et al. 2004)

animal moves about. **But how do HD cells discriminate between foreground and background cues?**

The psychophysical literature shows that relative depth in the visual field can be detected on the basis of several different stimulus attributes, including accommodation, occlusion (objects blocked by others are more distant), texture contrast, shadows, vergence and mechanisms like dynamic motion parallax (during displacements more distant objects appear to move less rapidly). Known brain systems specialised for detecting optic field flow could automatically confer the latter sensitivity on the HD system; for example, the optokinetic system is more sensitive to optic flow at low, rather than high, velocities (Hess et al., 1989). The experiment presented here was designed to test the **working hypothesis that ADN HD cells might distinguish anchoring background cues on the basis of dynamic visual processes** like motion parallax detection (see reprint of Zugaro & Arleo et al. 2004 for details).

Fig. 4.5 shows the experimental setup/protocol. A large card was placed in the background, and a small card was placed in the foreground, near the small central platform. The cards where identically marked, proportionally dimensioned and subtended identical visual angles from the central viewpoint. The rat was then disoriented in darkness and the cards were rotated by $90°$ in opposite directions about the centre, and the rat was returned. This rotation aimed at providing conflicting orienting cues: after this rotation the cards were again separated by $90°$ but inverted in their left-right relation. This procedure was first carried out under continuous lighting to permit normal visual processing. To test whether the selection of anchoring cues depended upon dynamic visual cues (such as motion parallax), we then repeated these experiments under stroboscopic light (flashes at 1.5 Hz).

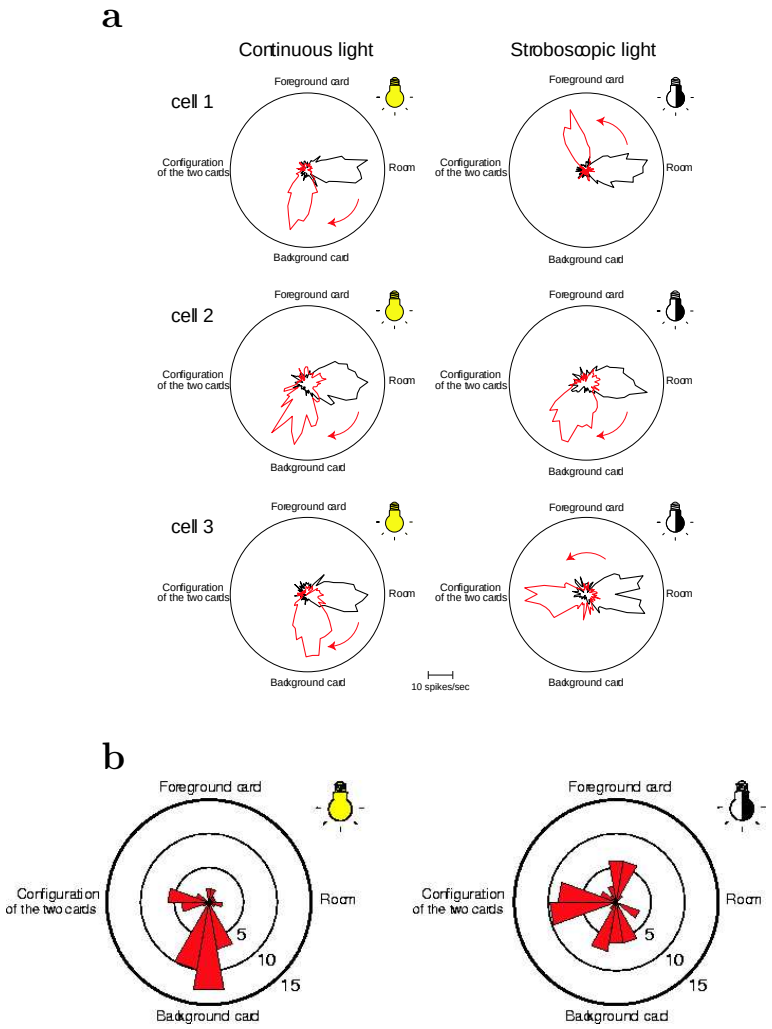

Figure 4.6: **(a)** Examples of shifts in preferred directions after card rotations under normal (left) and stroboscopic (rigth) lighting. The response curves were sampled during the recording preceding (black curves) and following (red curves) the rotation of the background card by $-90°$ and the foreground card by $+90°$ around the platform. The initial directional response curves were all oriented to point to the right (3 o'clock position) to facilitate comparisons. (Left column) Under continuous light conditions, the preferred directions of the HD cells shifted by approximately $-90°$, following the card in the background. (Right column) Under stroboscopic light conditions, the preferred directions of the HD cells could shifted $+90°$, following the foreground card (cell 1, in row 1), or $-90°$, following the background card (cell 2 in row 2), or shifted by 180°, following the barycentre of the two cards (cell 3 in row 3). The labels 'Foreground card', 'Background card' and 'Both cards' show the predicted angle of rotation of the preferred direction if the respective cues had dominantly influenced the anchoring of the preferred direction. Data have been rectified to compensate for the fact that background and foreground cards were rotated in different directions among sessions. **(b)** Circular histograms (bin size: 20°) representing the whole data set. The number of sessions corresponding to the respective shifts in preferred direction is indicated by the radius of the concentric circles that serve as calibration bars. The preferred directions after cue rotations are presented according to the same formalism as in (a) to facilitate comparisons. (Taken from Zugaro & Arleo et al. 2004)

As shown by the examples in Fig. 4.6a (left column), in the majority of the recording experiments the preferred directions of the HD cells stayed anchored to the background card after card rotations when recorded in continuous light. By contrast, Fig. 4.6a (right column) shows that the response curves of HD cells before and after rotation of the cards under stroboscopic lighting were equally likely to follow the background card, the foreground card or the configuration of both. The distributions of responses in the continuous and stroboscopic lighting condition (shown in Fig. 4.6b) were compared and proved to be significantly different.

Thus, the principal result of this study was that stroboscopic lighting at a frequency disturbing certain dynamic visual processes interfered with the preferential anchoring of HD responses by background cues. Thus, **dynamic visual signals are likely to play a critical role in selection of anchoring cues by HD cells**. Such inputs could include dynamic motion parallax-related signals. These would permit background visual cues to be discriminated from those in the foreground during head translation movements as more distant objects appear to move at lower velocities.

4.1.3 Optic field flow signals update the activity of head direction cells

We continued our investigations about the influence of dynamic visual information upon HD cell firing and we formulated the following **working hypothesis: can optic field flow information update the directional coding of HD neurons?**

Normally as a subject moves about, turning the head in one direction produces an opposite optic field flow of the visual image. Hence rotations of the visual scene convey information about rotations of the head in space. To **test our working hypothesis we designed an experiment to alter optic field flow signals relative to head rotations** (Arleo et al. 2004). All details about this experiment will be in the manuscript Arleo et al. 2006 which is about to be submitted (therefore it was not included in Appendix C). This section presents the basic protocol procedure and some preliminary results.

Fig. 4.7a shows the experimental setup. The animal was placed on a wall-less circular platform surrounded by a large cylindrical black curtain. A planetarium-like projector presented a field of points evenly distributed on the otherwise dark curtain.

One of the control procedures consisted of (i) switching off the planetarium, (ii) rotating it by 90° in the darkness, and then (iii) switching it back on. We did not observe any significant update of the preferred directions, meaning that the **uniformly distributed light points did not provided any salient static cue**.

In the basic protocol of Fig. 4.7b the preferred direction of the recorded neuron was first recorded during $5\,min$ with the planetarium still. Then, the latter was rotated at a constant velocity ($5\,^\circ/s$) for about $120\ s$, while directional firing was still recorded. Finally, baseline recordings were again made with the dot array stationary during $4\,min$. As shown in the example of Fig. 4.7c (top row), the point array provided sufficient information for stable HD responses when the planetarium was immobile.

Fig. 4.7c (central row) shows an example of preferred direction update during the

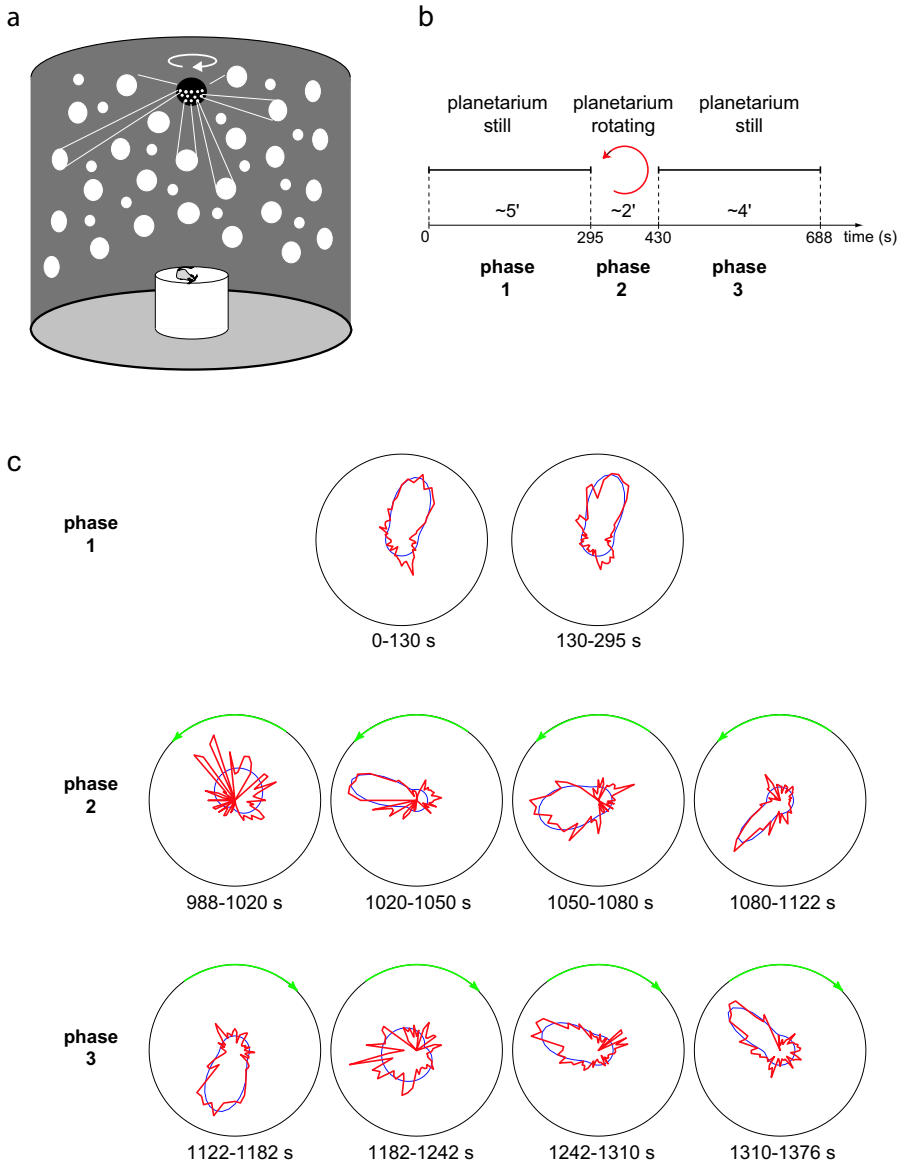

Figure 4.7: **(a)** The experimental setup. The animal moved on a wall-less circular platform (diameter $75\,cm$) placed at the center of a cylindrical black curtain (diameter $3\,m$). A planetarium projected spotlights on the dark curtain. **(b)** In the simplest protocol, the directional response of the HD cell was first recorded during $5\,min$ with the planetarium immobile. Second, the planetarium was made rotating at a constant velocity ($5\,^{\circ}/s$) for about $120\,s$. Third, the planetarium was stopped and the cell recorded for $4\,min$. **(c)** When the planetarium remained still (phase 1, top row) the preferred directions of the HD cells tended to remain stable. During planetarium rotation (phase 2, central row) the preferred direction shifted coherently with the rotating spotlight array. Finally, after the planetarium was stopped (phase 3, bottom row) the directional response drifted back toward the initial preferred direction.

planetarium rotation period. The directional response of the cell shifted coherently with the rotating point array. This may be due to the **optic field rotation inducing circular vection, and the HD system registering this as a shift in the animal's orientation**.

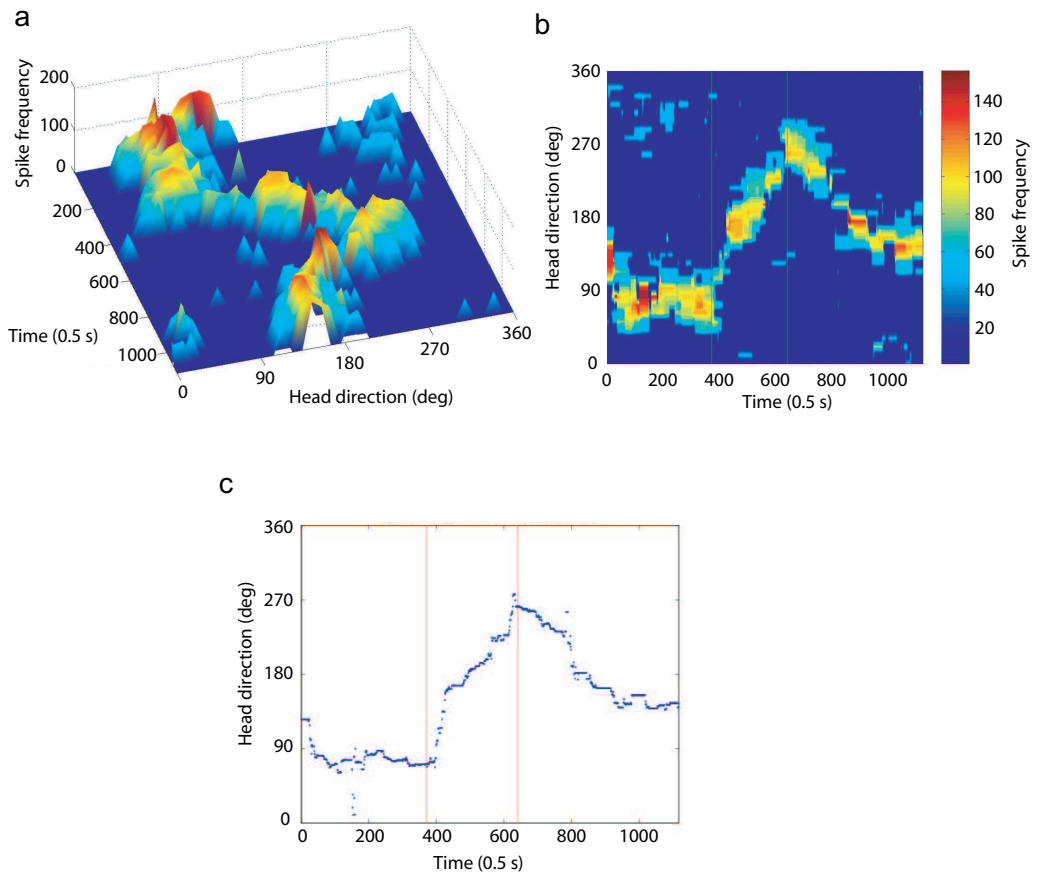

Figure 4.8: This example shows the time course of the shift of the preferred direction of one HD cell during the planetarium rotation and during the post-rotation period. **(a)** and **(b)** represent (in three- and two-dimension, respectively) the response histogram obtained by averaging over a $30\,s$ temporal window sliding over time at $500\,ms$ per step. **(c)** Preferred direction obtained by taking the center of mass of the spike frequency histograms in (a) or (b).

This would conflict with vestibular, motor command and efferent copy signals indicating no such self-rotation. Consistent with this, the optic field flow signals provoked directional shifts only when the animal was actively moving, not when it was immobile, where the intermodality discrepancy would be highly salient. Fig. 4.7c (bottom row) shows that during the post-rotation period, the directional response drifted back toward the initial preferred direction. This result, which is not representative of the entire data set, was chosen to show a case in which the HD cell could "recalibrate" its directional firing after the planetarium rotation.

Interestingly, HD cells did not exhibit a rapid (jump-like) update of its preferred direction (such as in Section 4.1.1, i.e. $80\,ms$). Rather, a progressive drift took place. See the example of Fig. 4.8 to compare the time course of the shift during and after the rotation period. Such a delayed re-alignment of the directional firing was likely due to an allothetic uncontrolled cue and resembled the progressive update reported by

Knierim et al. (1998) after a $180°$ conflict between a salient visual landmark (a cue card) and self-motion cues. This might indicate that during the planetarium rotation a self-motion illusion (e.g., vection) had primarily driven the preferred direction shift and generated the subsequent conflict situation.

4.1.4 Anterodorsal thalamic head direction neurons are modulated by the hippocampal theta rhythm

The hippocampal EEG signal exhibits two characteristic patterns depending on the animal's ongoing behaviour: *(i)* when the animal actively explores its environment, hippocampal local field potentials (LFPs) display prominent sinusoidal oscillations at $7 - 12\,Hz$ termed **theta rhythm** (Green and Arduini 1954; Miller 1991; O'Keefe and Recce 1993; Skaggs et al. 1996); the theta rhythm has also been observed during passive locomotion of the animal (Gavrilov et al. 1996) as well as during sensory scanning and REM sleep (Buzsáki 1996); *(ii)* when the animal is, for instance, eating, drinking, or grooming, the hippocampal EEG exhibits a rather irregular activity with large amplitude and broad frequency spectrum (Vanderwolf 1969; Buzsáki et al. 1990).

Theta oscillations seem to be involved in timing hippocampal cell assemblies (Lisman and Idiart 1995; Harris et al. 2003), as well as to be relevant to mnemonic functions including storage and recall of sequences of places or events (see Buzsáki 2002 for a recent review). There exists a phase correlation between the theta rhythm and hippocampal place cell firing. During each episode of elevated firing (corresponding for example to the traversal of a place field) pyramidal cells in the hippocampus follow a characteristic pattern, starting to fire at a certain phase, then firing at progressively earlier phases. This phenomenon has been referred to as 'phase precession' (O'Keefe and Recce 1993; Skaggs et al. 1996; Harris et al. 2002; Mehta et al. 2002; Zugaro et al. 2005). Thus, not only does the theta rhythm provide a timing mechanism to organise cell assemblies, it also permits more precise localisation (because the phase can indicate the position within the firing field and provide a mechanism for updating the active population of neurons during movements (Burgess and O'Keefe 1996; Jensen and Lisman 2000).

The anterodorsal thalamic nucleus (ADN) transmits directional information to the hippocampus via retrosplenial cortex and postsubiculum (both of which have neurons with both directional and theta modulation, Cho and Sharp 2001; Sharp 1996). Albo et al. (2003) showed that AD neurons have several types of theta related activity in recordings in urethan-anaesthetized rats (evoked by tail pinch). These types include 'theta-off' cells that cease tonic activity with the onset of theta, and 'theta-on' cells that increase their firing rate during theta. The latter type includes cells with rhythmic discharges synchronous with the theta rhythm, and cells with slightly rhythmic discharges with strong phase-locking to theta oscillations.

We recently **investigated the relationship between the theta rhythm and the activity of head direction neurons in the anterodorsal thalamus** (Arleo et al. 2005) (the manuscript Arleo & Battaglia et al. (2005) is under submission procedure and was

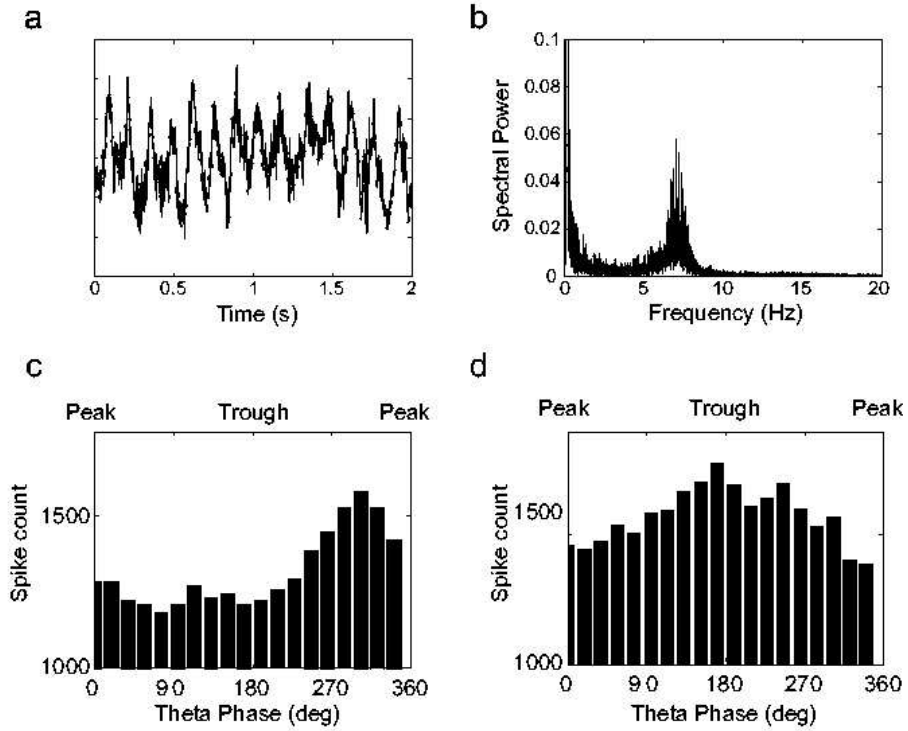

Figure 4.9: **(a)** Theta oscillations in skull-screw local field potential (LFP). A $2\,s$ segment of LFP showing prominent theta oscillations, which were constantly present during all recording sessions. **(b)** Power spectrum of the LFP signal, showing a theta related peak at around $7\,Hz$. **(c)**, **(d)** Theta modulation of two example HD cells. The Histograms show the number of spikes fired as a function of theta phase by the cells, one having a preferred phase near the peak of theta at 300° (c), the other near the trough (d).

not included in Appendix C).

EEG dipole recordings were made via two skull screws, one above the hippocampus and the other above the parietal cortex. Although higher amplitude theta can be recorded from intra-hippocampal electrodes, the skull screw dipole could capture the basic elements of hippocampal theta. Fig. 4.9a shows a $2\,s$ segment of local field potential (LFP) signal showing prominent theta oscillations which were constantly present during all recording sessions. Fig. 4.9b displays the power spectrum of the LFP signal, showing that the dominant frequency was centred at about $7\,Hz$. The theta amplitude was correlated with animal movement speed, as it has been demonstrated previously with intra-hippocampal electrodes.

The instantaneous theta phase at the moment of the emission of each action potential was logged in histograms. Preliminary results show that **most (71%) of the recorded cells showed a significant preferential firing during a particular phase of the theta cycle** (see examples in Fig 4.9c,d). The amount of activity modulation (firing rate at the preferred phase minus firing rate at the least preferred phase) represented typically 5 to 20% of the phase curve baseline activity level. Also, **AD head**

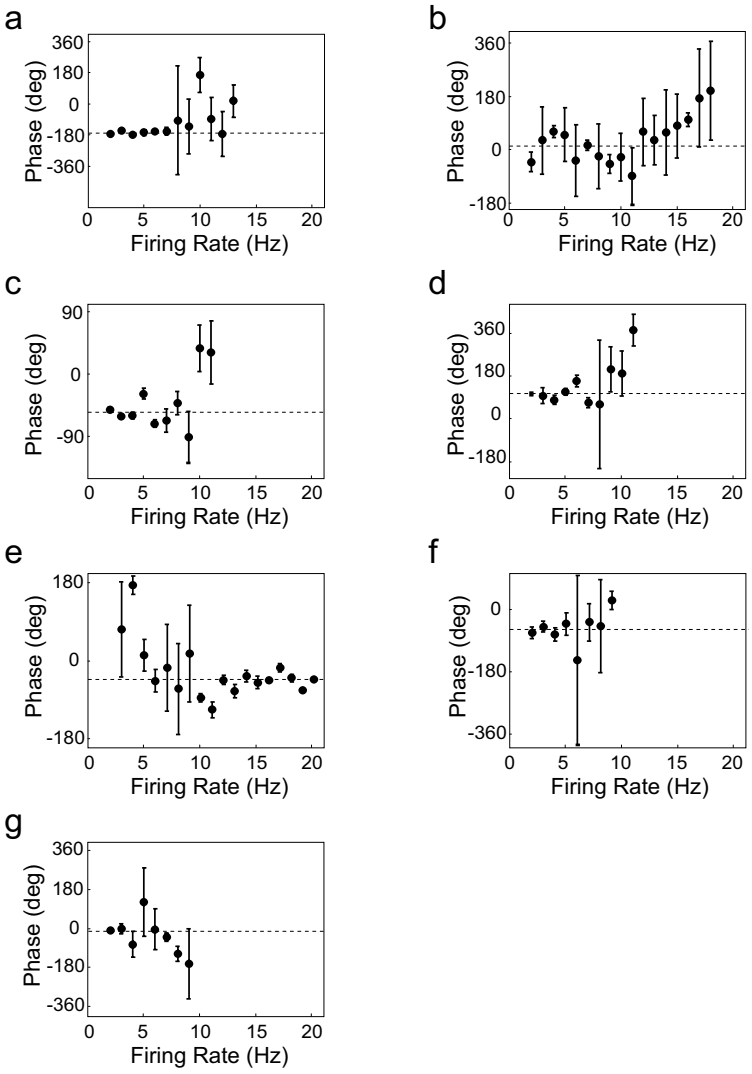

Figure 4.10: Preferred phase as a function of instantaneous firing rate. Data are represented for the seven cells for which a significant effect of rate on firing phase was observed **(a-g)**. The instantaneous firing rate, expressed as the number of spikes in a two-theta cycles period (x-axis), is plotted against the mean firing phase for all the spikes that occurred with that particular instantaneous firing rate and the 95% confidence interval for the mean. The dashed line represents the preferred theta firing phase for each cell.

direction cells did not show evident phase precession patterns (probably due to their high firing rate, i.e. many spikes were fired during each theta cycle). This does not rule out the possibility that theta oscillations interact with activity-related variables (for example the firing rate) in a non-trivial way. To test this, we applied the analysis by Harris et al. (2002) to our HD cell recordings. 70% of the cells that showed a significant phase preference showed also an effect of firing rate on preferred phase (Fig 4.10).

4.2 Theoretical modelling of head direction cells

4.2.1 A continuous attractor model for the maintenance and integration of the HD signal

Self-sustaining persistent activity in the brain is likely to mediate working memory functions (see e.g., Wang 2001). The discharge of HD cells constitutes an example of persistent neuronal activity that might serve an ongoing memory trace of the allocentric orientation of the rat, which could be used for navigation purposes (Wiener and Arleo 2003). If the head of the animal remains motionless and oriented in a given direction θ, the sub-population of HD cells with preferred directions close to θ remains active, demonstrating the persistence of the HD neural activity pattern in stationary conditions. The mechanisms of sustaining persistent activity could involve particular membrane properties as well as dynamic circuit interactions. These mechanisms as well as the functional role of persistent activity have been the subject of a large body of theoretical work. Most of these studies have identified **continuous attractor networks** (Amari 1977; Ermentrout 1998) **as a useful paradigm to describe the persistence of a pattern of activity** over time.

Continuous attractor network models have been proposed to account for selectivity properties of sensory (Ben-Yishai et al. 1995; Somers et al. 1995; Hansel and Sompolinsky 1998) and motor (Lukashin and Georgopoulos 1993) systems, for maintenance of a continuous variable in working memory in prefrontal and parietal cortices (Camperi and Wang 1998; Compte et al. 2000; Laing and Chow 2001; Gutkin et al. 2001), and for properties of hippocampal place cells (Tsodyks and Sejnowski 1995; Samsonovich and McNaughton 1997; Redish and Touretzky 1997; Battaglia and Treves 1998; Kali and Dayan 2000; Tsodyks 2005; Leutgeb et al. 2005).

HD cells have been hypothesised to constitute yet another system with one-dimensional continuous attractor dynamics (Skaggs et al. 1995; Zhang 1996; Redish et al. 1996; Goodridge and Touretzky 2000; Xie et al. 2002; Degris et al. 2004; Boucheny et al. 2005). As in most attractor systems, these models implement a recurrent neural network in which cells representing similar states (i.e., neighbouring orientations in the one-dimensional directional state space) are coupled by strong excitatory collaterals, whereas units representing distant states strongly inhibit each other. The intrinsic dynamics of the interaction between excitatory and inhibitory signals generates a centre-surround attractor scheme and allows the system to settle down to stable (self-sustained) states where sub-populations of HD neurons with similar preferred directions are active while others remain silent (sometimes called ‘bump’ states).

In these models, the integration of the head angular velocity is achieved by introducing an asymmetry in the centre-surround attractor dynamics, which makes the bump of activity shift over the continuous directional state space. To relate this asymmetric component to head rotations, Zhang (1996) and Redish et al. (1996) modulated the synaptic weights by means of angular velocity signals, whereas Goodridge and Touretzky (2000) utilised synapses with a non-linearity that is tuned to yield a perfect

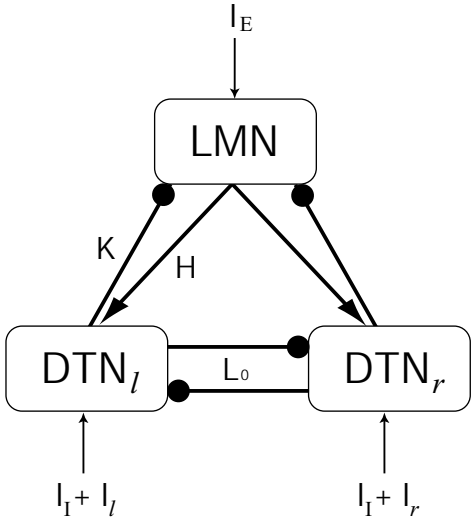

Figure 4.11: The attractor-integrator model included a population of excitatory directional units in the lateral mammillary nucleus (LMN) and two networks of inhibitory neurons in the dorsal tegmental nucleus ($\mathrm{DTN}_{l,r}$). Arrows and circles indicate excitatory and inhibitory synapses, respectively. The circuit did not contain recurrent excitatory collaterals. LMN received an external input current I_E, while $\mathrm{DTN}_{l,r}$ received modulatory external inputs $I_I + I_{l,r}$ providing the system with the head angular velocity signal. (Taken from Boucheny et al. 2005)

integration of angular velocity signals. Skaggs et al. (1995) hypothesised the existence of two groups of 'rotation cells' that receive vestibular inputs and fire as a function of the magnitude of the angular velocity. One group is responsive for clockwise head turns, the other for counterclockwise turns. The two groups project asymmetrically to the left and to the right of the HD bump of activity, respectively. However, Skaggs et al. (1995) did not simulate any model system to check the feasibility of this scenario. Blair et al. (1998) and Degris et al. (2004) realized a neural implementation of this scenario by proposing an attractor-integrator HD cell circuit. Finally, Xie et al. (2002) studied a two population network of left and right units, and showed that with appropriate connections and linear synapses, the network can integrate the inputs with good accuracy in a large velocity range.

All the aforementioned models rely on recurrent excitation to sustain persistent activity in HD neurons. However, **anatomical data show no evidence for recurrent excitatory collaterals in the structures of the HD cell system that seem to give rise to the self-sustained signal dynamics: the lateral mammillary nucleus (LMN) and the dorsal tegmental nucleus (DTN)** (Allen and Hopkins 1988; Allen and Hopkins 1989). On the other hand, reciprocal connections between LMN and DTN have been demonstrated experimentally. Anatomical studies suggest that LMN receives ascending inhibitory (GABAergic) afferents from DTN (Shibata 1987; Allen and Hopkins 1989; Gonzalo-Ruiz et al. 1992; Wirtshafter and Stratford 1993) and that, in turn, LMN sends descending excitatory efferents back to DTN (Allen and Hopkins 1989; Allen and Hopkins 1990). Finally, electrophysiological data suggest that a large fraction of cells in DTN are selective for angular velocity in either clockwise or counterclockwise

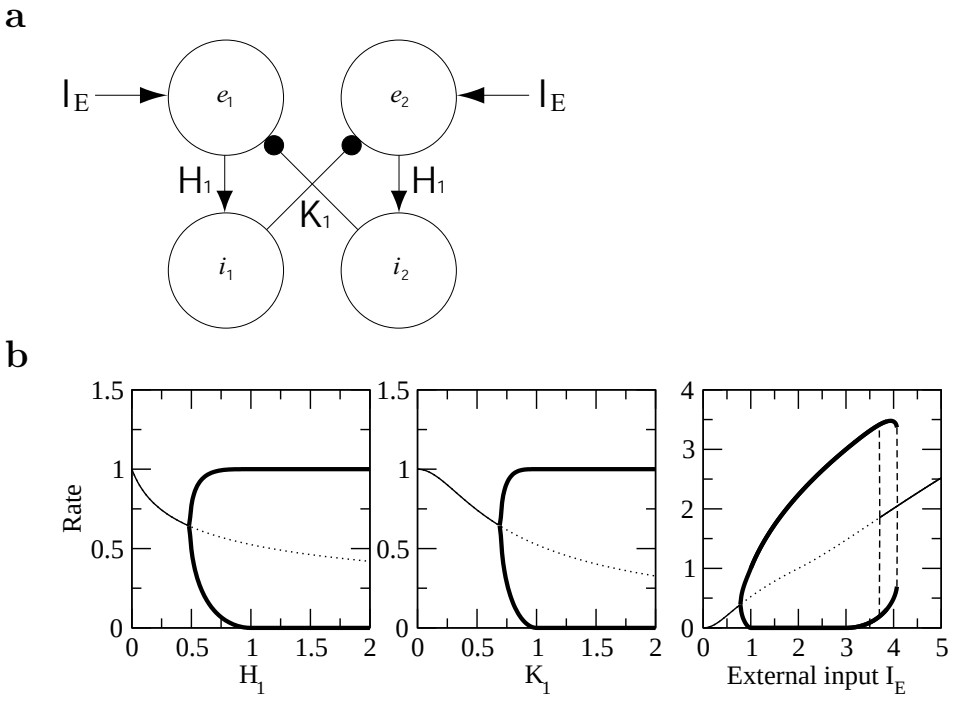

Figure 4.12: **(a)** Circuit composed of two excitatory $e_{1,2}$ and two inhibitory $i_{1,2}$ units. $e_{1,2}$ receive an external excitatory current I_E. H_1 is the strength of the iso-directional excitation from $e_{1,2}$ to $i_{1,2}$. K_1 denotes the amount of inhibition mediated by the offset projections from $i_{1,2}$ to $e_{1,2}$. **(b)** Bifurcation diagrams of the excitatory-inhibitory network. Firing rates of the excitatory populations e_1 and e_2 are shown as a function of H_1 (left), K_1 (centre) and I_E (right). Parameters: $H_1 = 1$ (except in left), $K_1 = 1$ (except in centre), $I_E = 1$ (except in right). The uniform states (thin solid line) become unstable (dotted line) above a critical value of H_1 (left) and K_1 (centre), and at intermediate values of I_E (right). The asymmetric states (one pair of populations suppressing the other pair) are indicated by thick black lines. At some intermediate level of I_E, the system is tristable (between the dashed lines in right panel).

directions (Bassett and Taube 2001b; Sharp et al. 2001). These cells could provide the basis for the 'rotation cells' postulated by Skaggs et al. (1995).

Taken together, this anatomical and electrophysiological data motivated our study Boucheny et al. (2005) investigating an **alternative continuous attractor model in which no recurrent excitation was present** (Rubin et al. 2001; Song and Wang 2003). This network was able to store in a short-term memory an angular variable (the head direction) as a spatial profile of activity across neurons in the absence of selective external inputs, and to accurately update this variable on the basis of angular velocity inputs. The network was composed of one excitatory population and two inhibitory populations, with inter-connections between populations but no connections within the neurons of a same population. In particular, there were no excitatory-to-excitatory connections. Angular velocity signals were represented as inputs in one inhibitory population (clockwise turns) or the other (counterclockwise turns).

The architecture of the network is shown in Fig. 4.11. The model included reciprocal connections between LMN and DTN, whose existence has been demonstrated

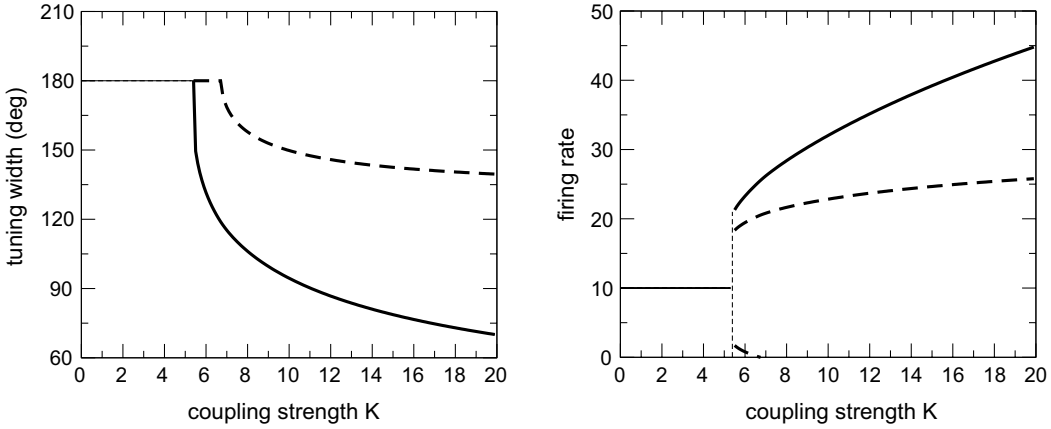

Figure 4.13: Characteristics of the tuned state vs connection strength K. Left: width of the tuned state as a function of K. Right: peak and background firing rates as a function of K (solid line: excitatory network; dashed line: inhibitory networks; thin lines: uniform state; thick lines: tuned state). For $K < 16/3$ (marked by dashed line), the uniform state was the only stable stationary state. Above $K = 16/3$, the tuned state became the only stable stationary state. Notice that the tuning widths decreased while K was increasing, while the peak firing rates increased with increasing K. (Taken from Boucheny et al. 2005)

experimentally. It assumed the existence of two DTN sub-populations, one selective for clockwise turns, the other selective for counterclockwise turns. Finally, the model also assumed that these two DTN networks mutually inhibit each other. As we will see later, such connections were not necessary for the model to operate, but they expanded greatly the performance of the system in terms of angular velocity integration. As far as we know, there is no experimental evidence for such a functional lateralisation within the rat DTN, nor for the presence of DTN intrastructural inhibition. However, Sharp et al. (2001) reported that DTNs in the left- and right-hemispheres exhibit reciprocal inhibitory projections, and show some preliminary electrophysiological data suggesting a tendency for DTN cells to be selective for ipsiversive head rotations.

4.2.2 Mathematical analysis of an attractor-integrator dynamics without recurrent excitation

We first studied the simplest circuits that exhibit bistability in spite of the absence of recurrent excitation: a model with two mutually coupled inhibitory populations, and a model with four populations, two excitatory and two inhibitory (Fig. 4.12). Then, we developed a mathematical analysis of an attractor-integrator model with the architecture of Fig. 4.11 by using analog (firing rate) simplified neurons. This model was a generalisation of previous ring attractor networks (Ben-Yishai et al. 1995; Zhang 1996; Redish et al. 1996; Ben-Yishai et al. 1997; Hansel and Sompolinsky 1998; Goodridge and Touretzky 2000; Xie et al. 2002; Degris et al. 2004), and its architecture was similar to the three-population architecture proposed by Song and Wang (2003): one excita-

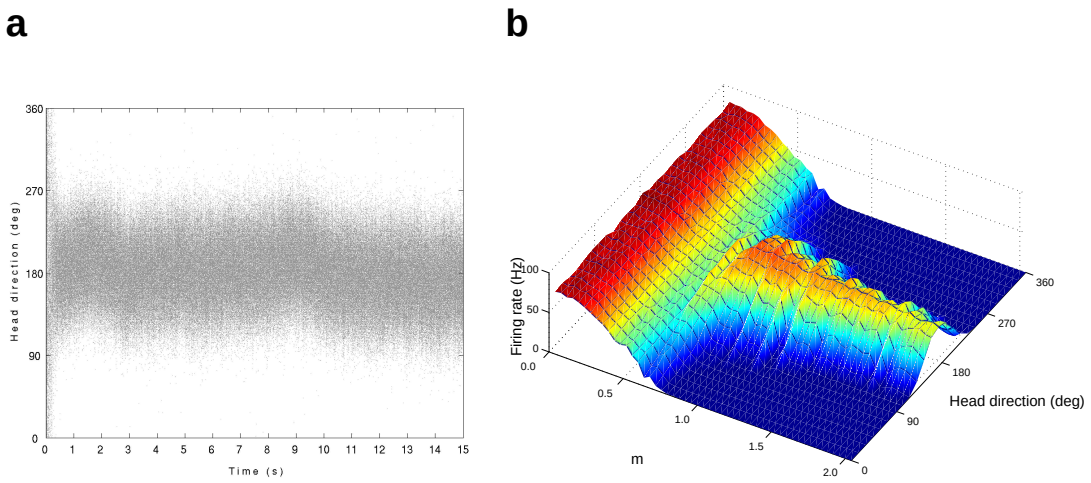

Figure 4.14: **(a)** Rastergram of the action potentials emitted by LMN HD cells over time. Each dot represents one spike. For zero angular velocity (i.e., $I_l = I_r = 0$), a stationary tuned state emerged from random noise after a transient $\Delta t \approx 200$ ms. This attractor state persisted over time providing a stable directional representation ($\bar{\theta}(t) = 181°$ computed by population vector coding). **(b)** Condition of emergence of a tuned state as a function of the strength H of the excitatory projections from LMN to DTN, and of the strength K of the inhibitory projections from DTN to LMN, given a fixed angular offset $\alpha = 50°$ of the connections from DTN to LMN. H and K vary according to the following rule: $H = m \cdot H_1$, $K = m \cdot K_1$, with $0 \leq m \leq 2$, where $H_1 = 0.06$ and $K_1 = 1.12$. For each m, we let the network evolve from $t = 0$ until $t = 1$ s and looked at the LMN ensemble activity profile $F_m(t = 1)$. The diagram displays all the LMN profiles $F_m(t = 1)$, for $0 \leq m \leq 2$, and shows that there existed a threshold value $m^* \approx 0.6$ above which a gaussian-shaped attractor state emerged. Notice that all the tuned states $F_m(t = 1)$ with $m > m^*$ had been aligned along the head direction 180°.

tory population (representing the LMN), and two inhibitory populations (representing two distinct populations in the DTN, one selective for clockwise turns, the other selective for counterclockwise turns). The mathematical analysis allowed us to derive the conditions on the connectivity for

- the emergence of the directionally selective HD profile: the study provided the **conditions under which the uniform state becomes unstable such that the system converges to a tuned stationary attractor regime (i.e., a 'bump of activity')** (Fig. 4.13);
- the reliable integration of angular velocity inputs: an analysis of the linear stability of the attractor state gave the **analytical solutions for the stationary bump to start moving around the ring**;
- the range of angular velocities that can be accurately integrated by the model: the study of the travelling bump solutions provided the **conditions for the linearity of the bump velocity function** (relative to the angular speed inputs I_r and I_l in Fig. 4.11).

Our work proposed the first analytical investigation of such an architecture using simplified network of threshold-linear neurons. The mathematical analysis provided

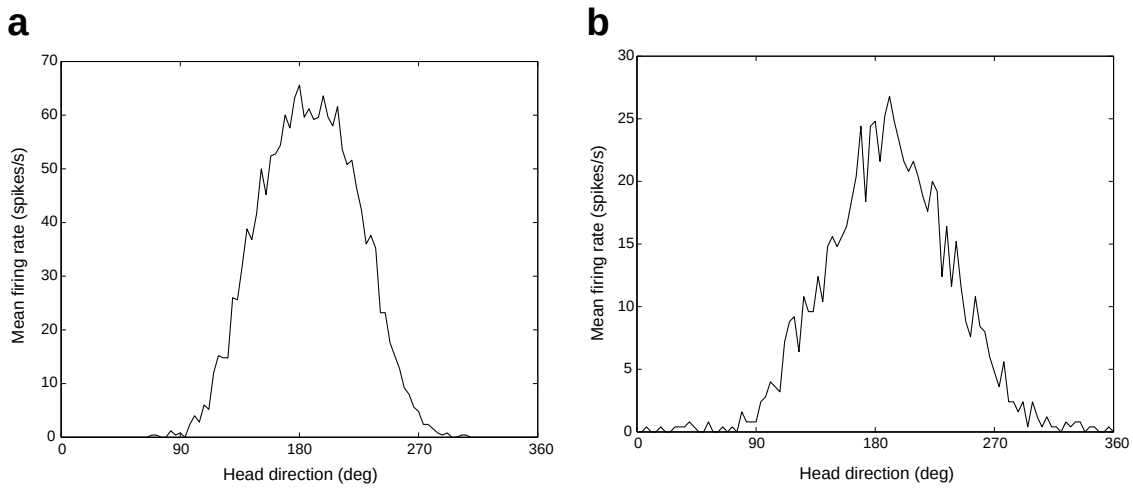

Figure 4.15: Tuning curves of the formal HD cells in LMN **(a)** and DTN **(b)**. The mean peak spike frequency is about $60 - 65$ spikes/s for LMN units and 25 spikes/s for DTN cells. The width of the gaussian activity profile is $180°$ for LMN and $250°$ for DTN. These tuning curve parameters are consistent with those observed experimentally in the rat LMN and DTN areas (Taube 1998; Bassett and Taube 2001b).

the boundaries of the parameter space for which stable direction selectivity can be present, and those for which the network is able to integrate accurately angular velocity information. The reader is referred to Secs. 2 and 3 of the reprint of Boucheny et al. (2005), Appendix C, for details about the analytical study.

4.2.3 An attractor-integrator network of spiking neurons

Following the analytical study, we derived a more realistic implementation of the HD model by means of large populations of spiking neurons forming an attractor-integrator network according to the architecture shown in Fig. 4.11. **LMN and DTN cells were modelled by means of spiking leaky integrate-and-fire neurons and synaptic currents followed the time courses of AMPA, NMDA, and GABA receptors** (see the reprint of Boucheny et al. (2005) in Appendix C for full details about the network architecture as well as neuronal and synaptic models).

Numerical simulations using this neural model allowed us:

- to **confirm our analytical predictions about the conditions on LMN-DTN interconnectivity (e.g., strength of inhibitory projections) to generate stable tuned states (i.e., emergence and persistence of HD cell signal)** (Fig. 4.14);

- to **obtain directionally selective activity profiles in our formal LMN and DTN HD cells comparable to the tuning curves electrophysiologically observed in LMN and DTN** (Fig. 4.15);

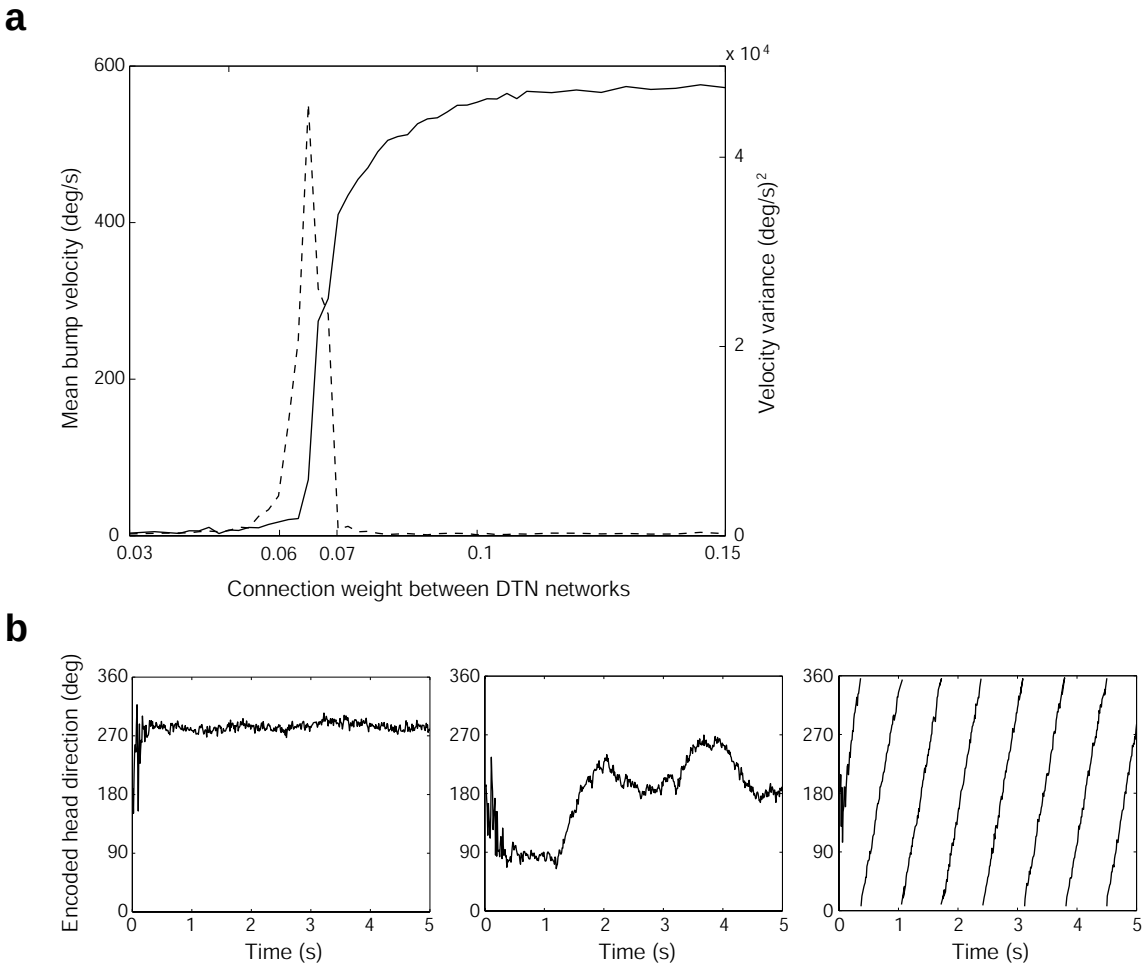

Figure 4.16: Stability of the tuned state as a function of the strength L_0 of the mutual inhibitory connections between the two DTNs. **(a)**: For each value $0.03 \leq L_0 \leq 0.15$ we measured the angular velocity v (solid curve) of the bump of activity in LMN and the variance around v over a 5 s period (dashed curve). For $L_0 < 0.06$, the tuned attractor state remained stable over time (angular speed v close to zero). Around $L_0 > 0.06$, the stationary bump became unstable, and the tuned state started moving around the ring. Close to the bifurcation, there were large fluctuations of the angular velocity: the bump moved in a very irregular fashion (v increased and the variance was very large). For $L_0 > 0.07$ the tuned state moved around the ring with a constant angular velocity v, with small fluctuations around v. **(b)**: Encoded head direction $\bar{\theta}(t)$ over a $5\,s$ trial for three particular values of L_0. The curves represent the centre of mass of the ensemble LMN activity computed by population vector coding. Left: for $L_0 = 0.03$ the bump of activity remained stable over time. Centre: for $L_0 = 0.062$ the attractor state exhibited a random angular velocity profile. Right: for $L_0 = 0.09$ the bump moved at constant angular velocity. (Taken from Boucheny et al. 2005)

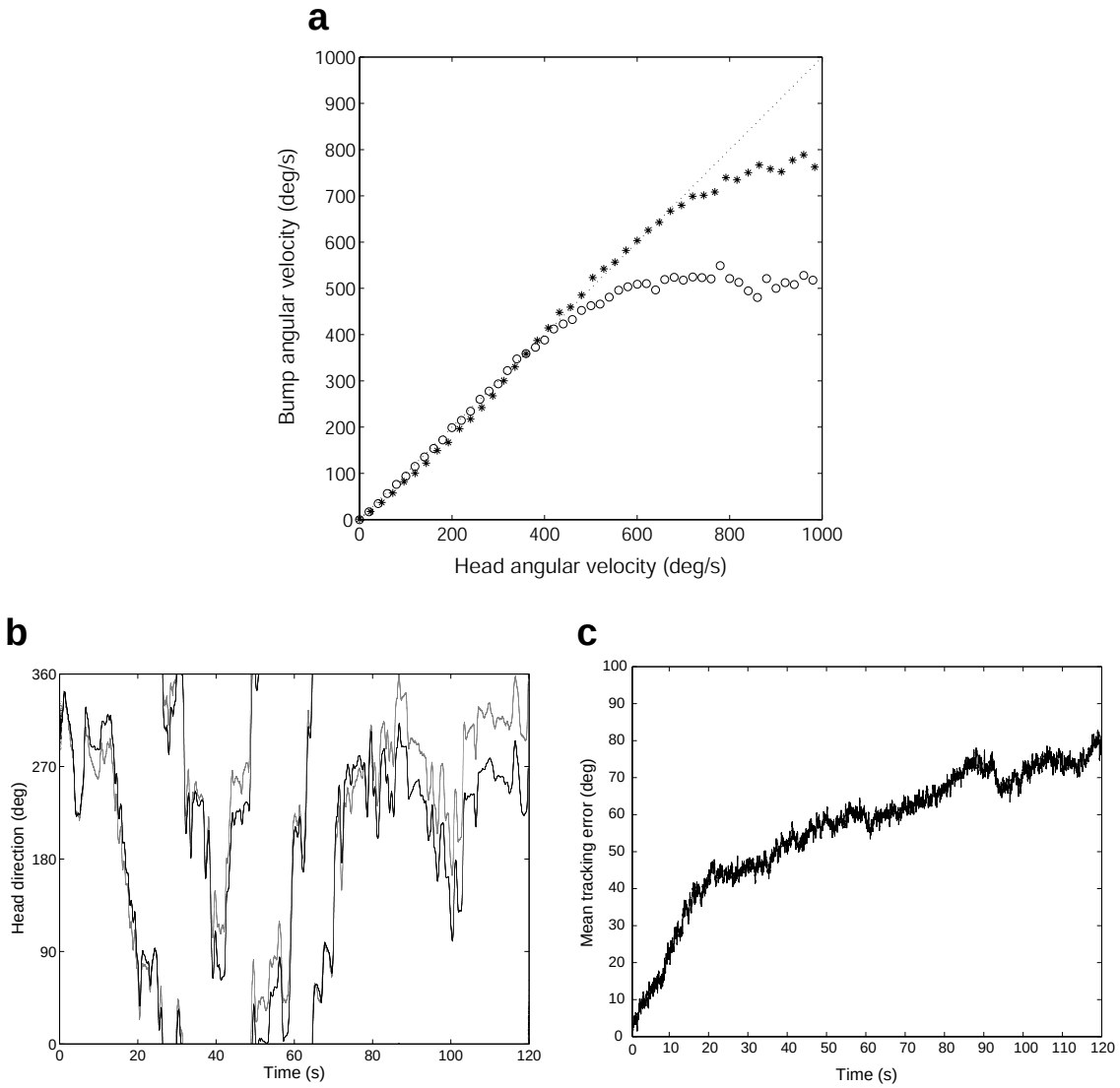

Figure 4.17: **(a)** For non-stationary regimes, e.g. $I_l > 0$ and $I_r = 0$, the tuned state shifted with a speed proportional to the angular velocity encoded by the differential input $\delta I(t)$, e.g. $\delta I(t) = I_l(t) - I_r(t)$. The two sets of symbols show the angular velocity of the tuned state (averaged over $4\,s$) as a function of constant head angular velocity, for two values of the angular offset α in the projections from $\mathrm{DTN}_{l,r}$ to LMN (circles: $\alpha = 50°$, saturation occurred at $\approx 520°/\mathrm{s}$; stars: $\alpha = 65°$, the saturation velocity increased to $v \approx 780°/\mathrm{s}$). **(b)** The angular velocity profile $v(t)$ of a freely moving rat was applied to the HD system for $120\,s$. The model integrated $v(t)$ over time providing an ongoing estimate $\bar{\theta}(t)$ (gray line) of the rat's heading $\theta(t)$ (black line). One example out of $n = 35$ simulations is shown here (for sake of clarity, the two curves have been smoothed by means of an averaging time window of $500\,ms$). **(c)** Mean reconstruction error, averaged over $n = 35$ trials, of the HD system when tracking angular velocity profiles of freely moving rats during $120\,s$. The diagram shows that the integration of head angular movements based on inertial signals only was prone to cumulative drift over time. (Taken from Boucheny et al. 2005)

- to **predict a role for the inhibitory projections existing within the DTN structure in determining the stability of the HD representation** (Fig. 4.16);
- to **study the response of the system to an external angular velocity input** (simulating vestibular signals converging onto DTN) (Fig. 4.17a);
- to **test the integration property of the system on a set of rat angular velocity profiles** (Fig. 4.17b,c);
- to investigate how the HD representation encoded by our attractor network could be updated by reorienting external inputs (e.g., visual cues) and **find update latencies consistent with those observed experimentally by Zugaro et al. (2003) in rat HD neurons** (Fig. 4.18).

Our simulation results complemented those by Song and Wang (2004), who showed how the network dynamics is influenced by the NMDA/AMPA ratio, and how the update of the HD signal by external cues can take either the form of a continuous rotation of the network state or a discontinuous jump to the new HD depending on the distance between the old and new HDs and the strength of the external cue. We showed how the network dynamics is influenced by the mutual inhibitory connections in DTN, and how the projections from DTN to LMN determine the saturation velocity above which the system is no longer able to integrate accurately. We showed how such an architecture can integrate real angular velocity data and that it how rapidly can update its HD representation (i.e., its attractor state) following a strong reorienting stimulus.

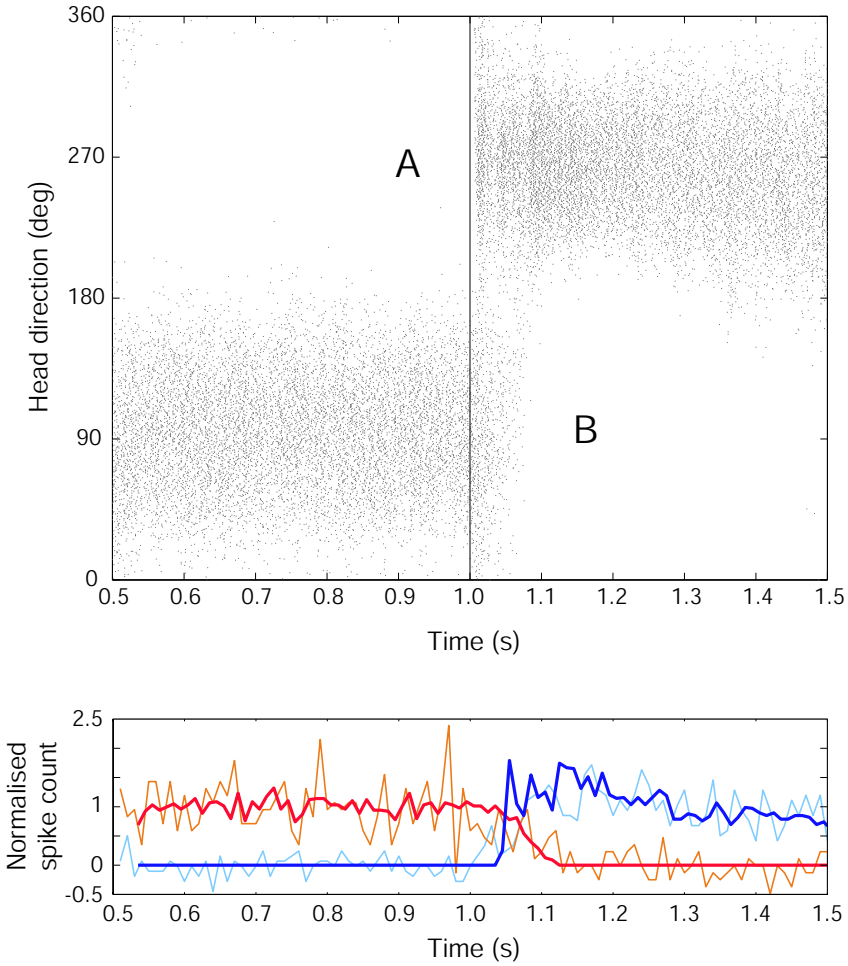

Figure 4.18: The HD model responded to reorienting external stimuli by rapidly relocating the bump of activity defined by the discharges of all LMN units. **Top:** Rastergram of the spikes emitted by LMN units over time. Each dot represents one spike. For $t < 1$ s the system had a self-sustained tuned state centred at $\bar{\theta} \approx 90°$; at $t = 1$ s a strong external input was applied to the system at $\theta = 180°$ and provoked the state transition. The new bump of activity (A) in turn extinguished the existing bump (B), through an increase in inhibition from DTN. **Bottom:** Spike peri-event histograms (bins of 10 ms) for the sub-population of HD cells that returned to baseline activity after the reorientation event (thick red line: numerical simulation data; thin orange line: experimental data from Zugaro et al. (2003)) and for sub-group of cells that became active after the stimulus onset (thick blue line: simulation; thin blue line: experimental data). The simulation data has been shifted in time by 25 ms to maximize the overlap between the two sets of curves. (Taken from Boucheny et al. 2005)

Chapter 5

Motor Behaviour Adaptation for Optimal Goal-oriented Navigation

Preface. *While being a member of the Neuroscience Group at the Sony Computer Science Lab in Paris (associate researcher 2004-2005), I also had the opportunity to participate to a project led by L. Rondi-Reig (LPPA, CNRS-Collège de France). This work focused on the role of the cerebellum in spatial navigation. Transgenic L7-PKCI mice (lacking cerebellar long-term synaptic depression, LTD, at the parallel fibre-Purkinje cell synapses) were tested with two navigation tasks in order to dissociate the relative contribution of the declarative and procedural components of spatial navigation. The results pointed towards a deficit of L7-PKCI mutants in performing a fine tuning of goal-oriented trajectories according to the ongoing sensory context. The use of transgenic mice permitted to characterise one of the underlying cellular mechanisms that may mediate the acquisition of this procedural-like function of the cerebellum (as opposed to the episodic-like functions ascribed to the hippocampus).*

In order to characterise the performances of mice undertaking a navigation task, we also developed an automated Navigation Analysis Tool (NAT). This MATLAB-based environment permitted to evaluate an extended set of behavioural parameters, and it was particularly adapted to achieve a detailed characterisation of the trajectory patterns performed by the animals. The rational behind developing NAT was threefold: (i) to provide an automated behavioural analysis allowing us to study navigation on a small time-scale basis (ms), (ii) to increase the reliability of the analysis (e.g., error minimisation), even when performed by multiple experimenters, (iii) to be flexible enough to adapt the analysis procedures to different navigation apparatus.

This chapter reviews the experimental work investigating the navigation capabilities of L7-PKCI cerebellar mice (Burguière et al. 2005). Then, it briefly outlines the main features of the developed behavioural analysis tool (Petit & Arleo et al. 2005). A reprint of Burguière et al. (2005) can be found in the Appendix C, whereas the contribution by Petit & Arleo et al. (2005) could not be included in the reprint collection because still under submission.

5.1 Spatial navigation impairment in mice lacking cerebellar long-term synaptic depression

Spatial cognition and navigation capabilities call upon two types of long-term memory: **declarative mnemonic capabilities** (e.g., the acquisition of representations encoding the spatio-temporal relations between environmental cues and places), and **procedural sensory-motor functions** (e.g., adaptive motor control for the fine tuning of trajectories based on contextual information) (Schenk and Morris 1985; Squire and Zola 1996; Petrosini et al. 1998; Burguière et al. 2005).

As discussed in Chapters 2 and 3, the hippocampal formation and several other limbic regions are likely to constitute the neural substrates mediating allocentric space coding (i.e., declarative-like functions). Recently, numerous experimental and clinical works have postulated a possible involvement of the cerebellum in the procedural components of spatial cognition (see reviews by Petrosini et al. 1998; Rondi-Reig and Burguière 2005). Also, the fact that the cerebellum receives multimodal spatial information and that it is anatomically interconnected to the limbic system as well as the frontal and parietal cortices (Schmahmann and Pandya 1989; Schmahmann 1996; Schmahmann and Pandya 1997), supports the hypothesis of a cerebellar role in spatial navigation.

We focused on the **cellular mechanisms subserving the contribution of the cerebellum in spatial learning** (Burguière et al. 2005). Our working hypothesis was that cerebellar **Long-Term synaptic Depression (LTD)**, occurring at the parallel fibre-Purkinje cell (PF-PC) synapses, and required for the acquisition of classical conditioning tasks (Thompson et al. 1997), may also be necessary for the acquisition of efficient trajectories toward a goal through a basic and common process of sensory-motor adaptation. Our hypothesis of a role of PF-PC LTD in the procedural component of navigation was inspired by the Marr-Albus-Ito theory that considers the cerebellar learning process as an error based system (Marr 1969; Albus 1971; Ito 1993). According to this theory, the climbing fibres convey error information to the PF-PC synapses and trigger a modulation of their strength via LTD. Ito showed that in VOR adaptation experiments PF-PC LTD is likely to constitute the neural substrate of such an error-driven motor learning process (Ito and Kano 1982). In the case of spatial navigation, the trajectory performed by the animal must be adapted to the spatial context and optimised to lead directly to the goal.

In order to test this hypothesis:

- We employed the L7-PKCI transgenic mice model (De Zeeuw et al. 1998), which presents a specific inactivation of the PF-PC LTD. De Zeeuw and colleagues have demonstrated that adult L7-PKCI mutant mice have intact motor capabilities and normal electrophysiological properties of Purkinje cells (e.g., baseline discharges) (Goossens et al. 2001). Likewise, we did not observe any abnormalities in the sensory-motor reflexes, physical characteristics, and general behaviour of L7-PKCI mice. In addition, hippocampal functions (synaptic transmission and long-term synaptic plasticity) were not impaired in L7-PKCI mutants (Burguière et al. 2005).

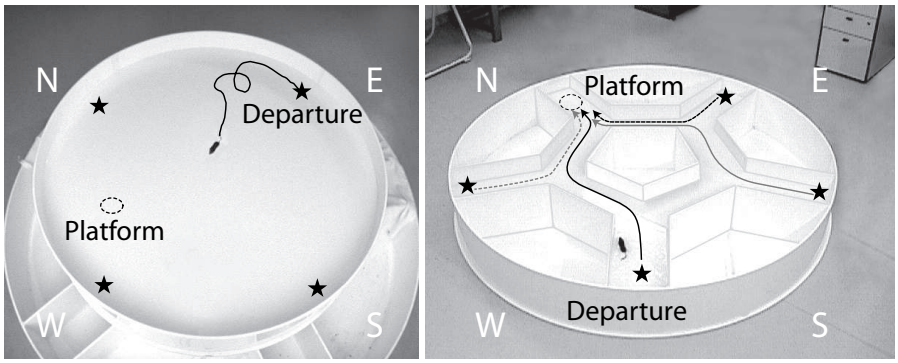

Figure 5.1: The two spatial navigation tasks employed for the experiments: the Morris water maze (MWM) **(a)** and the Starmaze task **(b)**. In both tasks the subject has to navigate to an escape platform submerged under opaque water (dashed circle) from four randomly selected departure points (black stars). However, in the Starmaze animals are constraint to swim within alleys that guide their movements, which reduces the possible deviations from an ideal trajectory. (Taken from Burguière et al. 2005)

- We adopted two different spatial learning tasks, the **Morris water maze** (MWM) (Morris et al. 1982) and a new task called the **Starmaze** (Rondi-Reig et al. 2004) (Fig. 5.1), to dissociate the relative importance of the declarative and procedural components of navigation. In both tasks, the animal has to find a fixed hidden platform from random departure locations, which requires declarative capabilities to learn a spatial representation of the environment. However, in contrast to the MWM task, the Starmaze allows the animal to only swim within alleys. This helps the subject to execute goal-directed trajectories effectively, reducing the procedural demand of the navigation task.

The results showed that **L7-PKCI mice were impaired in solving the MWM task compared to their control littermates** (Fig. 5.2, but see Burguière et al. 2005 for details). Nevertheless, the spatial navigation impairment was due to neither a deficit in swimming speed, nor a deficit in visual guidance abilities (Fig. 5.2d,e). Furthermore, the results suggested that both control and L7-PKCI mice were able to acquire a memory of the localisation of the platform. To investigate this difference we assessed the accuracy of the mice goal-oriented trajectories during learning (see Section 5.2 for a description of the employed analysis tool), and found that the trajectories of L7-PKCI mice toward the platform were significantly less effective compared to those employed by control mice. Thus, this findings suggested that **L7-PKCI mice could learn to locate the platform (declarative component) but they tended to execute non-optimal goal-directed trajectories (procedural component)** (see Fig. 5.3 for a qualitative comparison between the searching behaviour of controls and mutants over training).

We let the same groups of subjects undertake the allocentric starmaze task, which implies a lower procedural demand than the MWM. **No statistical difference was observed between the spatial learning capabilities and navigation performances of controls and mutants in the Starmaze** (Fig. 5.4). The absence of a deficit when the

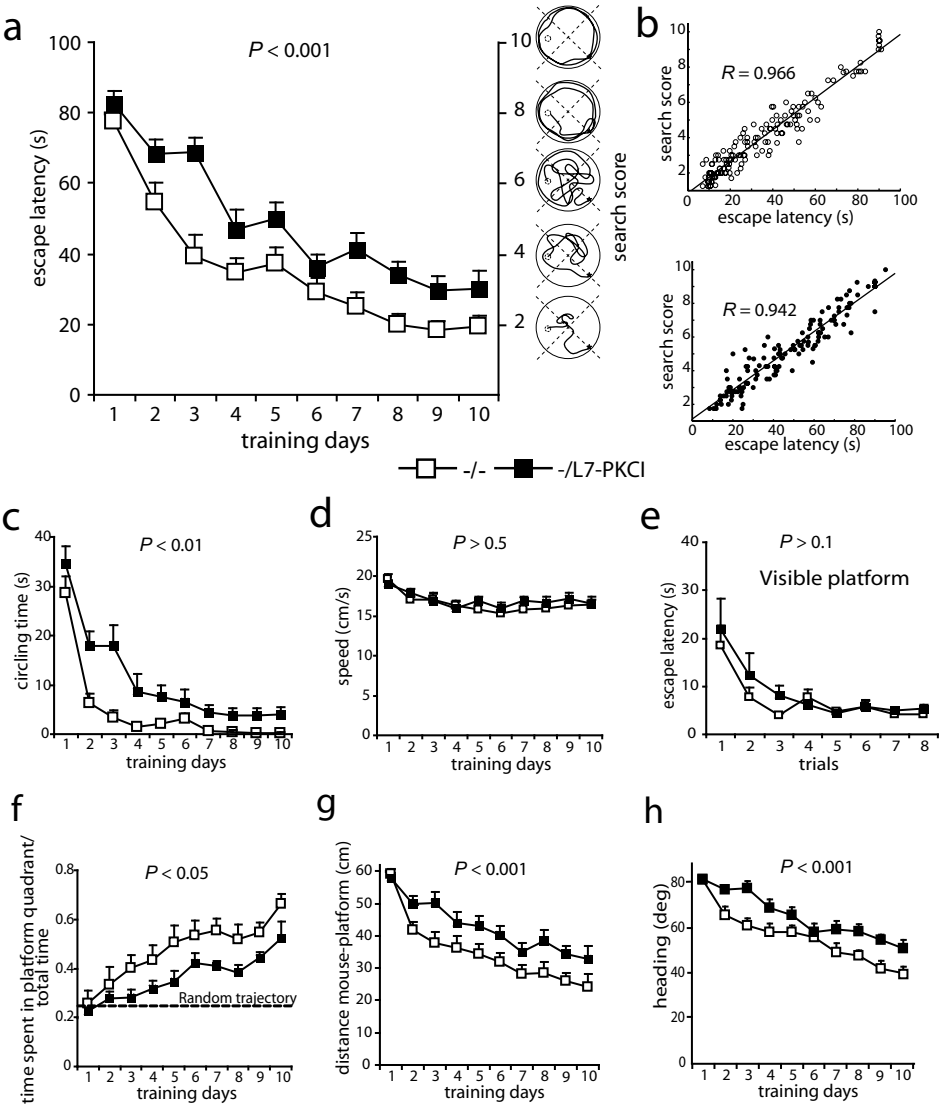

Figure 5.2: L7-PKCI mice were impaired in solving the hidden-platform version of MWM task. **(a)** The mean escape latencies of controls and mutants (white and black squares, respectively) were similar at the beginning of training (day 1). However, controls improved their performances significantly better than mutants over time. The behavioural patterns corresponding to the search scores defined by Petrosini et al. (1996) are illustrated by the cartoon trajectories on the right side. The lower the score, the better the searching behaviour. The search scores of L7-PKCI mice were significantly higher than those of control animals. **(b)** The escape latencies and the search scores were highly correlated for both control (top) and mutant (bottom) mice, suggesting that the longer time-to-goal needed by L7-PKCI mice was due to non-optimal searching trajectories. **(c)** L7-PKCI mutants exhibited a significantly larger amount of circling behaviour over training. **(d)** The mean swimming speeds of controls and mutants remained comparable over the entire training period. **(e)** Mutants were not impaired in solving the visible platform version of the MWM (i.e., visuo-guidance navigation task). **(f)** The mean ratio between the time spent within the target quadrant and the total duration of the trial of both controls and mutants increased significantly above the random trajectory level during training. However, controls improved their ratio significantly better than L7-PKCI. **(g)** The mouse-platform distance parameter suggested that mutants followed significantly longer trajectories than controls. **(h)** The mean angular deviation between ideal and actual trajectory showed that mutants had a deficit in maintaining an effective locomotion orientation (relative to the target) during navigation. (Taken from Burguière et al. 2005)

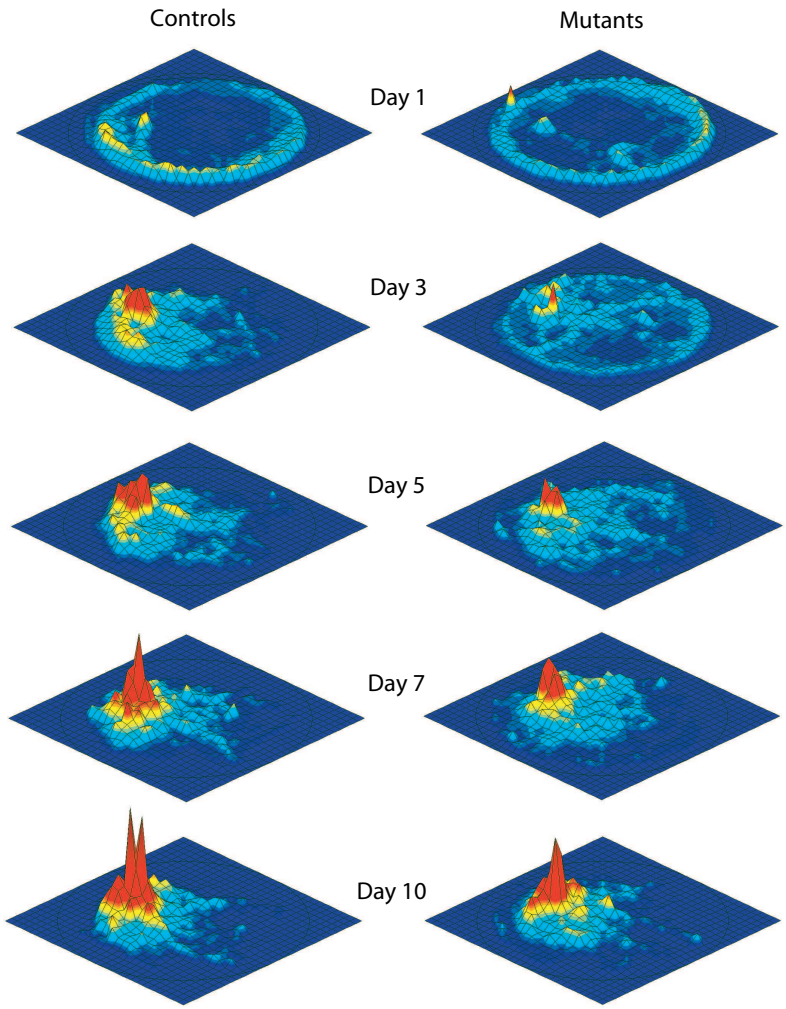

Figure 5.3: Three-dimensional plots of the mean spatial occupancy (i.e., the time, z axis, spent at each sampled region of the maze, x-y axes) of control and mutant mice at different training days. The value associated to each grid cell was obtained by normalizing the time spent in the cell region relative to the duration of each trial, then averaging over all day trials and over all the animals of a group. These qualitative representations suggested that, when solving the MWM task, mutants had larger searching zones than control animals during training. (Taken from Burguière et al. 2005)

trajectory was guided corroborated the results obtained with the MWM, which pointed towards the inability of L7-PKCI mice to adapt their goal-oriented behaviour effectively. Thus, the results obtained with the Starmaze strengthened our hypothesis that the declarative component was likely to be unimpaired in L7-PKCI mice.

This work corroborated previous spatial navigation studies with other cerebellar models (Leggio et al. 1999; Martin et al. 2003), but it also identified the **parallel fibre-Purkinje cell (PF-PC) LTD as being a possible core mechanism underlying the cerebellar spatial learning function**. How could the same cellular mechanism, i.e. PF-PC LTD, be involved in motor learning and more cognitive process such as

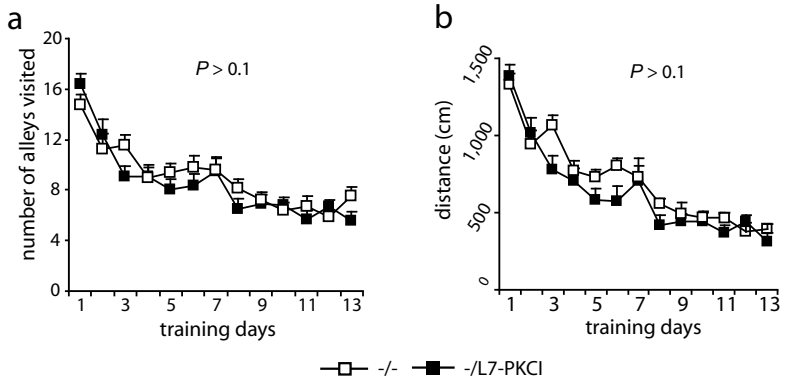

Figure 5.4: L7-PKCI mutants were not impaired in learning the allocentric version of the Starmaze task. **(a)** No statistically significant differences were observed between the number of alleys visited during a trial by control and mutant mice. **(b)** The mean distance swam to reach the target was also not significantly different between the two groups. (Taken from Burguière et al. 2005)

spatial learning? Several cognitive processes can be considered on the basis of the same sensory-motor coupling scheme observed in classical motor learning (Ito 1993). Spatial navigation requires a linkage between the spatial context (including sensory inputs and internal state information) and the explorative response (motor output) characterised by the animal's trajectory. While the spatial context may be conveyed by the mossy fibre - granule cell - parallel fibre pathway relaying information from the pontine nuclei (Thach et al. 1992), errors in the explorative response may be mediated by the climbing fibre signals that originate from the olivary subnuclei that are innervated by descending projections from the mesodiencephalic junction and cerebral cortex (De Zeeuw et al. 1998). Since induction of PF-PC LTD requires conjunctive activation of the parallel fibre and climbing fibre pathways, this form of synaptic plasticity could be responsible for the establishment of this linkage (Ito 1993).

Thus the cerebellum may mediate a general learning function to create a context-response linkage adapted to the task. During spatial learning, the subject could establish an appropriate context-response coupling resulting in effective motor behaviour (e.g., in the execution of optimal trajectories to the target). At the cerebellar level, procedural learning may result from a classical control learning scheme in which the feedback loop allows the system to converge towards an adapted context-motor linkage. The abstract model shown in Fig. 5.5 can be applied to study the process of sensory-response adaptation underlying both basic motor learning and higher cognitive learning. The absence of PF-PC LTD in L7-PKCI mice could lead to the accumulation of errors over time (i.e., during the execution of a goal-directed trajectory), due to the absence of continuous context-dependent corrections of the motor signals (Ito 1993). From a behavioural point of view, the accumulation of these errors would lead to a drift during unconstraint (not guided) navigation as in the MWM task, whereas it would be less relevant in the Starmaze task due to the reduced number of possible goal-directed trajectories.

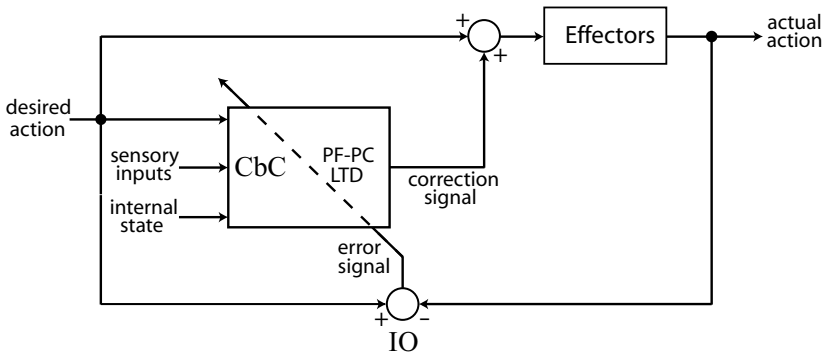

Figure 5.5: Abstract model describing the error-based cerebellar learning hypothesis (adapted from Ito 1993). This theoretical model can be applied to study the process of sensory-response adaptation underlying both basic motor learning and higher cognitive learning. Contextual information (i.e., multimodal sensory signals, animal's internal state, and desired action) enters the cerebellar cortex (CbC) via the mossy fibre - granule cell - parallel fibre pathway. The inferior olive (IO) generates an error signal based on the discrepancy between desired and actual action, and conveys this information to the cerebellum via the climbing fibers. The convergence of both contextual and error signals at precise timing can induce LTD at the parallel fibre - Purkinje cell (PF-PC) synapses. This learning process can lead to the acquisition of the optimal sensory-response linkage and, then, it can allow the cerebellum to compensate for the error dynamically. In the case of spatial navigation, this can result in the optimisation of the goal-directed trajectory performed by the animal. Specific inactivation of the PF-PC LTD mechanism would impair cerebellar learning and disrupt the correction signal. This would result in non-optimal spatial behaviour due to cumulative error over time. (Taken from Burguière et al. 2005)

5.2 A Navigation Analysis Tool (NAT) to evaluate spatial behaviour patterns

The complexity of spatial behaviour makes it necessary to develop automated analysis tools suitable for the computation of meaningful parameters (Dalm et al. 2000; Drai and Golani 2001; Graziano et al. 2003). Unfolding the spatial behaviour process by observing it through a multidimensional parameter space may yield heavy computational loads, especially if the temporal resolution of the observables is high (e.g., ms). As a consequence, the issue of automating the analysis procedures is relevant to the purpose of *(i)* optimising the use of available resources (especially time), *(ii)* improving the reliability of the analysis of large data sets.

We developed a new Navigation Analysis Tool (NAT) (Petit & Arleo et al. 2005) to extend the set of parameters classically used to quantify spatial navigation (e.g., escape latency). NAT was designed to better investigate the ability of a subject to acquire a motor behaviour that optimises the execution of goal-directed trajectories. Thus, NAT permits a **detailed characterisation of the trajectory patterns**. We employed NAT to assess the navigation performances of control and L7-PKCI mice solving both the starmaze and the Morris water maze (Burguière et al. 2005). In fact, NAT was programmed to account for a specific set of parameters adapted to the form of the starmaze apparatus (i.e., presence of alleys).

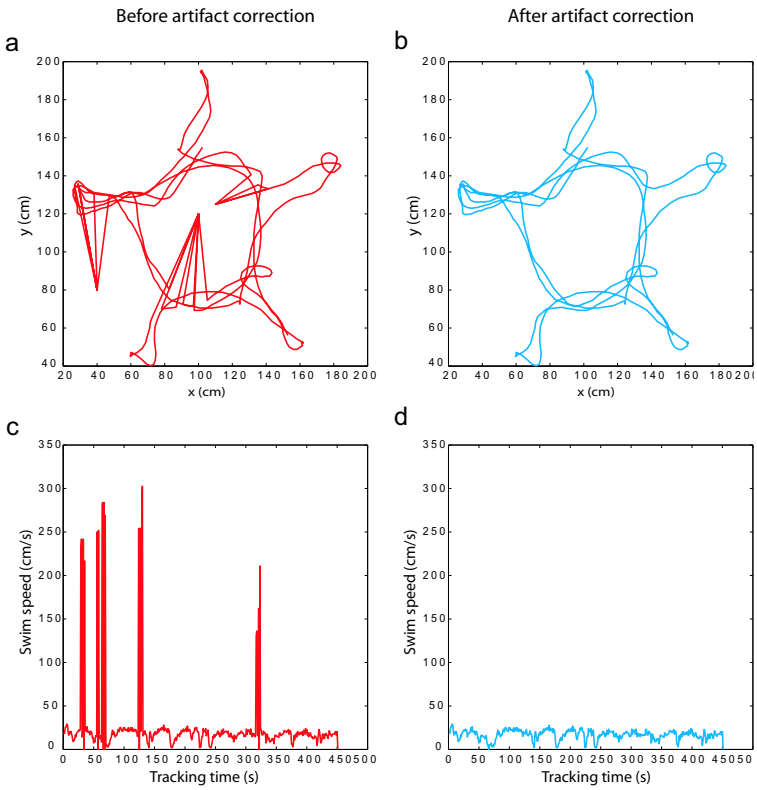

Figure 5.6: Example of artifact correction performed by NAT. Representations of a mouse's trajectory before **(a)** and after **(b)** applying the artifact correction algorithm. **(c)** and **(d)** Speed profiles before and after artifact correction, respectively. (Taken from Petit & Arleo et al. 2005)

A video-tracking system provided, for each training session, a time series of the animal positions $\{t, x(t), y(t)\}$, where x, y denote the cartesian coordinates of the body image sampled every $\Delta t = 40$ ms. However, the recorded traces can occasionally be affected by spurious data leading to inaccurate measures of the animal's spatial coordinates over time. Thus, as a first step, NAT pre-processes the time series to denoise them and to correct possible artifacts automatically (Fig. 5.6). After the artifact correction, NAT measures the following set of **basic parameters**:

- spatial locations are sampled by means of a uniform grid;
- each grid cell is given a value according to the measured function, which are the occupancy value normalised relative to the duration of the trial, the mean instantaneous speed in that area, and the sum of body rotation angles in that area;
- these grid-based functions are then averaged over all the trials of a subject (and eventually over all the trials of the subjects of a same group) and the mean values are used to perform some statistical tests (e.g., T-test) to evaluate the significance of the intergroup differences.

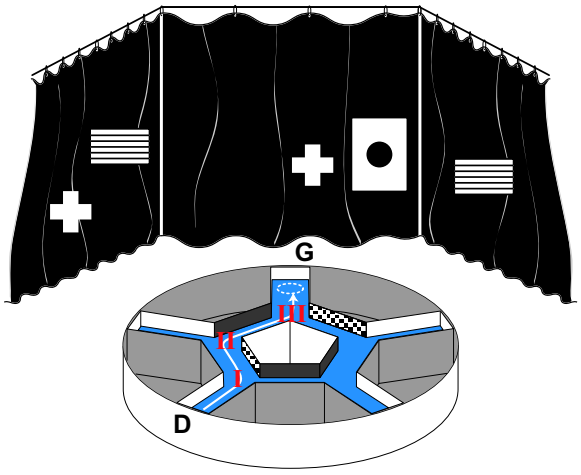

Figure 5.7: The 'multiple strategies' protocol of the starmaze. The alleys forming the central pentagonal ring have either black or chessboard-like walls, whereas the radial alleys have white walls. The maze is placed inside a black square curtain with distal visual cues attached on the curtains (crosses, circle, black and white stripes). D is the departure location, G is the goal consisting of an immerged platform (dotted circle). The arrow represents the optimal trajectory. To use optimal trajectory, animals have to go through to intersection I, then II, and finally III. (Taken from Petit & Arleo et al. 2005)

- the mean escape (or time-to-goal) latency;
- the mean distance covered by the subject before reaching the target;
- the instantaneous and mean travelling speed (useful to compare the escape latencies across trials, this parameter can also be used to characterise different training phases, Verbitsky et al. 2004);
- the mean and the cumulative distances between the animal and the target, $\bar{d} = \langle d(t) \rangle_{t \in [0,T]}$ and $D = \sum_{t \in [0,T]} d(t)$, respectively, where $d(t)$ is the subject-to-target distance at time t, and T is the duration of a trial (Gallagher et al. 1993);
- the mean and cumulative body rotations, which can inform us about the smoothness of the exploratory trajectory (Wolfer and Lipp 1992) (i.e., at each time step Δt, NAT computes the absolute directional change $\theta(\Delta t) \in [0°, 180°]$; then, it averages over the entire trial, i.e. $\bar{\theta} = \langle \theta(\Delta t) \rangle_{\Delta t \in T}$; and it also computes the cumulative angle $\Theta = \sum_{\Delta t \in T} \theta(\Delta t)$);
- the mean absolute egocentric angle $\bar{\phi} = \langle \phi(t) \rangle_{\Delta t \in T}$, where $\phi(t)$ is the angular deviation at time t between the optimal direction towards the target and the actual motion direction of the animal; the smaller the mean angle $\bar{\phi}$ the more the trajectory is optimal in terms of deviation from an ideal goal-directed trajectory;
- the time spent on average by a subject within some user-defined functionally relevant regions (e.g., the goal region) (Graziano et al. 2003).

The latter measure (i.e., the mean spatial occupancy) is then generalised in order to *(i)* remove any prior hypothesis about the relevance of specific regions, *(ii)* evaluate some location-dependent functions other than occupancy, *(iii)* increase the spatial resolution of the assessed functions. To do that, NAT performs a **grid-based behaviour analysis**: Finally, NAT computes a **specific set of parameters adapted to the starmaze setup**. In the starmaze task (Fig. 5.7), given a departure point D, the optimal trajectory to the goal G corresponds to a unique sequence of alleys. Nat measures:

- the number of visited alleys before reaching the goal, which is inversely proportional to the navigation performance;
- the specific sequences of visited alleys, which allows us to label and enumerate the subject's trajectories;
- the directions taken by the animal at specific choice points (e.g., intersections) of the maze.

The latter measures, which aims at **segmenting the animal trajectory into local decision events**, is carried out at different detail levels:

- at the first level, NAT considers all the intersection points visited by the subject as mutually independent (both spatially and temporally); then it scores each of them positively (negatively) if the choice made by the animal was adequate (inappropriate) relative to the optimal trajectory; finally it averages over all the choice points to assess the policy adopted by the subject over the entire trial;
- at the second level, NAT considers only the subset of intersections belonging to a specific sequence of alleys (e.g., the optimal goal-directed sequence) and scores them independently at each visit of the animal; then, for each choice point, it computes a mean score by averaging over all the times the animal passed through that intersection during a trial; these mean scores tell us about the ability of the subject to make, on average, the right choices at specific (spatially relevant) intersection points; finally, NAT stores the score obtained by the subject the very first time it has encountered each choice point; the larger these first-visit scores, the more the navigation policy learned by the animal tends to an automated optimal motor behaviour;
- at the third level, NAT focuses again on the subset of intersections belonging to a specific alley sequence (e.g., intersections I, II, and III of Fig. 5.7), but it takes into account their spatio-temporal relations (in contrast to the second level where it considers them as independent events). Let us assume, for instance, that the animal encounters the intersection point II at time t and that it takes the correct direction towards the goal (i.e., it turns to the right). Then, NAT computes the following score $s_{II} = 1/M_t$, where M_t is the number of alleys visited by the subject since its last visit of the intersection point I and before encountering the choice point II (at time t). At the end of each trial, NAT calculates the mean score

$\bar{C}_{II} = \langle s_{II}(t) \rangle_{t \in [0,T]}$ by averaging over all the times the animal has visited the intersection point II during a trial. In a similar way, NAT generates the mean scores $\bar{C}_I = \langle s_I(t) \rangle_{t \in [0,T]}$ and $\bar{C}_{III} = \langle s_{III}(t) \rangle_{t \in [0,T]}$; the larger these values, the better the subject has learned the spatio-temporal relations between the intersections of the optimal goal-directed sequence. Finally, similar to the second level, NAT pays a particular attention to the very first time the animal has encountered each of the three choice points. For instance, if the animal made a good choice the first time it visited the intersection II, NAT computes the score $s_{II}(t_{first}) = 1/N$, where N is the number of alleys visited between the first visit to the choice point I and the first visit to II.

Chapter 6

Exploring the Neural Code via Information Theory

Preface. *During my stay at the Neuroscience Group at Sony Computer Science Lab Paris (associate researcher 2004-2005) I had the opportunity to increase the detailedness of my theoretical neuroscience approach and focus on information processing at the level of single neurons. The project (done in collaboration with the Dept. of Physiological and Pharmacological Sciences, University of Pavia and INFM, Italy) aimed at quantifying the information transmission of cerebellar granule cells, and concentrated on the mossy fibre-granule cell (MF-GC) synaptic relay. This system has a peculiar structure because it is characterised by a very limited number of synapses (4 on average), permitting to dissect the noise sources during neurotransmission and to carry out an extensive analysis of the input stimuli.*

A stochastic release model of the MF-GC synapse and a Hodgkin-Huxley-like model of the GC were employed for the numerical simulations. Experimental data were obtained by means of in vitro whole-cell patch recordings of GCs. The information transmitted through a single GC was quantified before and after induction of long-term synaptic plasticity (LTP/LTD) at MF-GC synapses. Also, attention was payed to the role of spike time correlations across the MF inputs in regulating information transfer. Our results indicate that a major amount of information is conveyed by the spike time correlations across the inputs and that short- and long-term synaptic plasticity affects the information transmission process significantly. Interestingly, long-term synaptic potentiation increases the average amount of information transmitted, but not necessarily the contribution of the most informative set of stimuli.

This chapter outlines the information theoretic approach adopted for this study and presents some principal findings. This work has only been presented at conferences (Bezzi et al. 2004; D'Angelo et al. 2005; Bezzi et al. 2005; Coenen et al. 2005) and because the main manuscript Bezzi et al. (2005) is under submission procedure, it could not been included in Appendix C.

6.1 Information theoretic analysis

Understanding neural processing requires the knowledge about how information is represented by the activity of neurons (i.e. neural code) (Bezzi et al. 2005). Neurons are complex transmitting devices that encode information in terms of sequences of stereotyped voltage pulses (spikes or action potentials). The information content of these spike trains can be assessed by considering *(i)* their average frequency, *(ii)* their precise timing (e.g., the interspike interval distribution) (Rieke et al. 1997; Gerstner and Kistler 2002), or *(iii)* the exact timing of the first spike (Thorpe et al. 1996).

The approaches accounting for precise spike timing tend to be more efficient from the informative viewpoint because they permit to capture the fine temporal structure of the neural signal. In addition, the temporal pattern of the spike train can affect the dynamics of the synaptic contacts, and hence the processing. For instance, short-term memory effects (i.e., short-term facilitation and depression) may regulate postsynaptic temporal summation in a time-dependent manner (O'Donovan and Rinzel 1997; Buonomano 2000). Therefore, to fully understand information processing in neuronal assemblies we need theoretical tools that allow us to quantify the ability of a specific cell or group of cells to transmit information at different levels of resolutions, and to assess the robustness of this process. In this regard, **information theory** (Shannon 1948) has been proved to be suitable for studying information processing in different brain areas (Rieke et al. 1997). Within this framework it is possible to **quantify the amount of information that a given set of neural responses provides about a specific set of stimuli** or a set of activities of upstream neurons. Furthermore, Shannon information and similar quantities can be used to characterise different coding strategies or to discover the contribution of spatial and temporal correlations to the information transmission (Panzeri et al. 1999; Bezzi et al. 2002).

Mutual information (Shannon 1948) (MI) provides a measure of *how much* information is contained in the neural patterns. In this framework, **neurons can be treated as stochastic communication channels** and MI can be used to measure their transmitting properties. Assessing MI requires to determine the probability distribution of the output spike trains given any input spike train. Given a controlled set of stimuli $\mathcal{S}$, we record the elicited neural responses $r \in \mathcal{R}$ when one stimulus $s \in \mathcal{S}$ is repeatedly presented to the cell according to a prior probability $p(s)$. For example r can be defined in terms of firing rate, or of interspike interval distribution, or of the first spike timing. Once all the data have been collected, the joint probability $p(r,s)$[1] and the response probability distribution $p(r)$ can be estimated. Then, the **mutual information** can be calculated according to:

$$I(\mathcal{S};\mathcal{R}) = \sum_{s\in\mathcal{S}}\sum_{r\in\mathcal{R}} p(r,s)\ \log_2 \frac{p(r,s)}{p(r)p(s)} \tag{6.1}$$

[1]Estimating the joint probabilities from experimental data needs very large samples and it is often unfeasible, but approximation techniques exist (see for instance Panzeri and Treves 1996).

or equivalently in terms of conditional probability $p(r|s) = p(r,s)/p(s)$

$$I(\mathcal{S};\mathcal{R}) = \sum_{s\in\mathcal{S}}\sum_{r\in\mathcal{R}} p(s)p(r|s)\ \log_2\frac{p(r|s)}{p(r)} \tag{6.2}$$

Introducing the entropy $H(\mathcal{R}) = -\sum_{r\in\mathcal{R}} p(r)\log_2 p(r)$ of a probability distribution $p(r)$, we can rewrite Eq. 6.1 as:

$$I(\mathcal{S};\mathcal{R}) = H(\mathcal{R}) - H(\mathcal{R}|\mathcal{S}) \tag{6.3}$$

where $H(\mathcal{R}|\mathcal{S}) \equiv \sum_{s\in\mathcal{S}} p(s)H(\mathcal{R}|s)$ is the conditional entropy.

Shannon's MI provides a quantitative measure of the averaged information transmitted through the synapse by a set of responses given a set of input spike trains (or vice-versa). We were also interested in identifying those stimuli that were best encoded by the GC. Thus, for each stimulus $s \in \mathcal{R}$ we computed the **stimulus specific contribution** to the MI, termed **surprise**:

$$I(s) = \sum_{r\in\mathcal{R}} p(r|s)\log_2\frac{p(r|s)}{p(r)}$$

This allowed us to find the most informative set of stimuli, and to investigate in which conditions the cell coding capability was optimised.

6.2 Quantifying information transmission at cerebellar mossy fibre - granule cell synapses

6.2.1 The cerebellar granule cell constitutes a suitable neuronal channel for information theoretic studies

In most cases, *(i)* the multiple mechanisms of nonlinear integration at individual synapses, *(ii)* the large number of synapses (typically $10^3 - 10^4$), and *(iii)* their location on wide dendritic trees with complex electrotonic and active properties, make it infeasible to perform a thorough information theoretic analysis of the transmission properties of single neurons. Approximations have been attempted via dimensionality reduction of input-output space whereby the effect of an individual synapse on the neuron response was evaluated while considering the rest of the dendritic inputs as background noise (London et al. 2002).

We focused on a "simple" neuron, the cerebellar granule cell (GC), in which the excitatory input space could be explored extensively (Fig. 6.1a). GCs constitute a remarkable exception because: *(i)* they have a compact electrotonic structure (D'Angelo et al. 1995; Silver et al. 1996) and therefore their whole cell membrane can be considered as equipotential, disregarding spatial effects on computation (Koch and Segev 2000); *(ii)* they receive a very low number of mossy fibre (MF) afferents (4 on average) (Eccles et al. 1967; Jakab and Hamori 1988), which generates a tractable number of

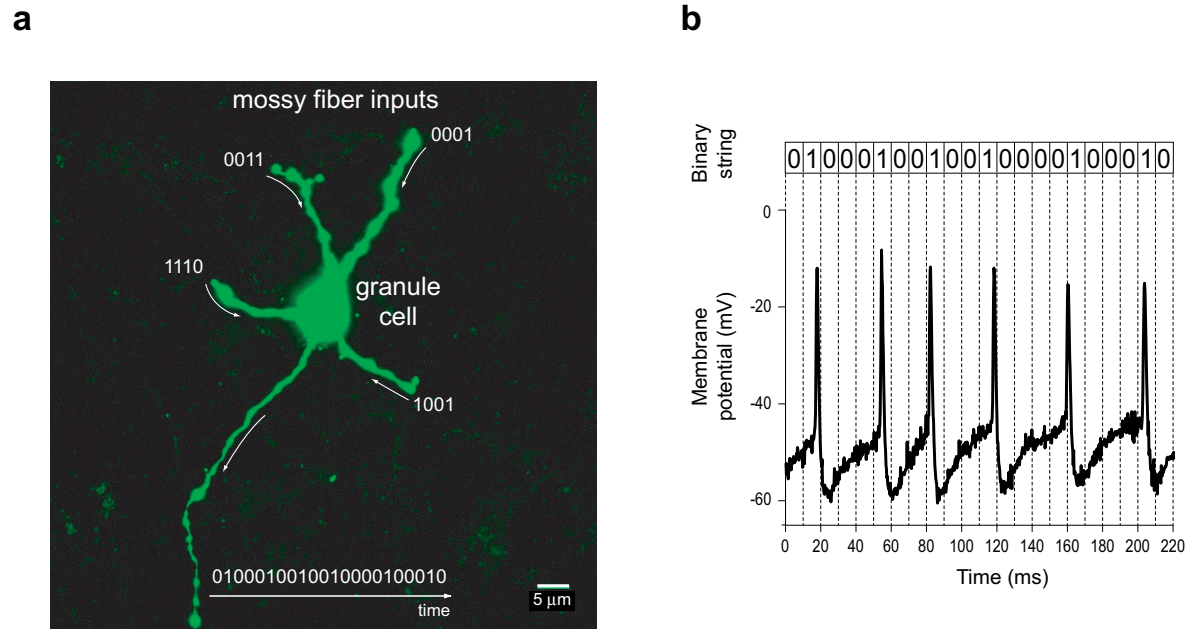

Figure 6.1: Cerebellar granule cell (GC) morphology and digitalization of neural signals. **(a)** Confocal image of a biocytin-stained GC in the rat cerebellum. GCs have a low number of mossy fiber (MF) afferents (4.17 on average). **(b)** The membrane potential of a GC recorded over 220 ms. Spike trains were digitised as strings of 0s and 1s within discrete time bins of 10 ms. (Taken from Bezzi et al. 2005)

possible combinations of presynaptic inputs and reduces the complexity of MI calculation. Moreover, the mechanisms of GCs intrinsic excitability and synaptic transmission and plasticity have been intensely investigated (e.g., D'Angelo et al. 2001; Nieus et al. 2005). GCs are tiny neurons (6 μm diameter, Jakab and Hamori 1988), they are very numerous ($\sim 10^{11}$ in humans, about half of the neurons of the whole brain), and constitute the major input stage of the cerebellum, the granular layer. Mossy fibres (MFs) are the primary afferents to the cerebellar cortex and convey multimodal sensory inputs to the GCs. The MF-GC synaptic transmission constitutes the core of the granular layer computation. Despite the structural simplicity of GCs, the temporal dynamics of the MF-GC synapses call upon the same complex mechanisms mediating information processing at most of brain synapses (Braitenberg 1967; Medina, Garcia, Nores, Taylor, and Mauk 2000). MF-GC synaptic transmission is based on nonlinear transformations determined by presynaptic short-term facilitation and depression, glutamate spillover, postsynaptic AMPA and NMDA receptor gating, and multiple voltage-dependent channel interactions regulating intrinsic electroresponsiveness (D'Angelo et al. 1995; Mitchell and Silver 2003; Nielsen et al. 2004; Sola et al. 2004; Nieus et al. 2005). According to classical theories of Marr (1969) and Albus (1971), the GC layer might encode multimodal afferent MF signals into a sparse representation to facilitate downstream discrimination of input patterns.

6.2.2 A model of the MF-GC synaptic transmission

In order to conjugate fundamental aspects of neurotransmission derived from physiological recordings with a detailed reconstruction of postsynaptic electroresponsiveness, we needed a detailed model of the synaptic transmission at the MF-GC relay (D'Angelo et al. 2005). A model of the GC was derived from D'Angelo et al. (2001). GCs are electrotonically compact (D'Angelo et al. 1995; Silver et al. 1996; Cathala et al. 2003), hence there was little need to simulate dendrites and a mono-compartmental structure was employed. The GC model included four independent synaptic contacts (Nieus et al. 2005), with three releasing sites per synapse. To account for the stochasticity of neurotransmission a stochastic version of the model was developed in which the neurotransmitter release at each site was generated by a probabilistic process modulating glutamate concentration. Independent postsynaptic receptor densities (AMPA and NMDA) could therefore be activated by the corresponding releasing sites according to a stochastic process. In the model, the state of the presynaptic terminal was computed according to a three-state scheme adapted from Tsodyks and Markram (1997). This integrated model permitted a systematic investigation of the multiple mechanisms regulating MF-GC synaptic transmission and driving synaptic plasticity. The NEURON simulator (Hines and Carnevale 2001) was employed to implement and validate the model.

6.2.3 Experimental measure of information transmission at the MF-GC synaptic relay

Experimental data were obtained by means of *in vitro* whole-cell patch clamp recordings of GCs of wistar rats. GC stimulations were carried out by means of a bipolar electrode positioned above the MF bundle (Nieus et al. 2005). To measure MI, one to four MFs were then stimulated simultaneously by a set of spike trains according to a protocol that allowed us to mimic the discharges of GCs following punctuate tactile stimulation *in vivo* (Chadderton et al. 2004). The information transmitted through a single GC was quantified before and after having induced long-term synaptic plasticity (both LTP and LTD) at MF-GC synapses, a condition known to modify the release probability at the MF synaptic terminals (Sola et al. 2004).

6.2.4 Outline of principal results

First, both our experimental and numerical results indicated that **the temporal structure of the spike trains conveys a large fraction of the total information transmitted**. We measured MI either by characterising the GC responses by means of their spike frequency, or by considering each spike train as a binary string, in which the position of each spike mattered (Fig. 6.1b). On average, the average amount of information carried by the firing frequency was 51%, meaning that half of the information transfer was due to temporal interspike relationships.

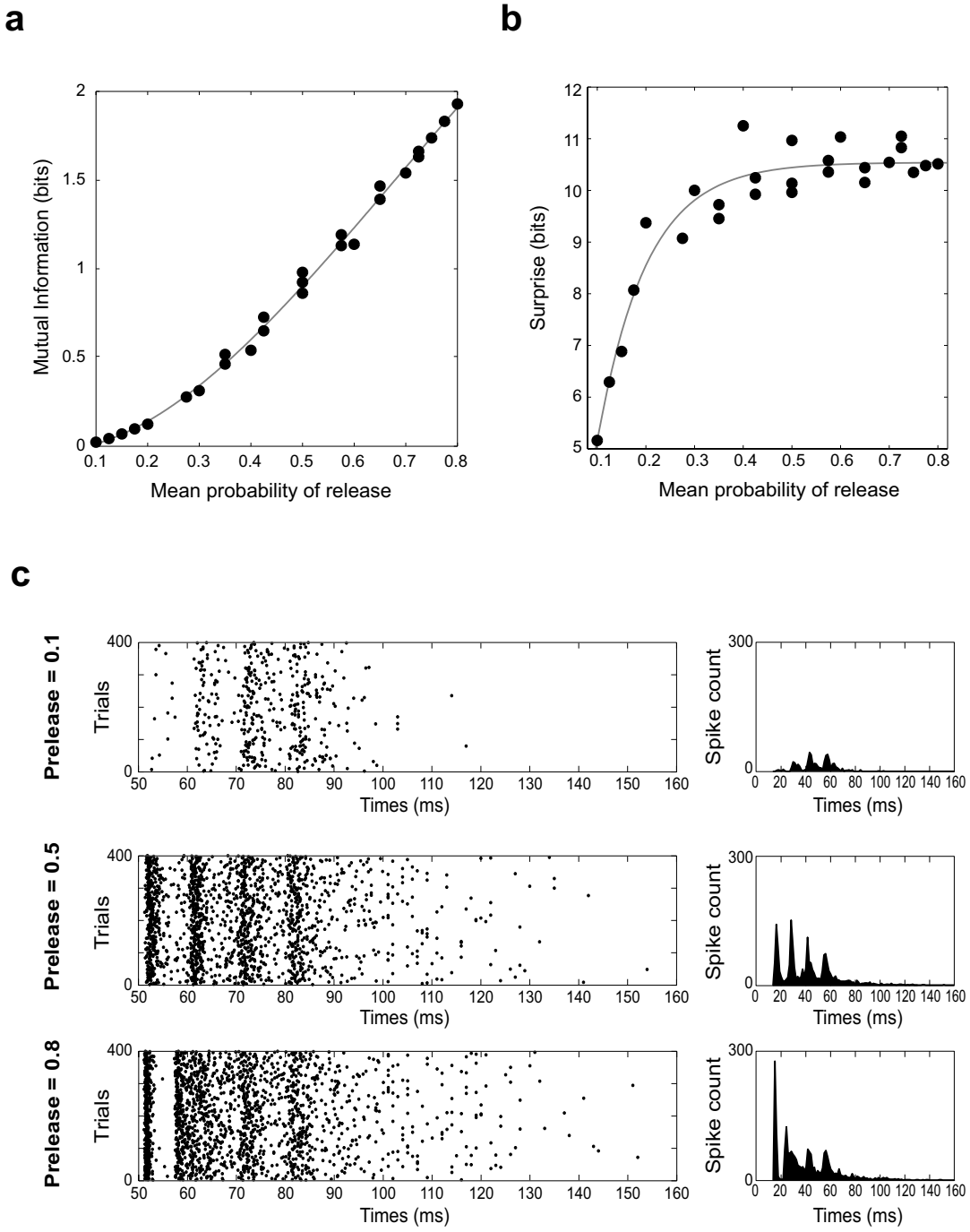

Figure 6.2: The effect of long-term plasticity upon MI and on the information transmitted by the subset of most informative inputs. **(a)** MI calculated by stimulating the formal MF-GC synapses with a rather large stimulus set (65536 stimuli) and by varying the release probability p on the four MFs independently, within the range $[0.1, 0.8]$. Each data point indicates the MI value corresponding to a different combination of p across the four MFs, and the x-axis provides the p averaged over the four MFs (therefore, different MI values can coexist for any value of p averaged). **(b** The mean surprise (averaged over the subset of stimuli with a surprise larger than 90% of the maximum surprise value) tends to a plateau as the mean release probability p (averaged over the four MF-GC synapses) is increased. **(c)** GC responses (spikegrams, left, and PSTH, right) to one of the most surprising stimuli ("1111" on all 4 MFs as indicated by the arrows) for three different values of release probability. This is an illustrative example of the general process described above in b. (Taken from Bezzi et al. 2005)

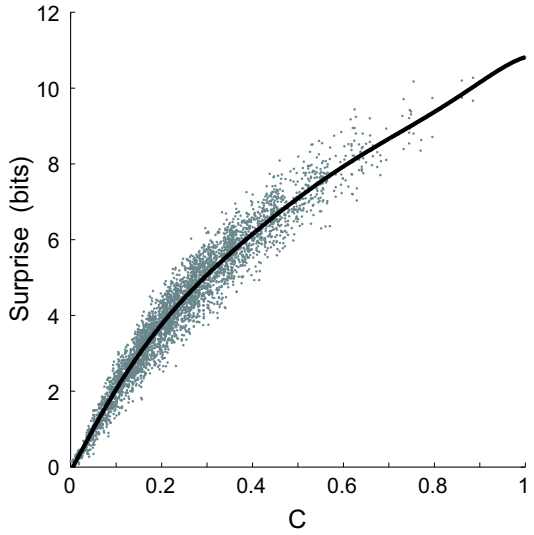

Figure 6.3: Correlated activity across the inputs contributes to information transmission. On average, the larger the temporal correlation coefficient C, which measures the average number of coincident spikes across the four MF afferents, the larger the surprise the information transmitted by a stimulus. (Adapted from Bezzi et al. 2005)

Second, again both experiments and theory showed that **long-term potentiation (LTP)**, which increases neurotransmitter release probability p, **affects the information transfer dynamics by enhancing MI significantly** (see Fig. 6.2a for the relationship between MI and p as predicted by the theoretical model). This finding suggested that optimal transmission might correspond to large p values.

To further investigate this hypothesis we run a series of numerical simulations to analyse the effect of long-term synaptic plasticity upon the information transmitted by the subset of the most informative stimuli. Fig. 6.2b shows the mean surprise as function of the release probability p. After an initial rapid growth, the surprise tended to a plateau. Thus, maximal transmission of the most informative inputs occurs already at intermediate values of p ($0.4 \leq p \leq 0.5$). Fig. 6.2c displays the GC responses to one of the most surprising stimuli for three different values of release probability. When p increased from 0.1 to 0.5, the time locking of the cell response to the input stimulation improved, augmenting information transmission. However, for larger p values (e.g., $p = 0.8$) short-term depression reduced the AMPA transients and depolarisation became driven by smoothly-varying currents (like the NMDA and persistent Na+ current) (D'Angelo et al. 2001; Nieus et al. 2005) decreasing the probability of having precise stimulus-elicited response spikes. Therefore, **although on average MI was maximised by LTP, an efficient transmission of most informative stimuli occurred at intermediate values of neurotransmitter release**, comparable to those measured in vitro in standard conditions (Sola et al. 2004).

The above findings may suggest that neurons as well as synaptic plasticity mechanisms have evolved for optimising the transmission of a limited set of relevant stimuli. We further examined the input spike train patterns to identify those features (e.g., dis-

charge frequency and spatio-temporal structure) that are relevant to optimal information transfer. Stimuli with large firing rates were usually highly informative, indicating that the spike count contributed to information transmission. Nevertheless, as noted above, information was not only encoded just in terms of spike count. We examined the most informative stimuli and noticed that they tended to be characterised by the presence of multiple coincident spikes across the four MFs, whereas no coincident spikes were observed in the least informative inputs. This result indicated that **correlated activity across the four MF afferents may largely contribute to information transmission**. To test this hypothesis, we measured the information transmitted by each stimulus as a function of the amount of temporal correlation C across the four MFs. Fig. 6.3 shows that, on average, the larger C, the larger the information transmitted by a stimulus. These results showed that the correlation across distinct afferent signals largely contributed to the information transferred by the neuron and they extended previous studies showing that GC firing requires the co-activation of two or more MFs (D'Angelo et al. 1995).

Chapter 7

Conclusions and Future Perspectives

The research work presented in this dissertation is characterised by a cross-disciplinary approach that brings together experimental, theoretical, and robotic techniques. This integrative neuroscience methodology can be employed to study the neural principles underlying the ability of animals to interact with their environment, process multimodal sensory information, and learn low-level sensory-motor couplings as well as more abstract context representations supporting flexible spatial behaviour.

The projects outlined by Chapters 3, 4, 5, and 6 have all given rise to collaborations and/or supervisions of master and Ph.D. works that are still ongoing. Thereupon, extending/improving most of the studies described in this report will constitute a large body of my future research.

Spatial learning and navigation in neuromimetic systems. A biologically-inspired model of the neural bases of spatial learning and goal-oriented navigation has been presented in Chapter 3. The model, which has been tested on a mobile robotic platform, reproduces the place and directional coding provided by hippocampal place (HP) and head direction (HD) cells, respectively. It also demonstrates that combining allothetic and idiothetic spatial information is crucial for generating reliable spatial memories. This model, which has already been extended thanks to the collaborations with W. Gerstner (Laboratory of Computational Neuroscience, Ecole Polytechnique Fédérale de Lausanne, EPFL) and J.-A. Meyer (Animatlab, Université Paris VI), has now become a module for a European integrated project (named ICEAbot, 2006-2010). Among the objectives of the international consortium that conceived ICEAbot there is the aim of synthesising a neuromimetic spatial learning system accounting for motivation-based action selection and for the anatomo-functional interactions between the hippocampus, several neocortices, the amygdala, and the basal ganglia. Furthermore, together with A. Guillot (Animatlab, Université Paris VI), we are supervising a Ph.D. project (2004-2007) that aims at extending the neuromimetic spatial cognition model by studying the role of the hippocampus-prefrontal cortex interaction (e.g., for “mental” planning of navigation trajectories).

Head direction cells: electrophysiological recordings. A series of electrophysiolog-

ical experiments focusing on the directional selective discharges of HD cells in the rat anterodorsal thalamic nuclei (ADN) has been outlined in the first part of Chapter 4. These experiments shed some light on the control of static (e.g., environmental landmarks) and dynamic (e.g., optic field flow) visual information upon HD cell activity. They also provide some insights on the relationship between the HD cell firing rate and the hippocampal theta rhythm. The study concerning the effect of visual optic field flow on the HD cell coding is being continued in collaboration with S. I. Wiener (Laboratory of Physiology of Perception and Action, LPPA, CNRS-Collège de France, Paris). In the future, we will attempt to complement our electrophysiological findings with a series of psychophysical experiments with subjects undergoing the same type of optical field flow stimulation. This might produce some results on the effect of vection phenomena (i.e., the self-motion perception induced by an optic field flow) upon the sense of direction of humans undertaking a spatial task. In particular, this might allow us to link the results at the level of single-cell discharges (i.e., ADN HD neurons) with those concerning high-level illusory perception in humans.

Head direction cells: theoretical modelling. A theoretical model of the HD cell system has been presented in the second part of Chapter 4. The objective of this theoretical work was to investigate (both analytically and numerically) the mechanisms underlying *(i)* the generation and maintenance of the directional coding of a large population of formal HD neurons; *(ii)* the integration of vestibular-like information (e.g., angular velocity signals); *(iii)* the update of the ensemble HD cell activity following reorienting visual cues. This work is the result of a collaboration with N. Brunel (Laboratory of Neurophysics and Physiology of the Motor System, Université Paris V) and S. I. Wiener (LPPA, CNRS-Collège de France, Paris). In the current version of the model, only static visual stimuli are employed to update the HD cell representation. A further step will consist of incorporating the dynamic visual signals (e.g., optic field flow) that may converge onto the HD cell circuit via the accessory optic system. This will allow us to study the mechanisms regulating the dynamics of the progressive shift of the preferred directions of ADN HD cells observed experimentally in the presence of visual optic flow.

The role of the cerebellum in spatial cognition. A behavioural study investigating how cerebellar learning can promote spatial navigation has been described in Chapter 5. This work has employed L7-PKCI mice, a transgenic model that lacks long-term synaptic depression (LTD) at the parallel fibre-Purkinje cell (PF-PC) synapses. The main result of this study is that PF-PC LTD (i.e., a mechanism at the synaptic level) may contribute to the procedural component of spatial navigation, in the sense it may mediate the adaptive tuning of navigation trajectories (planned outside the cerebellum) according to the ongoing sensory-motor contexts. This work has recently given rise to a theoretical study done in collaboration with L. Rondi-Reig (LPPA, CNRS-Collège de France), who led the original behavioural study, and N. Brunel (Laboratory of Neurophysics and Physiology of the Motor System, Université Paris V). The objective of this theoretical work consists of modelling the cerebellar macrocircuit (including mossy fibres, granule cells, parallel fibres, Purkinje cells, deep cerebellar nuclei, inferior olive, and interneurons such as Golgi cells) and to mimic the long-term synaptic plasticity oc-

curring at the synaptic relays of this network. This will allow us, for instance, to emulate a deficit of PF-PC LTD and, hopefully, to reproduce the same procedural impairments observed in L7-PKCI mice. Also, this will help us to study how synaptic modifications occurring at other learning sites of the cerebellar network (e.g., between the mossy fibres and the deep cerebellar nuclei) may compensate for the PF-PC LTD deficit.

Neural information processing and optimal neural coding. A study investigating neural information processing at the major input stage of the cerebellum, i.e. the granular layer, has been presented in Chapter 6. This work focuses on the information transmission properties of single granule cells (GCs) and has been carried out using both theoretical (i.e., Hodgkin-Huxley-like modelling) and experimental (i.e., in vitro patch-clamp recordings of rat GCs) methods. The cytoarchitectural properties of GCs (e.g., the fact they only receive four afferent synapses and they have a compact electrotonic structure) make them suitable for an information theoretic analysis of their input-output relationships. Both theory and experiments show that long-term synaptic plasticity influences the GC information transfer significantly and they support the hypothesis that the temporal structure of the spike trains (as opposed to their firing rate) conveys a large amount of information. This work, done in collaboration with O. Coenen (Neuroscience Group, CSL Sony, Paris) and E. D'Angelo (Dept. of Physiological and Pharmacological Sciences, University of Pavia and INFM, Italy), is now being extended along two main directions. First, the effect of changes of the cell's intrinsic excitability on information transmission will be investigated. Intrinsic electroresponsiveness will be regulated through the modulation of voltage-dependent ionic channel conductances (e.g., partial blockades of hyperpolarising K^+ channels or depolarising Ca^{2+} currents), or through the modulation of the cell's recovery time delay. Second, the information theoretic analysis will be extended to study a population of GCs. The cerebellar granular layer receives a large spectrum of afferent sensory signals and our information transmission analysis may help us to test the hypothesis that GCs provide an efficient encoding of multiple sensory-motor contexts to facilitate learning (e.g., to reduce destructive interference) at downstream synaptic relays (e.g., parallel fibre-Purkinje cell synapses).

Besides the new (ongoing) works described above, there are two future projects that will capitalise (principally) on the collaboration with L. Rondi-Reig (LPPA, CNRS-Collège de France). The first concerns a spatial learning study to investigate the functional interaction between the cerebellum (which is likely to mediate procedural-like memory) and the hippocampus (which mediates declarative memory). This study will involve both experiments (e.g., extracellular recordings) and theoretical methods (e.g., structural modelling). The second project will attempt to model the principal mechanisms regulating synaptic plasticity (e.g., the activation of NMDA receptors during induction of LTP) in the hippocampus, and to emulate high-level spatial memory impairments produced by deficits in these (low-level) plasticity mechanisms. This study will complement an ongoing experimental work (directed by J. Mariani of the Laboratory of Neurobiology of Adaptive Processes, Université Paris VI, and L. Rondi-Reig of the LPPA, CNRS-Collège de France) that aims at characterising the molecular and cellular bases of spatial orientation deficits in aged subjects.

Bibliography

Ahmed, A. K. M. F., N. G. Guison, and T. Yamadori (1996). A retrograde fluorescent-labeling study of direct relationship between the limbic (anterodorsal and anteroventral thalamic nuclei) and the visual system in the albino rat. *Brain Research 729*, 119–123.

Albo, Z., G. V. D. Prisco, and R. P. P. Vertes (2003). Anterior thalamic unit discharge profiles and coherence with hippocampal theta rhythm. *Thalamus & Related Systems 2*, 133–144.

Albus, J. S. (1971). A theory of cerebellar function. *Math Biosc 10*, 25–61.

Allen, G. V. and D. A. Hopkins (1988). Mamillary body in the rat: a cytoarchitectonic, Golgi, and ultrastructural study. *Journal of Comparative Neurology 275(1)*, 39–64.

Allen, G. V. and D. A. Hopkins (1989). Mamillary body in the rat: topography and synaptology of projections from the subicular complex, prefrontal cortex, and midbrain tegmentum. *Journal of Comparative Neurology 286*, 311–336.

Allen, G. V. and D. A. Hopkins (1990). Topography and synaptology of mammillary body projections to the mesencephalon and pons in the rat. *Journal of Comparative Neurology 301*, 214–231.

Amari, S. I. (1977). Dynamics of pattern formation in lateral-inhibition type neural fields. *Biological Cybernetics 27*, 77–87.

Arleo, A. (2000). *Spatial learning and navigation in neuromimetic systems, modeling the rat hippocampus*. ISBN 3-89825-247-7, Verlag-dissertation.

Arleo, A., F. Battaglia, C. Déjean, M. B. Zugaro, and S. I. Wiener (2005). Rat anterodorsal thalamic head direction neurons are modulated by hippocampal theta rhythm. In *Society for Neuroscience Abstracts*, pp. No. 198.18.

Arleo, A., C. Déjean, C. Boucheny, M. Khamassi, M. B. Zugaro, and S. I. Wiener (2004). Optic field flow signals update the activity of head direction cells in the rat anterodorsal thalamus. In *4th Forum of European Society for Neuroscience*, pp. 2:A007.19.

Arleo, A., C. Déjean, C. Boucheny, M. Khamassi, M. B. Zugaro, and S. I. Wiener (2006). Optic field flow signals update the activity of head direction cells in the rat anterodorsal thalamus. *(in preparation)*.

Arleo, A. and W. Gerstner (2000a). Modeling rodent head-direction cells and place cells for spatial learning in bio-mimetic robotics. In J.-A. Meyer, A. Berthoz, D. Floreano, H. Roitblat, and S. W. Wilson (Eds.), *From Animals to Animats VI*, Cambridge MA, pp. 236–245. MIT Press.

Arleo, A. and W. Gerstner (2000b). Spatial cognition and neuro-mimetic navigation: A model of hippocampal place cell activity. *Biological Cybernetics 83*, 287–299.

Arleo, A. and W. Gerstner (2001). Spatial orientation in navigating agents: Modeling head-direction cells. *Neurocomputing 38-40(1-4)*, 1059–1065.

Arleo, A. and W. Gerstner (2005). Head direction cells and place cells in models for navigation and robotic applications. In S. I. Wiener and J. S. Taube (Eds.), *Head direction cells and the neural mechanisms of spatial orientation*, Chapter 19. MIT Press.

Arleo, A. and L. Rondi-Reig (2005). Multimodal sensory integration and concurrent navigation strategies for spatial cognition in real and artificial organisms. In F. Dolins and R. Mitchell (Eds.), *Spatial Perception and Spatial Cognition*, Chapter 11. Cambridge University Press.

Arleo, A., F. Smeraldi, and W. Gerstner (2004). Cognitive navigation based on non-uniform Gabor space sampling, unsupervised growing networks, and reinforcement learning. *IEEE Transactions on Neural Networks 15(3)*, 639–652.

Arleo, A., F. Smeraldi, S. Hug, and W. Gerstner (2001). Place Cells and Spatial Navigation based on 2D Feature Extraction, Path Integration, and Reinforcement Learning. In T. K. Leen, T. G. Dietterich, and V. Tresp (Eds.), *Advances in Neural Information Processing Systems 13*, pp. 89–95. MIT-Press.

Arleo, A. & F. Battaglia, M. B. Zugaro, and S. I. Wiener (2005). Theta modulation of head direction cell discharges in the anterodorsal thalamic nucleus (submitted).

Barnes, C. A., M. S. Suster, J. Shen, and B. L. McNaughton (1997). Multistability of cognitive maps in the hippocampus of old rats. *Nature 388(6639)*, 272–275.

Bassett, J. P. and J. S. Taube (2001a). Lesions of the dorsal tegmental nucleus of the rat disrupt head direction cell activity in the anterior thalamus. *Society for Neuroscience Abstracts 27*, 852.29.

Bassett, J. P. and J. S. Taube (2001b). Neural correlates for angular head velocity in the rat dorsal tegmental nucleus. *The Journal of Neuroscience 21(15)*, 5740–5751.

Battaglia, F. P. and A. Treves (1998). Attractor neural networks storing multiple space representations: a model for hippocampal place fi elds. *Physical Review E 58*, 7738–7753.

Ben-Yishai, R., D. Hansel, and H. Sompolinsky (1997). Traveling waves and the processing of weakly tuned inputs in a cortical network module. *Journal of Computational Neuroscience 4*, 57–77.

Ben-Yishai, R., R. Lev Bar-Or, and H. Sompolinsky (1995). Theory of orientation tuning in visual cortex. *Proceedings of the National Academy of Sciences USA 92*, 3844–3848.

Best, P. J., A. M. White, and A. Minai (2001). Spatial processing in the brain: The activity of hippocampal place cells. *Annual Review of Neuroscience 24*, 459–486.

Bezzi, M., A. Arleo, and O. J.-M. D. Coenen (2005). Exploring the neural code by information theory. In *Proceedings of the NeuroMat Workshop*, Milan, Italy.

Bezzi, M., A. Arleo, T. Nieus, A. D'Errico, E. D'Angelo, and O. J.-M. Coenen (2005). Quantitative characterization of information transmission in a neuron. *(submitted)*.

Bezzi, M., M. Diamond, and A. Treves (2002). Redundancy and synergy arising from correlations in large ensembles. *Journal of Computational Neuroscience 12*, 165–174.

Bezzi, M., T. Nieus, A. Arleo, E. D'Angelo, and O. J.-M. Coenen (2004). Information transfer at the mossy fi ber-granule cell synapse of the cerebellum. *Society for Neuroscience Abstracts 827.5*.

Biegler, R. and R. G. M. Morris (1993). Landmark stability is a prerequisite for spatial but not discrimination learning. *Nature 361*, 631–633.

Blair, H. T., J. Cho, and P. E. Sharp (1998). Role of the lateral mammillary nucleus in the rat head direction circuit: A combined single unit recording and lesion study. *Neuron 21*, 1387–1397.

Blair, H. T. and P. E. Sharp (1995). Anticipatory head direction signals in anterior thalamus: Evidence for a thalamocortical circuit that integrates angular head motion to compute head direction. *The Journal of Neuroscience 15(9)*, 6260–6270.

Blair, H. T. and P. E. Sharp (1996). Visual and vestibular infl uences on head-direction cells in the anterior thalamus of the rat. *Behavioral Neuroscience 110(4)*, 643–660.

Bostock, E., R. U. Muller, and J. L. Kubie (1991). Experience-dependent modifi cations of hippocampal place cell fi ring. *Hippocampus 1(2)*, 193–206.

Boucheny, C., N. Brunel, and A. Arleo (2005). A continuous attractor network model without recurrent excitation: maintenance and integration in the head direction cell system. *Journal of Computational Neuroscience 18(2)*, 205–227.

Braitenberg, V. (1967). Is the cerebellar cortex a biological clock in the millisecond range? *Prog Brain Res 25*, 334–346.

Brown, M. A. and P. E. Sharp (1995). Simulation of spatial-learning in the Morris water maze by a neural network model of the hippocampal-formation and nucleus accumbens. *Hippocampus 5*, 171–188.

Buonomano, D. V. (2000). Decoding temporal information: A model based on short-term synaptic plasticity. *The Journal of Neuroscience 20(23)*, 1129–1141.

Burgess, N., K. J. Jeffery, and J. O'Keefe (1999). Integrating hippocampal and parietal functions: a spatial point of view. In N. Burgess, K. J. Jeffery, and J. O'Keefe (Eds.), *The Hippocampal and Parietal Foundations of Spatial Cognition*, Chapter 1, pp. 3–29. Oxford University Press.

Burgess, N., E. A. Maguire, and J. O'Keefe (2002). The human hippocampus and spatial and episodic memory. *Neuron 35(4)*, 625–641.

Burgess, N. and J. O'Keefe (1996). Neuronal computations underlying the fi ring of place cells and their role in navigation. *Hippocampus 6*, 749–762.

Burgess, N., M. Recce, and J. O'Keefe (1994). A model of hippocampal function. *Neural Networks 7*, 1065–1081.

Burguière, E., A. Arleo, M. R. Hojjati, Y. Elgersma, C. I. DeZeeuw, A. Berthoz, and L. Rondi-Reig (2005). Spatial navigation impairment in mice lacking cerebellar LTD: a motor adaptation defi cit? *Nature Neuroscience 8(10)*, 1292–1294.

Buzsáki, G. (1996). The hippocampo-neocortical dialogue. *Cerebral Cortex 6*, 81–92.

Buzsáki, G. (2002). Theta oscillations in the hippocampus. *Neuron 33*(3), 325–340.

Buzsáki, G., L. S. Chen, and F. H. Gage (1990). Spatial organization of physiological activity in the hippocampal region: Relevance to memory formation. *Progress in Brain Research 83*, 257–268.

Camperi, M. and X.-J. Wang (1998). A model of visuospatial short-term memory in prefrontal cortex: recurrent network and cellular bistability. *Journal of Computational Neuroscience 5*, 383–405.

Cathala, L., S. Brickley, S. Cull-Candy, and M. Farrant (2003). Maturation of EPSCs and intrinsic membrane properties enhances precision at a cerebellar synapse. *The Journal of Neuroscience 23(14)*, 6074–6085.

Chadderton, P., T. W. Margrie, and M. Häusser (2004). Integration of quanta in cerebellar granule cells during sensory processing. *Nature 428(6985)*, 856–860.

Chavarriaga, R. and W. Gerstner (2004). Combining visual and proprioceptive information in a model of spatial learning and navigation. In *Proceedings 2004 International Joint Conference on Neural Networks (IJCNN'2004)*, pp. 603–608. IEEE Press.

Chavarriaga, R., T. Strösslin, D. Sheynikhovich, and W. Gerstner (2005). A computational model of parallel navigation systems in rodents. *Neuroinformatics 3(3)*, 223–242.

Chen, L. L., L. Lin, C. A. Barnes, and B. L. McNaughton (1994). Head-direction cells in the rat posterior cortex. II. Contributions of visual and idiothetic information to the directional fi ring. *Experimental Brain Research 101*, 23–34.

Chen, L. L., L. Lin, E. J. Green, C. A. Barnes, and B. L. McNaughton (1994). Head-direction cells in the rat posterior cortex. I. Anatomical distribution and behavioral modulation. *Experimental Brain Research 101*, 8–23.

Cho, J. and P. E. Sharp (2001). Head direction, place, and movement correlates for cells in the rat retrosplenial cortex. *Behavioral Neuroscience 115(1)*, 3–25.

Coenen, O. J.-M., M. Bezzi, A. Arleo, T. Nieus, A. D'Errico, and E. D'Angelo (2005). Quantitative characterization of information transmission in a single neuron. *Society for Neuroscience Abstracts 823.3*.

Collingridge, G. L., S. J. Kehl, and H. McLennan (1983). Excitatory amino acids in synaptic transmission in the Schaffer collateral-commissural pathway of the rat hippocampus. *The Journal of Physiology 334*, 33–46.

Compte, A., N. Brunel, P. S. Goldman-Rakic, and X.-J. Wang (2000). Synaptic mechanisms and network dynamics underlying spatial working memory in a cortical network model. *Cerebral Cortex 10*, 910–923.

Cressant, A., R. U. Muller, and B. Poucet (1997). Failure of centrally placed objects to control fi ring fi elds of hippocampal place cells. *The Journal of Neuroscience 17(7)*, 2531–2542.

Dalm, S., J. Grootendorst, E. R. de Kloet, and M. S. Oitzl (2000). Quantifi cation of swim patterns in the Morris water maze. *Behavior research methods, instruments, & computers 32(1)*, 134–139.

D'Angelo, E., G. De Filippi, P. Rossi, and V. Taglietti (1995). Synaptic excitation of individual rat cerebellar granule cells in situ: evidence for the role of NMDA receptors. *The Journal of Physiology 484*, 397–413.

D'Angelo, E., T. Nieus, M. Bezzi, A. Arleo, and O. J.-M. D. Coenen (2005). Modeling synaptic transmission and quantifying information transfer in the granular layer of the cerebellum. In J. Cabestany, A. Prieto, and D. F. Sandoval (Eds.), *Artifi cial Neural Networks, Computational Intelligence and Bioinspired Systems*, pp. 107–114. Springer-Verlag LNCS series.

D'Angelo, E., T. Nieus, A. Maffei, S. Armano, P. Rossi, V. Taglietti, A. Fontana, and G. Naldi (2001). Theta-frequency bursting and resonance in cerebellar granule cells: experimental evidence and modeling of a slow k+-dependent mechanism. *The Journal of Neuroscience 21(3)*, 759–770.

Dayan, P. and T. Sejnowski (1994). TD(λ) converges with probability 1. *Machine Learning 14*, 295–301.

De Zeeuw, C. I., C. Hansel, F. Bian, S. K. Koekkoek, A. M. van Alphen, D. J. Linden, and J. Oberdick (1998). Expression of a protein kinase C inhibitor in Purkinje cells blocks cerebellar LTD and adaptation of the vestibulo-ocular reflex. *Neuron 20*(3), 495–508.

De Zeeuw, C. I., J. I. Simpson, C. C. Hoogenraad, N. Galjart, S. K. Koekkoek, and T. J. Ruigrok (1998). Microcircuitry and function of the inferior olive. *Trends Neurosci 21*(9), 391–400.

Degris, T., O. Sigaud, S. I. Wiener, and A. Arleo (2004). Rapid response of head direction cells to reorienting visual cues: A computational model. *Neurocomputing 58-60C*, 675–682.

d'Erfurth, A., A. Peyrache, A. Guillot, and A. Arleo (2005). Un modèle computationnel biomimétique de navigation pour le robot-rat Psikharpax. In Guéré (Ed.), *RJCIA*, pp. 327–330.

Drai, D. and I. Golani (2001). SEE: a tool for the visualization and analysis of rodent exploratory behavior. *Neuroscience and Biobehavioral Reviews 25*, 409–426.

Drai, D., N. Kafkafi , Y. Benjamini, G. Elmer, and I. Golani (2001). Rats and mice share common ethologically relevant parameters of exploratory behavior. *Behavioural Brain Research 125*, 133–140.

Eccles, J. C., M. Ito, and J. Szentagothai (1967). *The cerebellum as a neuronal machine*. Berlin: Springer-Verlag.

Ermentrout, G. B. (1998). Neural networks as spatio-temporal pattern-forming systems. *Rep. Prog. Phys. 61*, 353–430.

Etienne, A. S., J. Berlie, J. Georgakopoulos, and R. Maurer (1998). Role of dead reckoning in navigation. In S. Healy (Ed.), *Spatial Representation in Animals*, Chapter 3, pp. 54–68. Oxford University Press.

Etienne, A. S., V. Boulens, R. Maurer, T. Rowe, and C. Siegrist (2000). A brief view of known landmarks reorientates path integration in hamsters. *Naturwissenschaften 87*, 494–498.

Etienne, A. S. and K. J. Jeffery (2004). Path integration in mammals. *Hippocampus 14*, 180–192.

Etienne, A. S., E. Teroni, C. Hurni, and V. Portenier (1990). The effect of a single light cue on homing behaviour of the golden hamster. *Animal Behaviour 39*, 17–41.

Fortin, N. J., K. L. Agster, and H. B. Eichenbaum (2002). Critical role of the hippocampus in memory for sequences of events. *Nature Neuroscience 5(5)*, 458–462.

Foster, D. J., R. G. M. Morris, and P. Dayan (2000). A model of hippocampally dependent navigation, using the temporal difference learning rule. *Hippocampus 10(1)*, 1–16.

Foster, T. C., C. A. Castro, and B. L. McNaughton (1989). Spatial selectivity of rat hippocampal neurons: dependence on preparedness for movement. *Science 244*, 1580–1582.

Fyhn, M., S. Molden, M. P. Witter, E. I. Moser, and M.-B. Moser (2004). Spatial representation in the entorhinal cortex. *Science 305*(5688), 1258–1264.

Galambos, R., O. Szabo-Salfay, P. Barabas, J. Palhalmi, N. Szilagyi, and G. Juhasz (2000). Temporal distribution of the ganglion cell volleys in the normal rat optic nerve. *Proceedings of the National Academy of Sciences USA 97*, 13454–13459.

Gallagher, M., R. Burwell, and M. Burchinal (1993). Severity of spatial learning impairment in aging: development of a learning index for performance in the Morris water maze. *Behavioral Neuroscience 107(4)*, 618–626.

Gaussier, P., A. Revel, J. P. Banquet, and V. Babeau (2002). From view cells and place cells to cognitive map learning: Processing stages of the hippocampal system. *Biological Cybernetics 86(1)*, 15–28.

Gavrilov, V. V., S. I. Wiener, and A. Berthoz (1996). Whole-body rotations enhance hippocampal theta rhythm slow activity in awake rats passively transported on a mobile robot. *Annals of the New York Academy of Sciences 781*, 385–398.

Georgopoulos, A. P., A. Schwartz, and R. E. Kettner (1986). Neuronal population coding of movement direction. *Science 233*, 1416–1419.

Gerstner, W. and W. M. Kistler (2002). *Spiking Neuron Models*. Cambridge University Press.

Gonzalo-Ruiz, A., A. Alonso, J. M. Sanz, and R. R. Lliñas (1992). Afferent projections to the mammillary complex of the rat, with special reference to those from surrounding hypothalamic regions. *Journal of Comparative Neurology 321*, 277–299.

Goodridge, J. P., P. A. Dudchenko, K. A. Worboys, E. J. Golob, and J. S. Taube (1998). Cue control and head direction cells. *Behavioral Neuroscience 112(4)*, 749–761.

Goodridge, J. P. and J. S. Taube (1997). Interaction between the postsubiculum and anterior thalamus in the generation of head direction cell activity. *The Journal of Neuroscience 17(23)*, 9315–9330.

Goodridge, J. P. and D. S. Touretzky (2000). Modeling attractor deformation in the rodent head-direction system. *Journal of Neurophysiology 83(6)*, 3402–3410.

Goossens, J., H. Daniel, A. Rancillac, J. van der Steen, J. Oberdick, F. Crepel, C. I. De Zeeuw, and M. A. Frens (2001). Expression of protein kinase C inhibitor blocks cerebellar long-term depression without affecting Purkinje cell excitability in alert mice. *J Neurosci 21*(15), 5813–5823.

Graziano, A., L. Petrosini, and A. Bartoletti (2003). Automatic recognition of explorative strategies in the Morris water maze. *Journal of Neuroscience Methods 130(1)*, 33–44.

Green, J. and A. Arduini (1954). Hippocampal electrical activity in arousal. *Journal of Neurophysiology 17*, 533–557.

Gutkin, B. S., C. R. Laing, C. L. Colby, C. C. Chow, and G. B. Ermentrout (2001). Turning on and off with excitation: the role of spike time asynchrony and synchrony in sustained neural activity. *Journal of Computational Neuroscience 11*, 121–134.

Hafting, T., M. Fyhn, S. Molden, M.-B. Moser, and E. I. Moser (2005). Microstructure of a spatial map in the entorhinal cortex. *Nature 436*(7052), 801–806.

Hansel, D. and H. Sompolinsky (1998). Modeling feature selectivity in local cortical circuits. In C. Koch and I. Segev (Eds.), *Methods in Neuronal Modeling* (2nd ed.). MIT press, Cambridge, MA.

Harris, K. D., J. Csicsvari, H. Hirase, G. Dragoi, and G. Buzsaki (2003). Organization of cell assemblies in the hippocampus. *Nature 424*(6948), 552–556.

Harris, K. D., D. A. Henze, H. Hirase, X. Leinekugel, G. Dragoi, A. Czurko, and G. Buzsaki (2002). Spike train dynamics predicts theta-related phase precession in hippocampal pyramidal cells. *Nature 417*(6890), 738–741.

Hill, A. J. and P. J. Best (1981). Effects of deafness and blindness on the spatial correlates of hippocampal unit activity in the rat. *Experimental neurology 74*, 204–217.

Hines, M. L. and N. T. Carnevale (2001). NEURON: a tool for neuroscientists. *Neuroscientist 7(2)*, 123–135.

Itaya, S. K., G. W. V. Hoesen, and C.-B. Jenq (1981). Direct retinal input to the limbic system of the rat. *Brain Research 226*, 33–42.

Ito, M. (1993). New concepts in cerebellar function. *Rev Neurol (Paris) 149*(11), 596–599.

Ito, M. and M. Kano (1982). Long-lasting depression of parallel fi ber-Purkinje cell transmission induced by conjunctive stimulation of parallel fi bers and climbing fi bers in the cerebellar cortex. *Neurosci Lett 33*(3), 253–258.

Jaffard, R. and M. Meunier (1993). Role of the hippocampal formation in learning and memory. *Hippocampus 3*, 203–217.

Jakab, R. L. and J. Hamori (1988). Quantitative morphology and synaptology of cerebellar glomeruli in the rat. *Anatamy and Embryology 179*, 81–88.

Jeffery, K. J. (1998). Learning of landmark stability and instability by hippocampal place cells. *Neuropharmacology 37*, 677–687.

Jeffery, K. J. and J. M. O'Keefe (1999). Learned interaction of visual and idiothetic cues in the control of place fi eld orientation. *Experimental Brain Research 127*, 151–161.

Jensen, O. and J. E. Lisman (2000). Position reconstruction from an ensemble of hippocampal place cells: contribution of theta phase coding. *J Neurophysiol 83*(5), 2602–2609.

Kali, S. and P. Dayan (2000). The involvement of recurrent connections in area CA3 in establishing the properties of place fi elds: a model. *Journal of Neuroscience 20(19)*, 7463–7477.

Knierim, J. J., H. S. Kudrimoti, and B. L. McNaughton (1995a). Neuronal mechanisms underlying the integration between visual landmarks and path integration in the rat. *International Journal of Neural Systems 6*, 95–100.

Knierim, J. J., H. S. Kudrimoti, and B. L. McNaughton (1995b). Place cells, head direction cells, and the learning of landmark stability. *The Journal of Neuroscience 15*, 1648–1659.

Knierim, J. J., H. S. Kudrimoti, and B. L. McNaughton (1998). Interactions between idiothetic cues and external landmarks in the control of place cells and head direction cells. *Journal of Neurophysiology 80*, 425–446.

Koch, C. and I. Segev (2000). The role of single neurons in information processing. *Nature Neuroscience 3*, 1171–1177.

Laing, C. R. and C. C. Chow (2001). Stationary bumps in networks of spiking neurons. *Neural Computation 13*, 1473–1494.

Lee, I. and R. P. Kesner (2002). Differential contribution of NMDA receptors in hippocampal subregions to spatial working memory. *Nature Neuroscience 5(2)*, 162–168.

Leggio, M. G., P. Neri, A. Graziano, L. Mandolesi, M. Molinari, and L. Petrosini (1999). Cerebellar contribution to spatial event processing: characterization of procedural learning. *Exp Brain Res 127*(1), 1–11.

Lenck-Santini, P.-P., E. Save, and B. Poucet (2001). Evidence for a relationship between place-cell spatial fi ring and spatial memory performance. *Hippocampus 11*, 377–390.

Leonard, B. and B. L. McNaughton (1990). Spatial representation in the rat: Conceptual, behavioral, and neurophysiological perspectives. In R. P. Kesner and D. S. Olton (Eds.), *Neurobiology of Comparative Cognition*, pp. 363–422. Hillsdale, NJ: Erlbaum.

Leutgeb, S., J. K. Leutgeb, M. B. Moser, and E. I. Moser (2005). Place cells, spatial maps and the population code for memory. *Current Opinion in Neurobiology 15*, 1–9.

Lisman, J. E. and M. A. Idiart (1995). Storage of 7 +/- 2 short-term memories in oscillatory subcycles. *Science 267*(5203), 1512–1515.

Liu, R., L. Chang, and G. Wickern (1984). The dorsal tegmental nucleus: an axoplasmic transport study. *Brain Research 310*, 123–132.

London, M., A. Schreibman, M. Hausser, M. E. Larkum, and I. Segev (2002). The information effi cacy of a synapse. *Nature Neuroscience 5*, 332–340.

Lukashin, A. V. and A. P. Georgopoulos (1993). A dynamical neural network model for motor cortical activity during movement: population coding of movement trajectories. *Biological Cybernetics 69*, 517–524.

Markus, E. J., C. A. Barnes, B. L. McNaughton, V. L. Gladden, and W. E. Skaggs (1994). Spatial information content and reliability of hippocampal CA1 neurons: Effects of visual input. *Hippocampus 4*, 410–421.

Marr, D. (1969). A theory of cerebellar cortex. *Journal of Physiology 220(2)*, 437–470.

Martin, L. A., D. Goldowitz, and G. Mittleman (2003). The cerebellum and spatial ability: dissection of motor and cognitive components with a mouse model system. *Eur J Neurosci 18*(7), 2002–2010.

McNaughton, B. L., C. A. Barnes, J. L. Gerrard, K. Gothard, M. W. Jung, J. J. Knierim, H. Kudrimoti, Y. Qin, W. E. Skaggs, M. Suster, and K. L. Weaver (1996). Deciphering the hippocampal polyglot: The hippocampus as a path integration system. *The Journal of Experimental Biology 199*, 173–185.

McNaughton, B. L., L. L. Chen, and E. J. Markus (1991). Dead reckoning, landmark learning, and the sense of direction: A neurophysiological and computational hypothesis. *Journal of Cognitive Neuroscience 3*, 190–202.

Medina, J. F., K. S. Garcia, W. L. Nores, N. M. Taylor, and M. D. Mauk (2000). Timing mechanisms in the cerebellum: testing predictions of a large-scale computer simulation. *The Journal of Neuroscience 20(14)*, 5516–5525.

Mehta, M. R., A. K. Lee, and M. A. Wilson (2002). Role of experience and oscillations in transforming a rate code into a temporal code. *Nature 417*(6890), 741–746.

Miller, R. (1991). *Cortico-Hippocampal interplay and the representation of contexts in the brain*. Springer-Verlag.

Mitchell, S. J. and R. A. Silver (2003). Shunting inhibition modulates neuronal gain during synaptic excitation. *Neuron 38(3)*, 433–445.

Mittelstaedt, H. and M. L. Mittelstaedt (1982). Homing by path integration. In F. Papi and H. G. Wallraff (Eds.), *Avian navigation*. Berlin Heidelberg: Springer.

Mittelstaedt, M. L. and H. Mittelstaedt (1980). Homing by path integration in a mammal. *Naturwissenschaften 67*, 566–567.

Mizumori, S. J. Y. and J. D. Williams (1993). Directionally selective mnemonic properties of neurons in the lateral dorsal nucleus of the thalamus of rats. *The Journal of Neuroscience 13*, 4015–4028.

Morris, R. G. M., E. Anderson, G. S. Lynch, and M. Baudry (1986). Selective impairment of learning and blockade of long-term potentiation by an N-methyl-D-aspartate receptor antogonist, AP5. *Nature 319*, 774–776.

Morris, R. G. M. and U. Frey (1999). Hippocampal synaptic plasticity: Role in spatial learning or the automatic recording of attended experience? In N. Burgess, K. J. Jeffery, and J. O'Keefe (Eds.), *The Hippocampal and Parietal Foundations of Spatial Cognition*, Chapter 12, pp. 220–246. Oxford University Press.

Morris, R. G. M., P. Garrud, J. N. P. Rawlins, and J. O'Keefe (1982). Place navigation impaired in rats with hippocampal lesions. *Nature 297*, 681–683.

Muller, R. U. and J. L. Kubie (1987). The effects of changes in the environment on the spatial fi ring of hippocampal complex-spike cells. *The Journal of Neuroscience 7*, 1951–1968.

Nakazawa, K., M. C. Quirk, R. A. Chitwood, M. Watanabe, M. F. Yeckel, L. D. Sun, A. Kato, C. A. Carr, D. Johnston, M. A. Wilson, and S. Tonegawa (2002). Requirement for hippocampal CA3 NMDA receptors in associative memory recall. *Science 297*, 211–218.

Nielsen, T. A., D. A. DiGregorio, and R. A. Silver (2004). Modulation of glutamate mobility reveals the mechanism underlying slow-rising AMPAR EPSCs and the diffusion coeffi cient in the synaptic cleft. *Neuron 42*, 757–771.

Nieus, T., E. Sola, J. Mapelli, E. Saftenku, P. Rossi, and E. D'Angelo (2005). LTP regulates burst initiation and frequency at mossy fi ber - granule cell synapses of rat cerebellum: experimental observations and theoretical predictions. *Journal of Neurophysiology*, (to appear).

O'Donovan, M. J. and J. Rinzel (1997). Synaptic depression: a dynamic regulator of synaptic communication with varied functional roles. *Trends Neurosci 20(10)*, 431–433.

O'Keefe, J. and D. H. Conway (1978). Hippocampal place units in the freely moving rat: why they fi re where they fi re. *Experimental Brain Research 31*, 573–590.

O'Keefe, J. and J. Dostrovsky (1971). The hippocampus as a spatial map: Preliminary evidence from unit activity in the freely moving rat. *Brain Research 34*, 171–175.

O'Keefe, J. and L. Nadel (1978). *The Hippocampus as a cognitive map*. Oxford: Clarendon Press.

O'Keefe, J. and M. Recce (1993). Phase relationship between hippocampal place units and the EEG theta rhythm. *Hippocampus 3*, 317–330.

O'Keefe, J. and A. Speakman (1987). Single unit activity in the rat hippocampus during a spatial memory task. *Experimental Brain Research 68*, 1–27.

Panzeri, S., S. R. Schultz, A. Treves, and E. T. Rolls (1999). Correlations and the encoding of information in the nervous system. *Proceedings of the Royal Society of London Series B: Biological Sciences 266*, 1001–1012.

Panzeri, S. and A. Treves (1996). Analytical estimates of limited sampling biases in different information measures. *Network 7*, 87–107.

Petit, G. & A. Arleo, C. Fouquet, and L. Rondi-Reig (2005). A Navigation Analysis Tool (NAT) to evaluate spatial behavior patterns in a new paradigm: the starmaze. *(submitted)*.

Petrosini, L., M. Leggio, and M. Molinari (1998). The cerebellum in the spatial problem solving: a co-star or a guest-star? *Progress in Neurobiology 56(2)*, 191–210.

Petrosini, L., M. Molinari, and M. E. Dell'Anna (1996). Cerebellar contribution to spatial event processing: Morris water maze and T-maze. *European Journal of Neuroscience 9*, 1882–1896.

Poucet, B. (1993). Spatial cognitive maps in animals: New hypotheses on their structure and neural mechanisms. *Psychological Review 100*, 163–182.

Quirk, G. J., R. U. Muller, and J. L. Kubie (1990). The fi ring of hippocampal place cells in the dark depends on the rat's recent experience. *The Journal of Neuroscience 10(6)*, 2008–2017.

Quirk, G. J., R. U. Muller, J. L. Kubie, and J. B. J. Ranck (1992). The positional fi ring properties of medial entorhinal neurons: Description and comparison with hippocampal place cells. *The Journal of Neuroscience 12(5)*, 1945–1963.

Ranck, J. B. J. (1984). Head-direction cells in the deep cell layers of dorsal presubiculum in freely moving rats. *Society for Neuroscience Abstracts 10*, 599.

Redish, A. D. (1999). *Beyond the Cognitive Map, From Place Cells to Episodic Memory*. London: MIT Press-Bradford Books.

Redish, A. D., A. N. Elga, and D. S. Touretzky (1996). A coupled attractor model of the rodent head direction system. *Network 7(4)*, 671–685.

Redish, A. D. and D. S. Touretzky (1997). Cognitive maps beyond the hippocampus. *Hippocampus 7(1)*, 15–35.

Reep, R. L., H. C. Chandler, V. King, and J. V. Corwin (1994). Rat posterior parietal cortex: topography of corticocortical and thalamic connections. *Exp Brain Res 100*(1), 67–84.

Rieke, F., D. Warland, R. R. Steveninck, and W. Bialek (1997). *Spikes - Exploring the neural code*. The MIT Press.

Rondi-Reig, L. and E. Burguière (2005). Is the cerebellum ready for navigation? *Progress in Brain Research 148*, 199–212.

Rondi-Reig, L., G. Petit, C. Tobin, S. Tonegawa, J. Mariani, and A. Berthoz (2004). Impaired sequential-egocentric and allocentric memories in hippocampal CA1-NMDA receptor knockout mice during a new task of spatial navigation. *Society for Neuroscience Abstracts n. 329.2*.

Rubin, J., D. Terman, and C. Chow (2001). Localized bumps of activity sustained by inhibition in a two-layer thalamic network. *Journal of Computational Neuroscience 10*, 313–331.

Samsonovich, A. and B. L. McNaughton (1997). Path integration and cognitive mapping in a continuous attractor neural network model. *The Journal of Neuroscience 17(15)*, 5900–5920.

Sanger, T. D. (1989). Optimal unsupervised learning in a single-layer linear feedforward neural network. *Neural Networks 2*, 459–473.

Save, E., A. Cressant, C. Thinus-Blanc, and B. Poucet (1998). Spatial fi ring of hippocampal place cells in blind rats. *The Journal of Neuroscience 18(5)*, 1818–1826.

Save, E. and B. Poucet (2000). Hippocampal-parietal cortical interactions in spatial cognition. *Hippocampus 10(4)*, 491–499.

Schenk, F. and R. G. M. Morris (1985). Dissociation between components of spatial memory in rats after recovery from the effects of retrohippocampal lesions. *Experimental Brain Research 58*, 11–28.

Schmahmann, J. D. (1996). From movement to thought: anatomic substrates of the cerebellar contribution to cognitive processing. *Human Brain Mapping 4*, 174–198.

Schmahmann, J. D. and D. N. Pandya (1989). Anatomical investigation of projections to the basis pontis from posterior parietal association cortices in Rhesus monkey. *Journal of Comparative Neurology 289*, 53–73.

Schmahmann, J. D. and D. N. Pandya (1997). Anatomic organization of the basilar pontine projections from prefrontal cortices in rhesus monkeys. *Journal of Neuroscience 17*, 438–458.

Schölkopf, B. and H. A. Mallot (1995). View-based cognitive mapping and path planning. *Adaptive Behavior 3*, 311–348.

Schultz, W., P. Dayan, and R. R. Montague (1997). A neural substrate of prediction and reward. *Science 275*, 1593–1599.

Shannon, C. E. (1948). A mathematical theory of communication. *Bell System Technical Journal 27*, 379–423.

Sharp, P. E. (1996). Multiple spatial/behavioral correlates for cells in the rat postsubiculum: Multiple regression analysis and comparison to other hippocampal areas. *Cerebral Cortex 6(2)*, 238–259.

Sharp, P. E., J. L. Kubie, and R. U. Muller (1990). Firing properties of hippocampal neurons in a visually symmetrical environment: Contributions of multiple sensory cues and mnemonic processes. *The Journal of Neuroscience 10(9)*, 3093–3105.

Sharp, P. E., A. Tinkelman, and J. Cho (2001). Angular velocity and head direction signals recorded from the dorsal tegmental nucleus of gudden in the rat: Implications for path integration in the head direction cell circuit. *Behavioral Neuroscience 115(3)*, 571–588.

Sheynikhovich, D., R. Chavarriaga, T. Strösslin, and W. Gerstner (2005). Spatial representation and navigation in a bio-inspired robot. In S. Wermter, G. Palm, and M. Elshaw (Eds.), *Biomimetic Neural Learning for Intelligent Robots*.

Shibata, H. (1987). Ascending projections to the mammillary nuclei in the rat: A study using retrograde and anterograde transport of wheat germ agglutinin conjugated to horseradish peroxidase. *The Journal of Comparative Neurology 264*, 205–215.

Silver, R. A., S. G. Cull-Candy, and T. Takahashi (1996). Non-NMDA glutamate receptor occupancy and open probability at a rat cerebellar synapse with single and multiple release sites. *The Journal of Physiology 494*, 231–250.

Skaggs, W. E., J. J. Knierim, H. S. Kudrimoti, and B. L. McNaughton (1995). A model of the neural basis of the rat's sense of direction. In G. Tesauro, D. S. Touretzky, and T. K. Leen (Eds.), *Advances in Neural Information Processing Systems 7*, Cambridge, MA, pp. 173–180. MIT Press.

Skaggs, W. E., B. L. McNaughton, M. A. Wilson, and C. A. Barnes (1996). Theta phase precession in hippocampal neuronal populations and the compression of temporal sequences. *Hippocampus 6(2)*, 149–173.

Sola, E., F. Prestori, P. Rossi, V. Taglietti, and E. D'Angelo (2004). Increased neurotransmitter release during long-term potentiation at mossy fi bre-granule cell synapses in rat cerebellum. *The Journal of Physiology 557*, 843–861.

Somers, D. C., S. B. Nelson, and M. Sur (1995). An emergent model of orientation selectivity in cat visual cortical simple cells. *The Journal of Neuroscience 15*, 5448–5465.

Song, P. and X.-J. Wang (2003). A three-population attractor network model of rodent head direction system. *Society for Neuroscience Abstracts*, 939.3.

Song, P. and X.-J. Wang (2004). Time integration by moving 'hill of activity': a spiking neural model without recurrent excitation of the head-direction system. *Unpublished manuscript*.

Squire, L. R. and S. M. Zola (1996). Structure and function of declarative and nondeclarative. *Proc. Natl. Acad. Sci. USA 93*, 13515–13522.

Stackman, R. W. and J. S. Taube (1997). Firing properties of head direction cells in the rat anterior thalamic nucleus: Dependence on vestibular input. *The Journal of Neuroscience 17(11)*, 4349–4358.

Stackman, R. W. and J. S. Taube (1998). Firing properties of rat lateral mammillary single units: Head direction, head pitch, and angular head velocity. *The Journal of Neuroscience 18(21)*, 9020–9037.

Steele, R. J. and R. G. M. Morris (1999). Delay-dependent impairment of a matching-to-placetask with chronic and intrahippocampal infusion of the NMDA-antagonist D-AP5. *Hippocampus 9*, 118–136.

Strösslin, T., C. Krebser, A. Arleo, and W. Gerstner (2002). Combining multimodal sensory input for spatial learning. In J. R. Dorronsoro (Ed.), *Artifi cial Neural Networks*, pp. 87–92. Springer LNCS.

Strösslin, T., D. Sheynikhovich, R. Chavarriaga, and W. Gerstner (2005). Robust self-localisation and navigation based on hippocampal place cells. *Neural Networks*. To appear.

Sutton, R. S. (1988). Learning to predict by the methods of temporal differences. *Machine Learning 3*, 9–44.

Sutton, R. S. and A. G. Barto (1998). *Reinforcement learning, an introduction*. Cambridge, Massachusetts: MIT Press-Bradford Books.

Tabuchi, E. T., A. B. Mulder, and S. I. Wiener (2000). Position and behavioral modulation of synchronization of hippocampal and accumbens neuronal discharges in freely moving rats. *Hippocampus 10*, 717–728.

Taube, J. S. (1995). Head direction cells recorded in the anterior thalamic nuclei of freely moving rats. *The Journal of Neuroscience 15(1)*, 70–86.

Taube, J. S. (1998). Head direction cells and the neurophysiological basis for a sense of direction. *Progress in Neurobiology 55*, 225–256.

Taube, J. S. and J. P. Bassett (2003). Persistent neural activity in head direction cells. *Cerebral Cortex 13*, 1162–1172.

Taube, J. S., R. I. Muller, and J. B. J. Ranck (1990a). Head direction cells recorded from the postsubiculum in freely moving rats. I. Description and quantitative analysis. *The Journal of Neuroscience 10*, 420–435.

Taube, J. S., R. I. Muller, and J. B. J. Ranck (1990b). Head direction cells recorded from the postsubiculum in freely moving rats. II. Effects of environmental manipulations. *The Journal of Neuroscience 10*, 436–447.

Taube, J. S. and R. U. Muller (1998). Comparisons of head direction cell activity in the postsubiculum and anterior thalamus of freely moving rats. *Hippocampus 8*, 87–108.

Thach, W. T., H. P. Goodkin, and J. G. Keating (1992). The cerebellum and the adaptive coordination of movement. *Annu Rev Neurosci 15*, 403–442.

Thompson, R. F., S. Bao, L. Chen, B. D. Cipriano, J. S. Grethe, J. J. Kim, J. K. Thompson, J. A. Tracy, M. S. Weninger, and D. J. Krupa (1997). Associative learning. *Int. Rev. Neurobiol. 41*, 151–189.

Thorpe, S., D. Fize, and C. Marlot (1996). Speed of processing in the human visual system. *Nature 381*, 520–522.

Trullier, O. and J.-A. Meyer (2000). Animat navigation using a cognitive graph. *Biological Cybernetics 83*, 271–285.

Tsien, J. Z., P. T. Huerta, and S. Tonegawa (1996). The essential role of hippocampal CA1 NMDA receptor dependent synaptic plasticity in spatial memory. *Cell 87*, 1327–1338.

Tsodyks, M. (2005). Attractor neural networks and spatial maps in hippocampus. *Neuron 48*(2), 168–169.

Tsodyks, M. and T. Sejnowski (1995). Associative memory and hippocampal place cells. *International Journal of Neural Systems 6*, 81–86.

Tsodyks, M. V. and H. Markram (1997). The neural code between neocortical pyramidal neurons depends on neurotransmitter release probability. *Proceedings of the National Academy of Sciences USA 94(2)*, 719–23.

Vanderwolf, C. H. (1969). Hippocampal electrical activity and voluntary movement in the rat. *Electroencephalography and Clinical Neurophysiology 26*, 407–418.

Verbitsky, M., A. L. Yonan, G. Malleret, E. R. Kandel, T. C. Gilliam, and P. Pavlidis (2004). Altered hippocampal transcript profi le accompanies an age-related spatial memory defi cit in mice. *Learning and Memory 11(3)*, 253–260.

Vogt, B. A. and M. W. Miller (1983). Cortical connections between rat cingulate cortex and visual, motor, and postsubicular cortices. *J Comp Neurol 216*(2), 192–210.

Wang, X.-J. (2001). Synaptic reverberation underlying mnemonic persistent activity. *Trends in Neuroscience 24(8)*, 455–463.

Wiener, S. I. (1993). Spatial and behavioral correlates of striatal neurons in rats performing a self-initiated navigation task. *The Journal of Neuroscience 13*, 3802–3817.

Wiener, S. I. and A. Arleo (2003). Persistent activity in limbic system neurons: Neurophysiological and modeling perspectives. *Journal of Physiology Paris 97(4-6)*, 547–555.

Wiener, S. I. and J. S. Taube (2005). *Head Direction Cells and the Neural Mechanisms of Spatial Orientation*. Cambridge, MA: MIT Press.

Wilson, M. A. and B. L. McNaughton (1993). Dynamics of the hippocampal ensemble code for space. *Science 261*, 1055–1058.

Wirtshafter, D. and T. R. Stratford (1993). Evidence for GABAergic projections from the tegmental nuclei of Gudden to the mammillary body in the rat. *Brain Research 630*, 188–194.

Witter, M. P. (1993). Organization of the entorhinal-hippocampal system: A review of current anatomical data. *Hippocampus 3*, 33–44.

Wolfer, D. P. and H. P. Lipp (1992). A new computer program for detailed off-line analysis of swimming navigation in the Morris water maze. *Journal of Neuroscience Methods 41(1)*, 65–74.

Xie, X., R. H. R. Hahnloser, and H. S. Seung (2002). Double-ring network model of the head direction system. *Physical Review E 66*, 041902–1–9.

Zhang, K. (1996). Representation of spatial orientation by the intrinsic dynamics of the head-direction cell ensemble: A theory. *The Journal of Neuroscience 16(6)*, 2112–2126.

Zugaro, M. B., A. Arleo, A. Berthoz, and S. I. Wiener (2003). Rapid spatial reorientation and head direction cells. *The Journal of Neuroscience 23(8)*, 3478–3482.

Zugaro, M. B., A. Berthoz, and S. I. Wiener (2001). Background, but not foreground, spatial cues are taken as references for head direction responses by rat anterodorsal thalamus neurons. *The Journal of Neuroscience 21*, RC154(1–5).

Zugaro, M. B., L. Monconduit, and G. Buzsaki (2005). Spike phase precession persists after transient intrahippocampal perturbation. *Nat Neurosci 8*(1), 67–71.

Zugaro, M. B., E. Tabuchi, C. Fouquier, A. Berthoz, and S. I. Wiener (2001). Active locomotion increases peak fi ring rates of anterodorsal thalamic head direction cells. *Journal of Neurophysiology 86*, 692–702.

Zugaro, M. B., E. Tabuchi, and S. I. Wiener (2000). Influence of conflicting visual, inertial and substratal cues on head direction cell activity. *Experimental Brain Research 133*, 198–208.

Zugaro, M. B. & A. Arleo, C. Déjean, E. Burguière, M. Khamassi, and S. I. Wiener (2004). Rat anterodorsal thalamic head direction neurons depend upon dynamic visual signals to select anchoring landmark cues. *European Journal of Neuroscience 20*, 530–536.